Neutrino interactions
importance to nuclear physics

. . .

José Enrique Amaro

Departamento de Física Atómica, Molecular y Nuclear

Universidad de Granada

Overview

Neutrino scattering formalism

- Response functions
- Polarization observables
- Connection to electron scattering
- Scaling

Overview

Neutrino scattering formalism

- Response functions

Nuclear and reaction mechanisms ingredients

- Electro-weak current matrix elements
- Long-range nuclear correlations (RPA)
- Final-state interactions
- Finite-size effects
- Coulomb corrections
- Relativistic effects

Overview

Neutrino scattering formalism

Nuclear and reaction mechanisms ingredi-

Resuls for different reaction channels

- Charge-changing quasi-elastic scattering
- Neutral-current quasielastic scattering
- Delta excitation
- Coherent pion production

- Relativistic effects

Overview

Neutrino scattering formalism

Nuclear and reaction mechanisms ingredi-

Resuls for different reaction channels

Kinematics

- Low energy
- Intermediate to high energy
- Coherent pion production
- Relativistic effects

Overview

Neutrino scattering formalism
- Response functions

Nuclear and reaction mechanisms ingredi-ents

Resuls for different reaction channels

Kinematics

Observables

- Inclusive cross sections
- Integrated cross sections
- Angular distributions
- Polarization observables

Overview

- Neutrino scattering formalism
  - Response functions
- Nuclear and reaction mechanisms ingredients
- Resuls for different reaction channels
- Kinematics
- Observables
- Nuclear models
  - Local fermi gas
  - Relativistic Fermi Gas
  - Shell Model (SM)
  - Relativistic Mean Field (RMF)
  - Super-Scaling Analysis (SuSA)

Overview

Neutrino scattering formalism

- Response functions

Nuclear and reaction mechanisms ingredi-ents

Resuls for different reaction channels

Kinematics

Observables

Nuclear models

Special Topics

- Theoretical uncertainties
- Strangeness content of the nucleon
- Flux-averaged coherent pion production
- Super-Scaling Analysis (SuSA)

1 General formalism

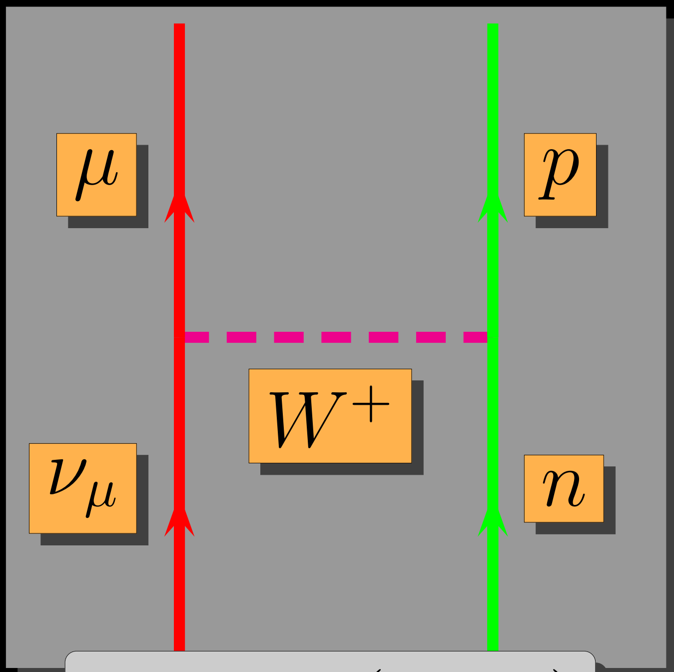

CC QE (ν_l, l^-)

1 General formalism

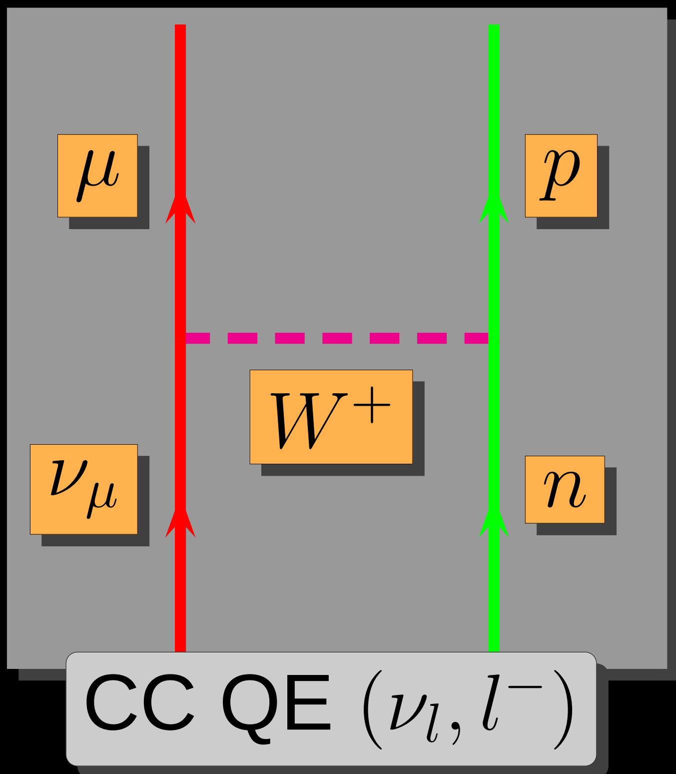

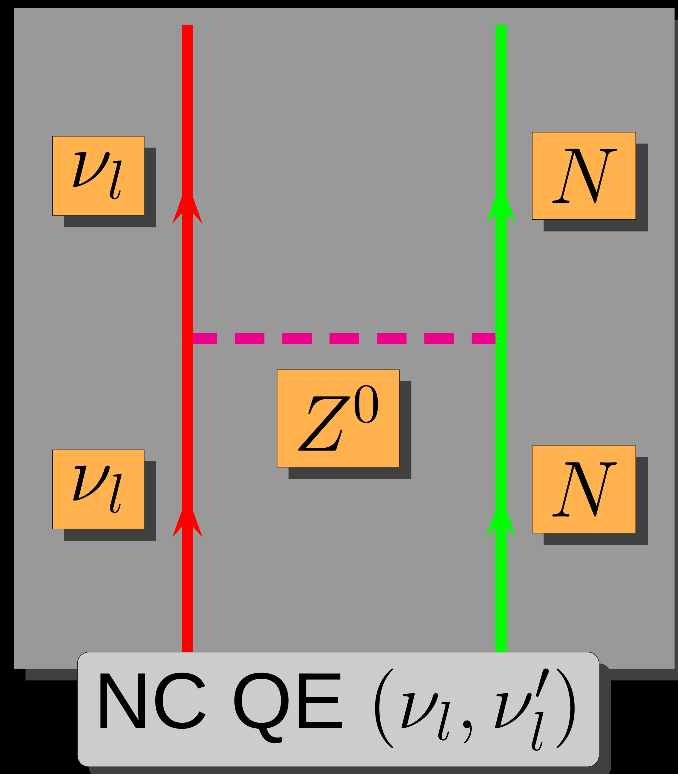

Kinematics

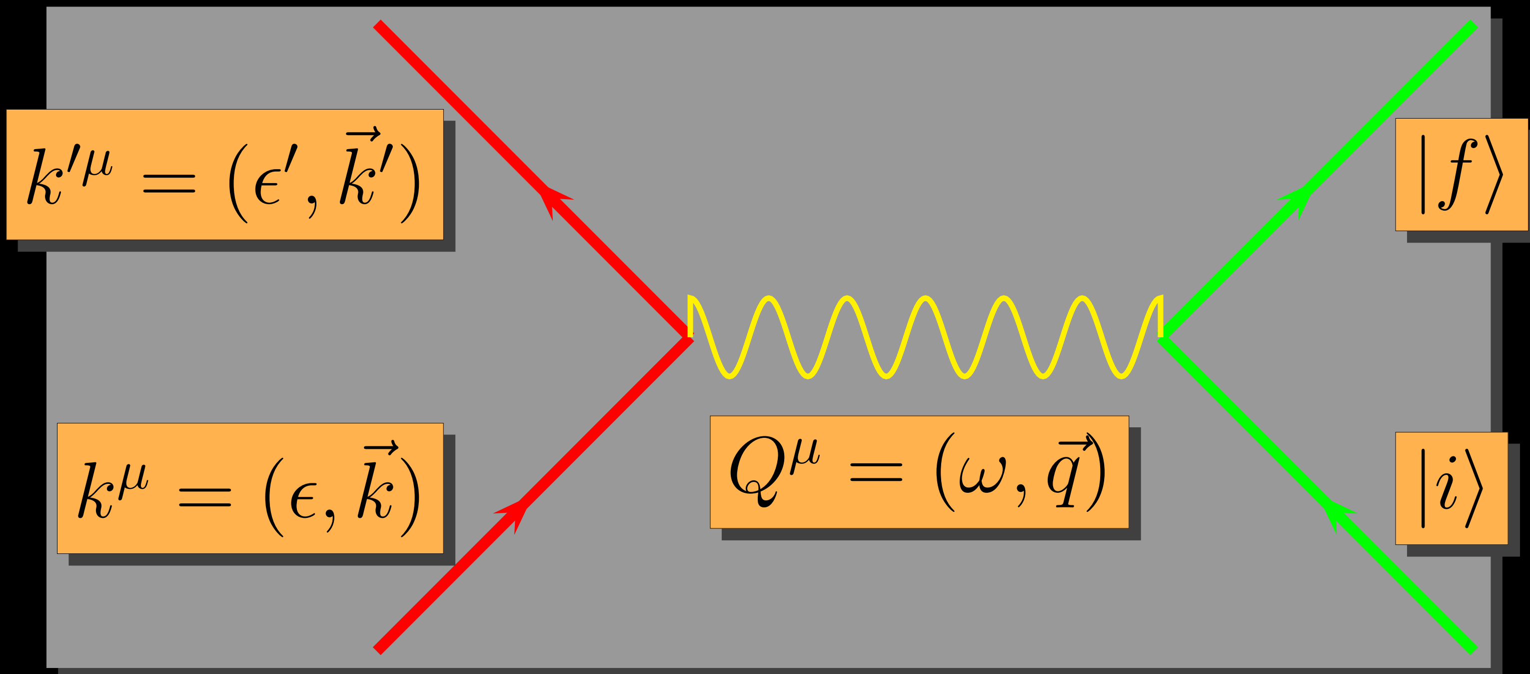

$$Q^2 = \omega^2 - q^2 < 0$$

Adimensional variables

$$\lambda = \frac{\omega}{2m_N} \qquad \kappa = \frac{q}{2m_N} \qquad \tau = \kappa^2 - \lambda^2$$

Example: CC neutrino reaction

$$\nu + A \rightarrow l^- + B$$

Effective Hamiltonian

$$\mathcal{H}_{eff} = \frac{G\cos\theta_c}{\sqrt{2}} j^\mu(x)\hat{J}_\mu(x)$$

Couplig constant: $G = 1.1664 \times 10^{-5}\mathrm{GeV}^{-2}$
Cabibbo angle: $\theta_c = 0.974$
Leptonic current ($\nu \rightarrow l$):

$$j^\mu = \overline{u}_l(\mathbf{k}')\gamma^\mu(1-\gamma_5)u_\nu(\mathbf{k})$$

Hadronic current (single nucleon $n \rightarrow p$) is of the form $V - A$

$$\boxed{\hat{J}_\mu = \overline{u}_p(\mathbf{p}')\left[F_1(Q^2)\gamma_\mu + F_2(Q^2)i\sigma_{\mu\nu}\frac{Q^\nu}{2m_N} - G_A(Q^2)\gamma_\mu\gamma_5 - G_P(Q^2)\frac{Q_\mu}{2m_N}\gamma_5\right]u_n(\mathbf{p})}$$

Momentum transfer

$$Q^\mu = K^\mu - K'^\mu = P'^\mu - P^\mu$$

Example: S-matrix element

Neutrino scattering with initial and final hadronic states $|i\rangle \longrightarrow |f\rangle$
Transition matrix element to first order in the interaction

$$S_{fi} = -i \int d^4 \, \langle l, f | \mathcal{H}_{eff}(x) | \nu_l, i \rangle = \boxed{-2\pi i \delta(E_f - E_i - \omega) \frac{G \cos\theta_c}{\sqrt{2}} l^\mu J_\mu}$$

Lepton current matrix element

$$l^\mu = \left[\frac{m'}{V\epsilon'} \frac{m}{V\epsilon} \right]^{1/2} \overline{u}_l(\mathbf{k}') \gamma^\mu (1 - \gamma_5) u_\nu(\mathbf{k})$$

Hadronic current matrix element

$$J_\mu = \langle f | \hat{J}_\mu(\mathbf{q}) | i \rangle$$

Example: cross Section

Inclusive: only the final lepton is detected

$$d\sigma = \frac{\overline{\sum}|S_{fi}|^2}{T}\frac{V}{v_{rel}}\frac{V d^3k'}{(2\pi)^3}$$

Performing the lepton traces

$$\boxed{\frac{d\sigma}{d\Omega' d\epsilon'} = \frac{G^2\cos^2\theta_c}{4\pi^2}\frac{k'}{\epsilon}(s_{\mu\nu}+ia_{\mu\nu})W^{\mu\nu}}$$

Hadronic tensor

$$\boxed{W^{\mu\nu} = \overline{\sum_{fi}}\delta(E_f - E_i - \omega)\langle f|J^\mu(\mathbf{q})|i\rangle^*\langle f|J^\nu(\mathbf{q})|i\rangle}$$

Leptonic tensors

$$\boxed{\begin{aligned} s^{\mu\nu} &= 2P^\mu P^\nu - \frac{1}{2}Q^\mu Q^\nu + \frac{Q^2 - m'^2}{2}g^{\mu\nu} \\ a^{\mu\nu} &= \epsilon^{\mu\nu\alpha\beta}Q_\alpha P_\beta \end{aligned}}$$

$$P^\mu = \frac{K^\mu + K'^\mu}{2}$$
$$Q^\mu = K^\mu - K'^\mu$$

(ν_l, l^-) *formalism*

Cross section:

$$\frac{d\sigma}{d\Omega' d\epsilon'} = \sigma_0 \mathcal{F}_+^2$$

Similar to $\sigma_{\rm Mott}$:

$$\sigma_0 = \frac{G^2 \cos^2\theta_c}{2\pi^2} k'\epsilon' \cos^2\frac{\tilde\theta}{2}$$

Fermi constant: $G = 1.166 \times 10^{-11} \quad {\rm MeV}^{-2}$

Cabibbo angle: $\cos\theta_c = 0.975$

Generalized scattering angle:

$$\tan^2\frac{\tilde\theta}{2} = \frac{|Q^2|}{(\epsilon+\epsilon')^2 - q^2}$$

(ν_l, l^-) *formalism (II)*

Nuclear structure information:

$$\mathcal{F}_+^2 = \widehat{V}_{CC}R_{CC} + 2\widehat{V}_{CL}R_{CL} + \widehat{V}_{LL}R_{LL} + \widehat{V}_T R_T + 2\widehat{V}_{T'}R_{T'}$$

(ν_l, l^-) *formalism (II)*

Nuclear structure information:

$$\mathcal{F}_+^2 = \widehat{V}_{CC} R_{CC} + 2\widehat{V}_{CL} R_{CL} + \widehat{V}_{LL} R_{LL} + \widehat{V}_T R_T + 2\widehat{V}_{T'} R_{T'}$$

kinematical factors $\widehat{V}_K$ from the leptonic tensor

$$\begin{aligned}
\widehat{V}_{CC} &= 1 - \delta^2 \tan^2 \frac{\tilde{\theta}}{2} \\
\widehat{V}_{CL} &= \frac{\omega}{q} + \frac{\delta^2}{\rho'} \tan^2 \frac{\tilde{\theta}}{2} \\
\widehat{V}_{LL} &= \frac{\omega^2}{q^2} + \left(1 + \frac{2\omega}{q\rho'} + \rho\delta^2\right) \delta^2 \tan^2 \frac{\tilde{\theta}}{2} \\
\widehat{V}_{T} &= \tan^2 \frac{\tilde{\theta}}{2} + \frac{\rho}{2} - \frac{\delta^2}{\rho'} \left(\frac{\omega}{q} + \frac{1}{2}\rho\rho'\delta^2\right) \tan^2 \frac{\tilde{\theta}}{2} \\
\widehat{V}_{T'} &= \frac{1}{\rho'} \left(1 - \frac{\omega\rho'}{q}\delta^2\right) \tan^2 \frac{\tilde{\theta}}{2}
\end{aligned}$$

(ν_l, l^-) formalism (II)

Nuclear structure information:

$$\mathcal{F}_+^2 = \widehat{V}_{CC} R_{CC} + 2\widehat{V}_{CL} R_{CL} + \widehat{V}_{LL} R_{LL} + \widehat{V}_T R_T + 2\widehat{V}_{T'} R_{T'}$$

kinematical factors $\widehat{V}_K$ from the leptonic tensor

$$\begin{aligned}
\widehat{V}_{CC} &= 1 - \delta^2 \tan^2 \frac{\tilde{\theta}}{2} \\
\widehat{V}_{CL} &= \frac{\omega}{q} + \frac{\delta^2}{\rho'} \tan^2 \frac{\tilde{\theta}}{2} \\
\widehat{V}_{LL} &= \frac{\omega^2}{q^2} + \left(1 + \frac{2\omega}{q\rho'} + \rho\delta^2\right) \delta^2 \tan^2 \frac{\tilde{\theta}}{2} \\
\widehat{V}_T &= \tan^2 \frac{\tilde{\theta}}{2} + \frac{\rho}{2} - \frac{\delta^2}{\rho'}\left(\frac{\omega}{q} + \frac{1}{2}\rho\rho'\delta^2\right) \tan^2 \frac{\tilde{\theta}}{2} \\
\widehat{V}_{T'} &= \frac{1}{\rho'}\left(1 - \frac{\omega\rho'}{q}\delta^2\right) \tan^2 \frac{\tilde{\theta}}{2}
\end{aligned}$$

Adimensional variables:

$$\begin{aligned}
\delta &= \frac{m'}{\sqrt{|Q^2|}} \\
\rho &= \frac{|Q^2|}{q^2} \\
\rho' &= \frac{q}{\epsilon + \epsilon'} .
\end{aligned}$$

The only dependence on the muon mass m' is in δ

(ν_l, l^-) *formalism (III)*

Weak response functions

$$
\begin{aligned}
R_{CC} &= W^{00} \\
R_{CL} &= -\frac{1}{2}\left(W^{03} + W^{30}\right) \\
R_{LL} &= W^{33} \\
R_{T} &= W^{11} + W^{22} \\
R_{T'} &= -\frac{i}{2}\left(W^{12} - W^{21}\right)
\end{aligned}
$$

(ν_l, l^-) formalism (III)

Weak response functions

$$
\begin{aligned}
R_{CC} &= W^{00} \\
R_{CL} &= -\frac{1}{2}\left(W^{03} + W^{30}\right) \\
R_{LL} &= W^{33} \\
R_T &= W^{11} + W^{22} \\
R_{T'} &= -\frac{i}{2}\left(W^{12} - W^{21}\right)
\end{aligned}
$$

Weak CC hadronic tensor:

$$
W^{\mu\nu}(q,\omega) = \overline{\sum_{fi}} \delta(E_f - E_i - \omega) \langle f|J^\mu(Q)|i\rangle^* \langle f|J^\nu(Q)|i\rangle \ .
$$

(ν_l, l^-) formalism (III)

Weak response functions

$$\begin{aligned} R_{CC} &= W^{00} \\ R_{CL} &= -\frac{1}{2}\left(W^{03} + W^{30}\right) \\ R_{LL} &= W^{33} \\ R_T &= W^{11} + W^{22} \\ R_{T'} &= -\frac{i}{2}\left(W^{12} - W^{21}\right) \end{aligned}$$

Weak CC hadronic tensor:

$$W^{\mu\nu}(q,\omega) = \overline{\sum_{fi}} \delta(E_f - E_i - \omega) \langle f|J^\mu(Q)|i\rangle^* \langle f|J^\nu(Q)|i\rangle \; .$$

$J^\mu(Q)$: the hadronic CC current operator

Nuclear Weak responses

Expand into vector and axial-vector contributions

$$R_{CC} = R_{CC}^{VV} + R_{CC}^{AA} \qquad R_{CL} = R_{CL}^{VV} + R_{CL}^{AA}$$
$$R_{LL} = R_{LL}^{VV} + R_{LL}^{AA}$$
$$R_{T} = R_{T}^{VV} + R_{T}^{AA} \qquad R_{T'} = R_{T'}^{VA}$$

$$R_{CL}^{VV} = -\frac{\omega}{q} R_{CC}^{VV} \qquad R_{LL}^{VV} = \frac{\omega^2}{q^2} R_{CC}^{VV}$$

Conserved vector current

$$\widehat{V}_{CC} R_{CC}^{VV} + 2\widehat{V}_{CL} R_{CL}^{VV} + \widehat{V}_{LL} R_{LL}^{VV} = \widehat{V}_L R_L^{VV} \equiv X_L^{VV}$$

traditional longitudinal contribution

$$\widehat{V}_{CC} R_{CC}^{AA} + 2\widehat{V}_{CL} R_{CL}^{AA} + \widehat{V}_{LL} R_{LL}^{AA} \equiv X_{C/L}^{AA}$$

Collapse does not occur for the AA terms.

$$\widehat{V}_T \left[R_T^{VV} + R_T^{AA} \right] \equiv X_T$$

Transverse components

$$2\widehat{V}_{T'} R_{T'}^{VA} \equiv X_{T'}$$

V/A interference term

Full response: $\mathcal{F}_\chi^2 = X_L^{VV} + X_{C/L}^{AA} + X_T + \chi X_{T'}$

2 The relativistic Fermi gas (RFG)

Nuclear response functions for (ν_μ, μ^-) reactions

$$R_K = N\Lambda_0 U_K f_{RFG}(\psi), \quad K = CC, CL, LL, T, T',$$

- N is the neutron number,
- $\Lambda_0 = \dfrac{\xi_F}{m_N \eta_F^3 \kappa}, \quad \eta_F = k_F/m_N, \quad \xi_F = \sqrt{1+\eta_F^2} - 1.$
- Scaling function $f_{RFG}(\psi) = \frac{3}{4}(1-\psi^2)\theta(1-\psi^2)$
- Scaling variable

$$\psi = \frac{1}{\sqrt{\xi_F}} \frac{\lambda - \tau}{\sqrt{(1+\lambda)\tau + \kappa\sqrt{\tau(1+\tau)}}}$$

- single-nucleon responses U_K

Single-nucleon responses, $K = CC$

$$U_{CC} = U^V_{CC} + \left(U^A_{CC}\right)_{\mathrm{c.}} + \left(U^A_{CC}\right)_{\mathrm{n.c.}}$$

$$U^V_{CC} = \frac{\kappa^2}{\tau}\left[(2G^V_E)^2 + \frac{(2G^V_E)^2 + \tau(2G^V_M)^2}{1+\tau}\Delta\right] ,$$

$$\Delta = \frac{\tau}{\kappa^2}\xi_F(1-\psi^2)\left[\kappa\sqrt{1+\frac{1}{\tau}} + \frac{\xi_F}{3}(1-\psi^2)\right]$$

The axial-vector response is the sum of conserved (c.) plus non conserved (n.c.) parts,

$$\left(U^A_{CC}\right)_{\mathrm{c.}} = \frac{\kappa^2}{\tau}G_A^2\Delta \quad , \quad \left(U^A_{CC}\right)_{\mathrm{n.c.}} = \frac{\lambda^2}{\tau}{G'_A}^2 .$$

Single-nucleon responses, $K = CL, LL$

$$
\begin{aligned}
U_{CL} &= U^V_{CL} + \left(U^A_{CL}\right)_{\rm c.} + \left(U^A_{CL}\right)_{\rm n.c.} \\
U_{LL} &= U^V_{LL} + \left(U^A_{LL}\right)_{\rm c.} + \left(U^A_{LL}\right)_{\rm n.c.} \quad ,
\end{aligned}
$$

The vector and conserved axial-vector parts are determined by current conservation

$$
U^V_{CL} = -\frac{\lambda}{\kappa} U^V_{CC} \qquad \left(U^A_{CL}\right)_{\rm c.} = -\frac{\lambda}{\kappa} \left(U^A_{CC}\right)_{\rm c.}
$$

$$
U^V_{LL} = \frac{\lambda^2}{\kappa^2} U^V_{CC} \qquad \left(U^A_{LL}\right)_{\rm c.} = \frac{\lambda^2}{\kappa^2} \left(U^A_{CC}\right)_{\rm c.} \quad ,
$$

Non-conserved n.c. parts:

$$
\left(U^A_{CL}\right)_{\rm n.c.} = -\frac{\lambda\kappa}{\tau} {G'_A}^2 \quad , \quad \left(U^A_{LL}\right)_{\rm n.c.} = \frac{\kappa^2}{\tau} {G'_A}^2 \quad .
$$

Single-nucleon responses, $K = T, T'$

$$
\begin{aligned}
U_T &= U_T^V + U_T^A \\
U_T^V &= 2\tau(2G_M^V)^2 + \frac{(2G_E^V)^2 + \tau(2G_M^V)^2}{1+\tau}\Delta \\
U_T^A &= 2(1+\tau)G_A^2 + G_A^2\Delta \\
U_{T'} &= 2G_A(2G_M^V)\sqrt{\tau(1+\tau)}[1+\tilde{\Delta}]
\end{aligned}
$$

with

$$
\tilde{\Delta} = \sqrt{\frac{\tau}{1+\tau}\frac{\xi_F(1-\psi^2)}{2\kappa}}\ .
$$

3 Local Fermi gas (LFG)

Easy model to include many nuclear effects

- Local Density Approximation (LDA): use a local Fermi momentum $k_F(r) = (3\pi^2\rho(r))^{1/3}$ and average the responses over the nuclear interior weigthed by $\rho(r)$ (integrating over r)
- RPA nuclear correlations
- Correct energy balance and Coulomb distortion effects
- FSI effects

The RPA series

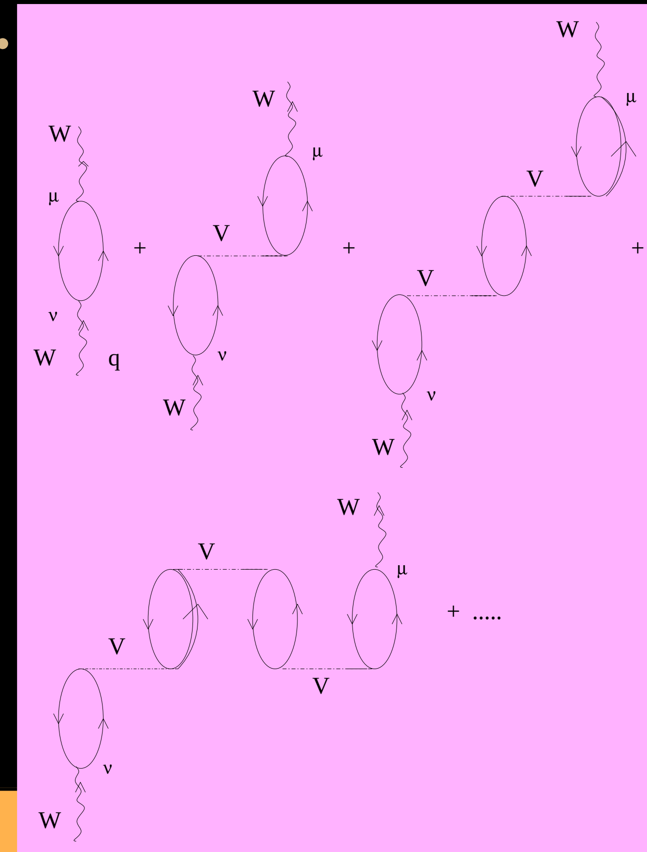

- ph-ph interaction of Landau-Migdal

$$V = c_0 \left[f_0(\rho) + f_0'(\rho)\vec{\tau}_1 \cdot \vec{\tau}_2 + g_0(\rho)\vec{\sigma}_1 \cdot \vec{\sigma}_2 + g_0'(\rho)\vec{\tau}_1 \cdot \vec{\tau}_2 \vec{\sigma}_1 \cdot \vec{\sigma}_2 \right]$$

- Parameters fitted to electromagnetic nuclear properties and transitions Speth et al.
- Includes Δ excitations in the medium, and ph-Δh, Δ-hΔh effective interactions
- renormalization of the hadronic tensor (axial and vector) in the medium

Coulomb corrections

- Correct the energy balance by the minumum nuclear excitation energy gap $Q = M(X_f) - M(X_i)$ instead of the LFG value $Q_{LFG}(r) = E_F^p(r) - E_F^n(r)$ Replacing

$$\omega \longrightarrow \omega - [Q - Q_{LFG}(r)]$$

- Self-energy (Coulomb potential) of the final lepton

$$\Sigma_C = 2\epsilon' V_C(r)$$

($V_C(r)$ is the nuclear Coulomb potential) Modification of the charged lepton propagator

$$\frac{1}{k^2 - m_l^2 - 2k_0 V_C(r) + i\epsilon}$$

$\longrightarrow$ new local energy-momentum relation for the final lepton (Modified effective momentum approximation)

RPA predictions for LSND

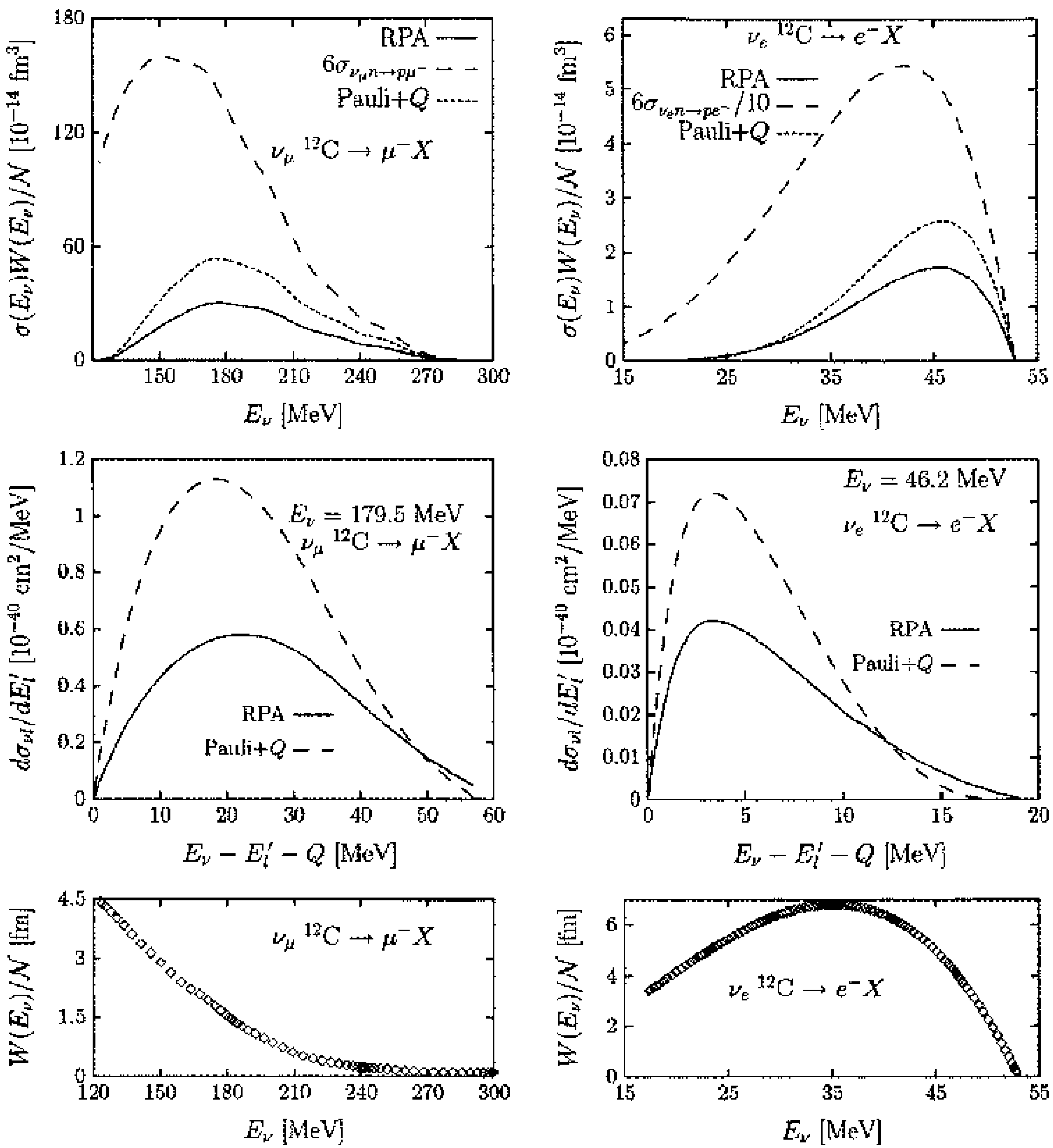

FIG. 7. Predictions for the LSND measurement of the ^{12}C $(\nu_\mu,\mu^-)X$ reaction (left panels) and the ^{12}C $(\nu_e,e^-)X$ reaction near threshold (right panels). Results have been obtained by using nonrelativistic kinematics for the nucleons and without FSI. Top: ν_μ and ν_e cross sections multiplied by the neutrino fluxes, as a function of the neutrino energy. In addition to the RPA calculation (solid line), we show results without RPA correlations and Coulomb corrections (dotted line), and also (dashed line) the low-density limit of Eq. (31). Middle: Differential muon and electron neutrino cross sections at $E_{\nu_\mu}=179.5$ MeV (left) and $E_{\nu_e}=46.2$ MeV (right), as a function of the energy transfer. Bottom: Neutrino spectra from Ref. [50] (left) and Eq. (65) (right).

RPA predictions for LSND

Experimental and theoretical Flux averaged cross section

TABLE II. Experimental and theoretical flux averaged $^{12}C(\nu_\mu,\mu^-)X$ and $^{12}C(\nu_e,e^-)X$ cross sections in 10^{-40} cm^2 units. We label our predictions as in Fig. 7. We also quote results from other calculations (see text for details).

	LDT	Pauli+Q	RPA	SM [15]	SM [27]	CRPA [18]	Exp.		
							LSND'95 [50]	LSND'97 [51]	LSND'02 [52]
$\bar\sigma(\nu_\mu,\mu^-)$	66.1	20.7	11.9	13.2	15.2	19.2	8.3±0.7±1.6	11.2±0.3±1.8	10.6±0.3±1.8
							KARMEN [53]	LSND [54]	LAMPF [55]
$\bar\sigma(\nu_e,e^-)$	5.97	0.19	0.14	0.12	0.16	0.15	0.15±0.01±0.01	0.15±0.01±0.01	0.141±0.023

Final State Interaction (FSI)

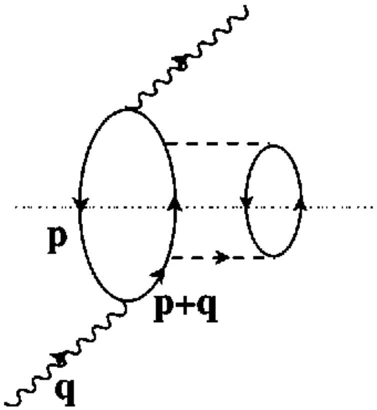

FIG. 4. W^+ self-energy diagram obtained from the first diagram epicted in Fig. 2 by dressing up the nucleon propagator of the article state in the ph excitation.

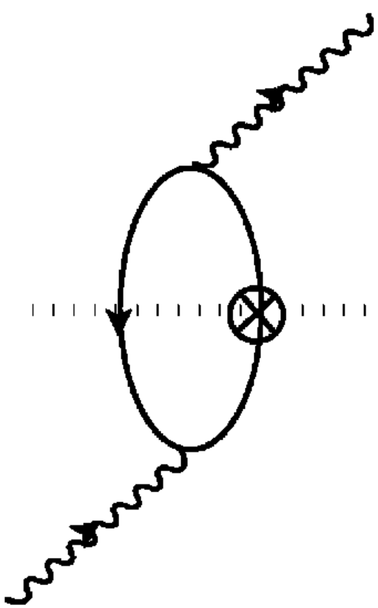

FIG. 5. Insertion of the nucleon self-energy on the nucleon line f the particle state.

- Use a renormalized nucleon propagator in the medium

$$G_{FSI}(p) = \frac{1}{p^0 - E(\vec{p}) - \Sigma(p)}$$

- $\Sigma(p)$: Nucleon self-energy in the medium
- Aproximation: $\mathrm{Im}\Sigma_h \simeq 0$ for hole states
- Nucleon self energy taken from P. Fernadez de Cordoba and E. Oset, PRC 46 (1992)

FSI on the LFG model

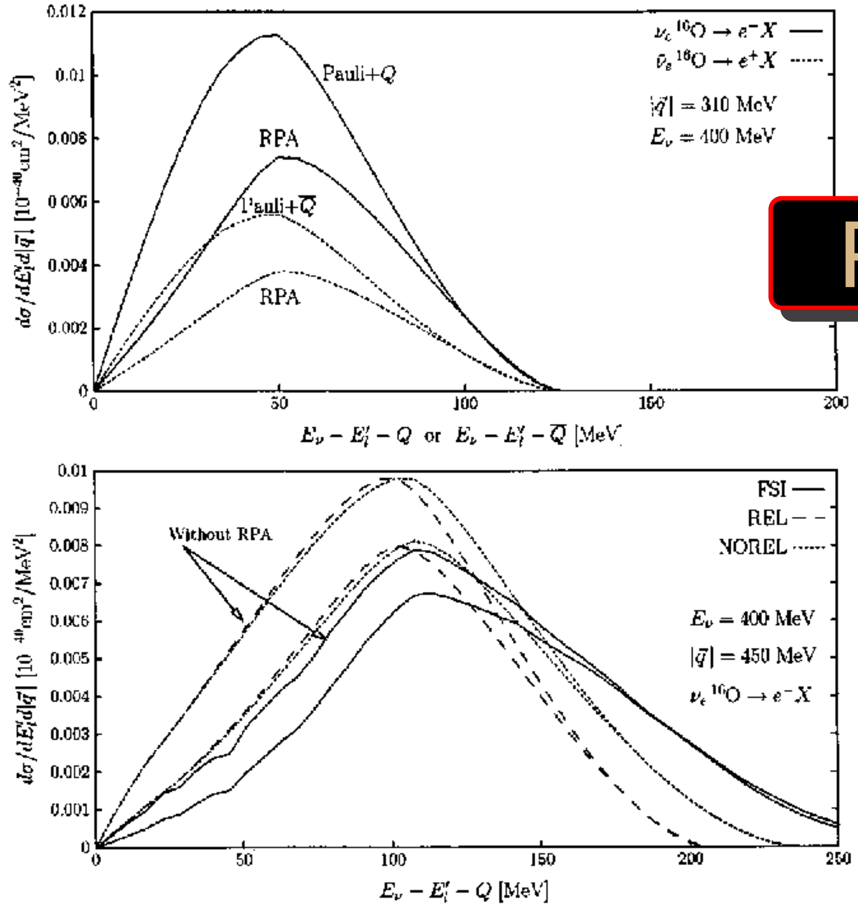

FIG. 13. ν_e and $\bar{\nu}_e$ differential cross sections in ^{16}O as a function of the excitation energy, for fixed values of the momentum transfer and $E_{\nu,\bar{\nu}}$=400 MeV. Top: Results obtained from the full relativistic model without FSI, with (RPA) and without RPA and Coulomb corrections (Pauli+$Q(\bar{Q})$). Bottom: Results obtained by using relativistic (long dashed line, REL) and nonrelativistic nucleon kinematics. In this latter case, we present results with (solid line, FSI) and without (short dashed line, NOREL) FSI effects. For the three cases, we also show the effect of taking into account RPA and Coulomb corrections (lower lines at the peak). The areas (in units of 10^{-40} cm^2/MeV) below the curves are 1.02 (REL), 1.13 (NOREL), and 1.01 (FSI) when RPA and Coulomb corrections are not considered, and 0.79 (REL), 0.90 (NOREL), and 0.85 (FSI) when these nuclear effects are taken into account.

- The FSI is implemented on the non relativistic model
- The RPA correction is less important in presence of FSI

Theoretical uncertainties

Central values and errors of the model input parameters

Form Factors					Nucleon Interaction				
M_D	=	0.843	$\pm$	0.042 GeV	$f_0^{\prime(in)}$	=	0.33	$\pm$	0.03
λ_n	=	5.6	$\pm$	0.6	$f_0^{(\prime ex)}$	=	0.45	$\pm$	0.05
M_A	=	1.05	$\pm$	0.14 GeV	f	=	1.00	$\pm$	0.10
g_A	=	1.26	$\pm$	0.01	f^*	=	2.13	$\pm$	0.21
					Λ_π	=	1200	$\pm$	120 MeV
					C_ρ	=	2.0	$\pm$	0.2
					Λ_ρ	=	2500	$\pm$	250 MeV
					g'	=	0.63	$\pm$	0.06

We have also included 10% uncertainties in both the real part of the nucleon selfenergy and densities

The Montecarlo simulation

- Generate 2000 sets of input parameters
- Gaussian distributions
- Compute the different observables
- Obtain the distribution of the observable values
- Theoretical errors are obtained discarding the highest and lowest 16% of the obtained values
- Keep a 68% confidence level (CL) interval

M. Valverde, Amaro, J. Nieves, Phys. Lett. B 638 (2006)

Uncertainty bands

Integrated inclusive QE cross section uncertainties for the full model, compared to the LFG without nuclear corrections

M. Valverde et al. / Physics Letters B 638 (2006) 325–332

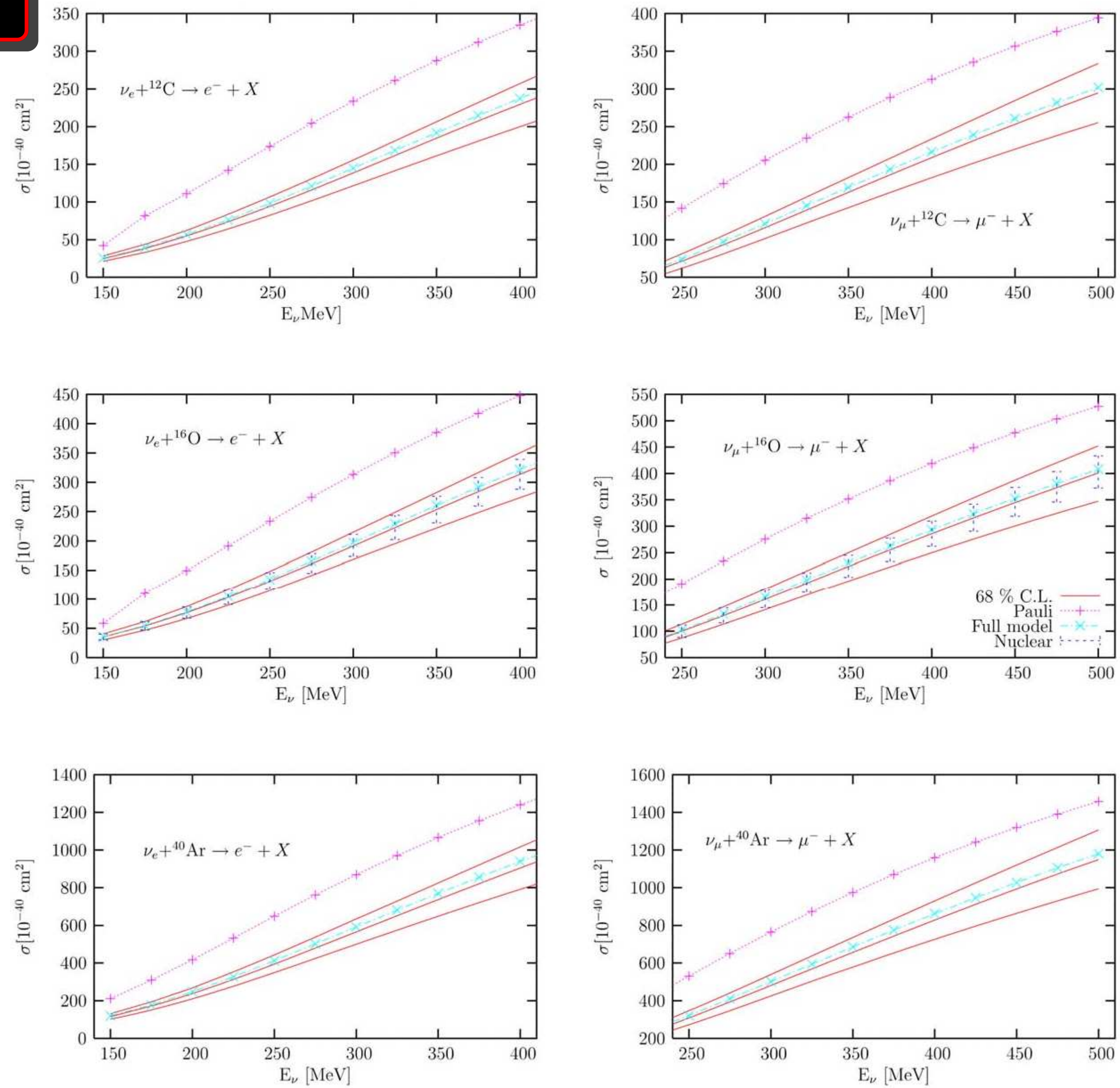

Fig. 1. (Color online.) Electron and muon neutrino inclusive QE integrated cross sections from carbon, oxygen and argon, as a function of the neutrino energy. In all cases non-relativistic nucleon kinematics has been employed. Results denoted as "Full model" are obtained from the full model developed in Ref. [14], while those denoted as "Pauli" have been obtained without including RPA, Coulomb and nucleon self-energy effects. We also give the 68% CL band (red or solid lines). For oxygen, the error bars (denoted as "Nuclear") account for the uncertainties due to the imprecise knowledge of the nucleon densities and of the parameters entering in the model used (Ref. [14]) to compute nuclear effects (RPA and nucleon self-energy).

Uncertainties cancellations on ratios

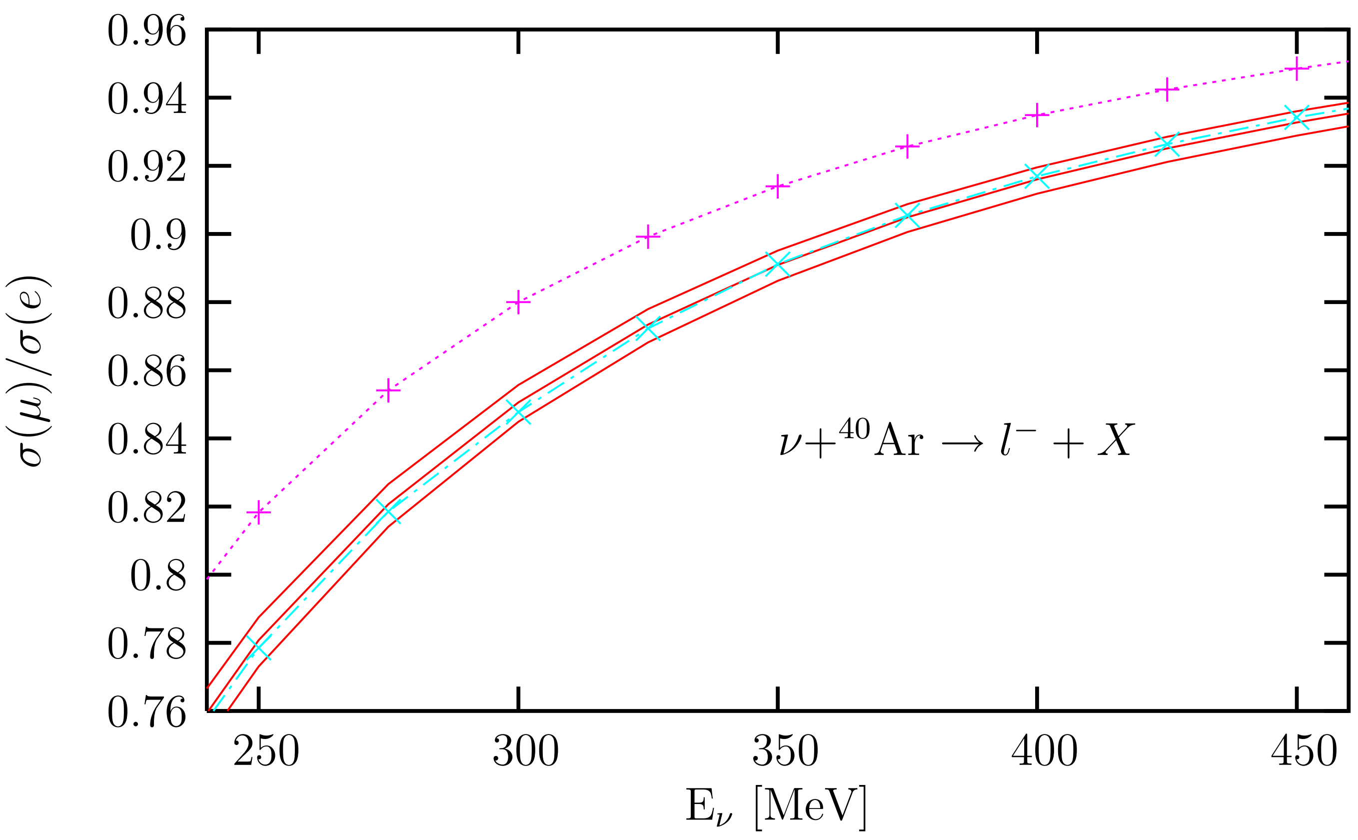

ν_μ/ν_e ratio

$$\frac{\sigma(\mu)}{\sigma(e)} = \frac{\sigma(\nu_\mu, \mu)}{\sigma(\nu_e, e)}$$

- of interest for experiments on atmospheric neutrinos
- Theoretical errors partially cancel out

Polarization observables

Polarization in (ν_τ, τ) reactions

- Of interest for $\nu_\mu \longrightarrow \nu_\tau$ oscillation experiments.
- τ decay particle distribution depend on the τ spin direction
- Theoretical information on the τ polarization will be valuable
- Also needed in $\nu_\mu \longrightarrow \nu_e$ oscillation experiments to disentangle (ν_e, e) events from background electron productions following the $\nu_\mu \longrightarrow \nu_\tau$ oscillation

Polarization vector and asymmetries

Polarized differential cross section in $(\nu_l, \vec{l})$ reactions

Final lepton polarization meassured in the direction $\vec{s}$

$$\Sigma(\vec{s}) \equiv \frac{d^2\sigma}{d\Omega' dE'_l} \boxed{= \frac{1}{2}\Sigma_0 \left(1 + s_\mu P^\mu\right)}$$

- Σ_0: unpolarized cross section
- Lepton polarization vector components P_l (longitudinal), P_t (transverse)
- They can be obtained as asymmetries

$$s_\mu P_\mu = \frac{\Sigma(\vec{s}) - \Sigma(-\vec{s})}{\Sigma(\vec{s}) + \Sigma(-\vec{s})}$$

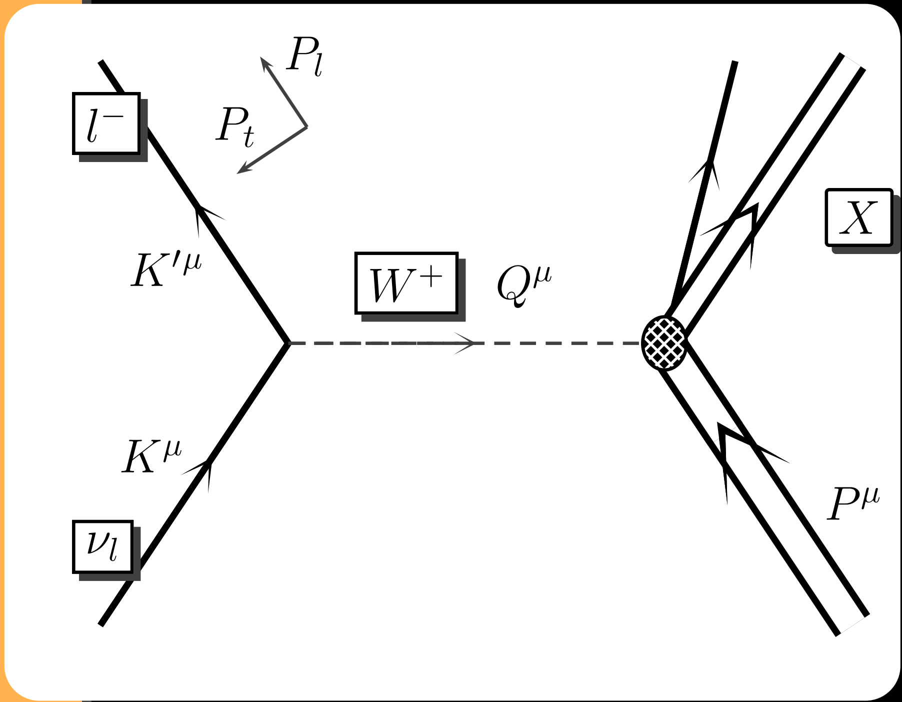

Polarization results

Dotted: LFG
Dashed: RPA
Solid: FSI

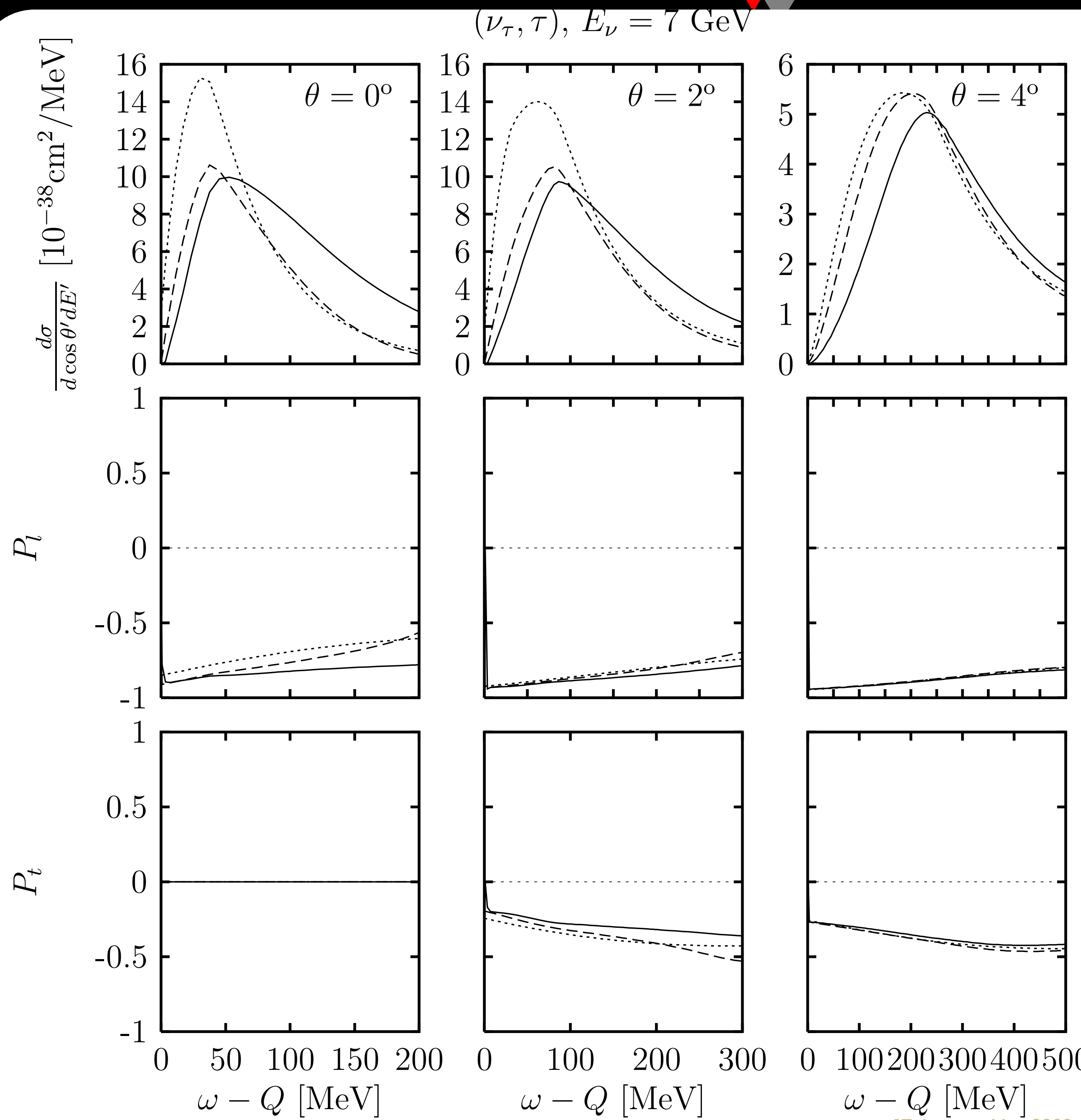

Polarization results

Total polarization and angle

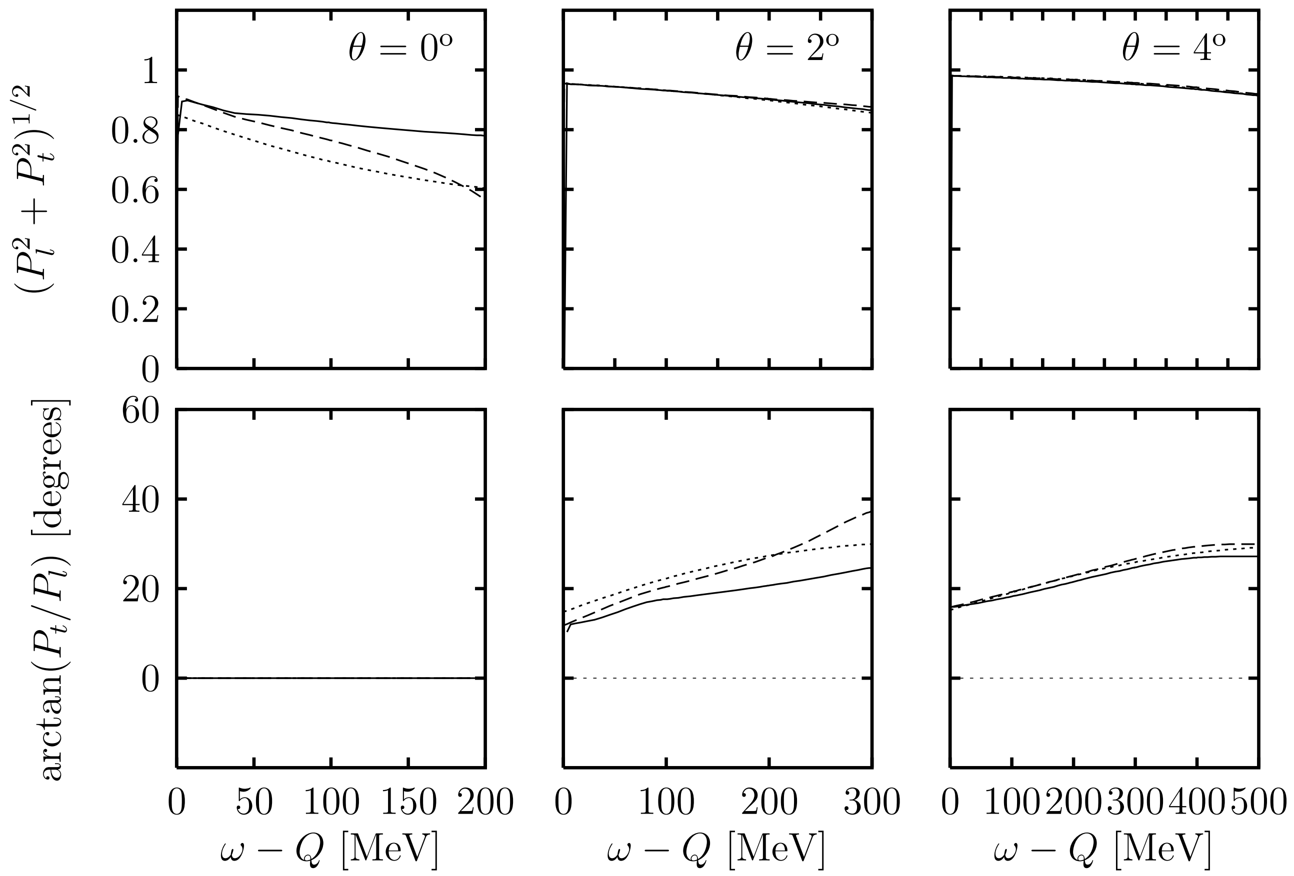

4 Super-Scaling Analysis (SuSA)

Scaling in the RFG (Relativistic Fermi gas)

$$R_K = G_K f_{RFG}(\psi)$$

Functions G_K from the RFG for electrons ($K = L, T$) and neutrinos $K = CC, CL, LL, T, T'$.

Scaling function in the RFG

$$f_{RFG}(\psi) = \frac{3}{4}(1-\psi^2)\theta(1-\psi^2)$$

Scaling variable:

$$\psi = \frac{1}{\sqrt{\xi_F}} \frac{\lambda - \tau}{\sqrt{(1+\lambda)\tau + \kappa\sqrt{\tau(1+\tau)}}}$$

Experimental scaling function from (e, e')

$$f(\psi') = \frac{\left(\frac{d\sigma}{d\Omega' d\epsilon'}\right)_{exp}}{\sigma_{Mott}(v_L G_L + v_T G_T)}$$

shifted $\longrightarrow \psi' = \frac{1}{\sqrt{\xi_F}} \frac{\lambda' - \tau'}{\sqrt{(1+\lambda')\tau' + \kappa\sqrt{\tau'(1+\tau')}}}$

$$\lambda' = (\omega - E_s)/2m_N, \quad \tau' = \kappa^2 - \lambda'^2$$

k_F y E_s are fitted to the data

$f_L = \frac{R_L}{G_L}$ Longitudinal $\qquad f_T = \frac{R_T}{G_T}$ Transverse

Superscaling

- Plot the experimental $f(\psi')$ versus ψ' for different kinematics and nuclei
- Fit E_s and k_F to get scaling (one universal scaling function)

no q dependence → 1st kind scaling

no A dependence → 2nd kind scaling

1st kind scaling + 2nd kind scaling → Superscaling

Scaling in the QE peak

Summary of past work by Donnelly & Sick PRC 60 (1999)

T. W. DONNELLY AND INGO SICK PHYSICAL REVIEW C **60** 065502

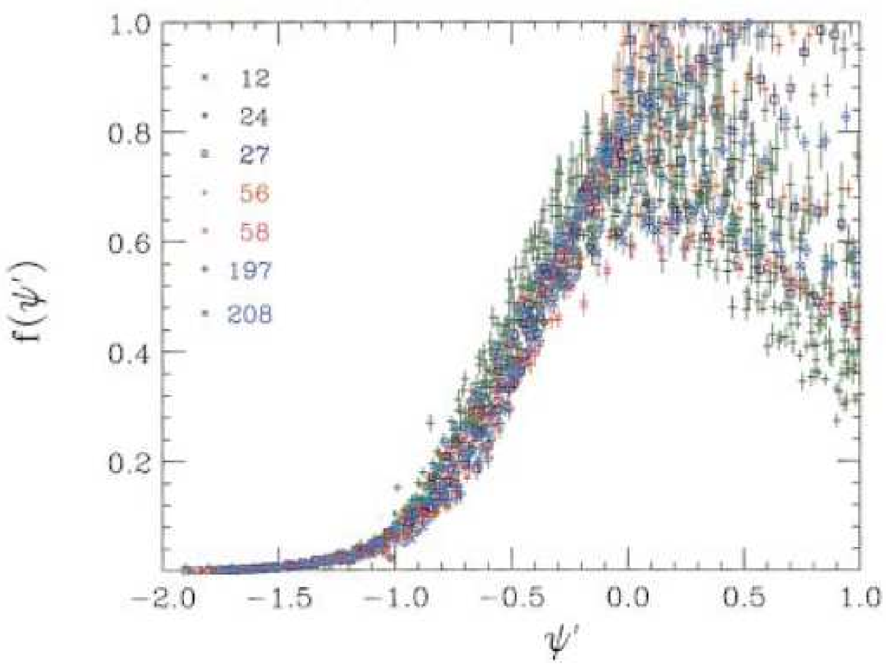

FIG. 2. (Color) Scaling function $f(\psi')$ as function of ψ' for all nuclei $A \geq 12$ and all kinematics. The values of A corresponding to different symbols are shown in the inset.

Scaling in the QE peak

Summary of past work by Donnelly & Sick PRC 60 (1999)

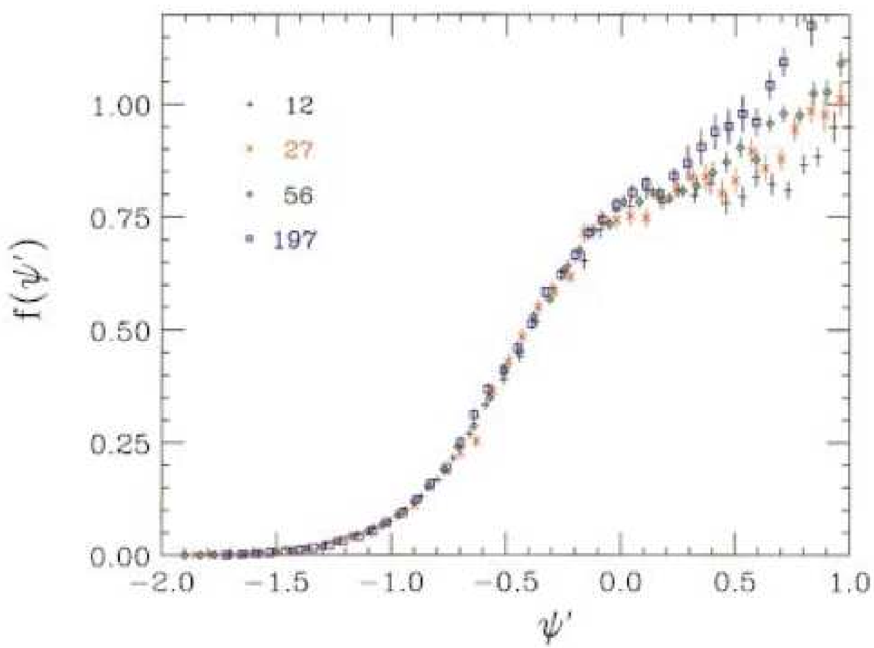

FIG. 3. (Color) Scaling function for C, Al, Fe, and Au and fixed kinematics ($q \approx 1000$ MeV/c).

065502-6

Scaling in the QE peak

Summary of past work by Donnelly & Sick PRC 60 (1999)

SUPERSCALING OF INCLUSIVE ELECTRON . . . PHYSICAL REVIEW C **60** 065502

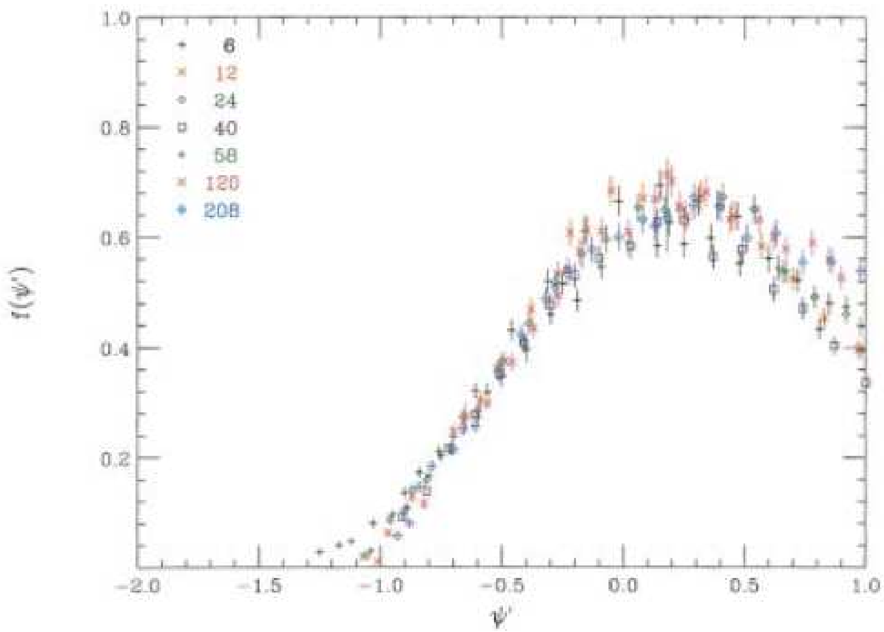

FIG. 4. (Color) Scaling function for Li, C, Mg, Ca, Ni, Sn, and Pb and fixed kinematics ($q \approx 460$ MeV/c).

Scaling in the QE peak

Summary of past work by Donnelly & Sick PRC 60 (1999)

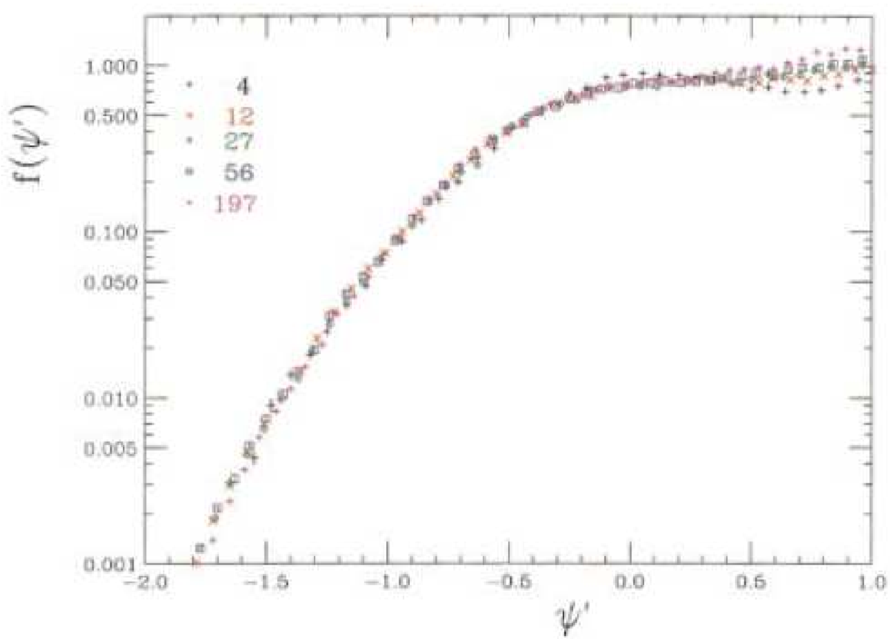

FIG. 5. (Color) Scaling function for nuclei $A = 4-197$ and fixed kinematics ($q \approx 1000$ MeV/c) on a logarithmic scale.

065502-7

Scaling in the QE peak

Summary of past work by Donnelly & Sick PRC 60 (1999)

T. W. DONNELLY AND INGO SICK — PHYSICAL REVIEW C **60** 065502

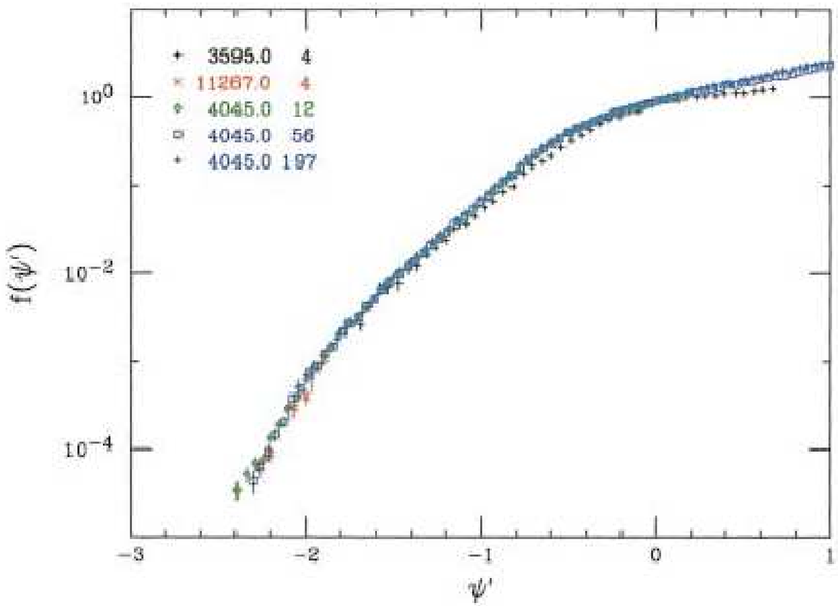

FIG. 6. (Color) Scaling function for nuclei $A = 4-197$ at $q \approx 1650$ MeV/c. The 4.405 GeV data have been taken at 23° scattering angle, the ^{4}He data at 25° and 8°.

Scaling in the QE peak

Summary of past work by Donnelly & Sick PRC 60 (1999)

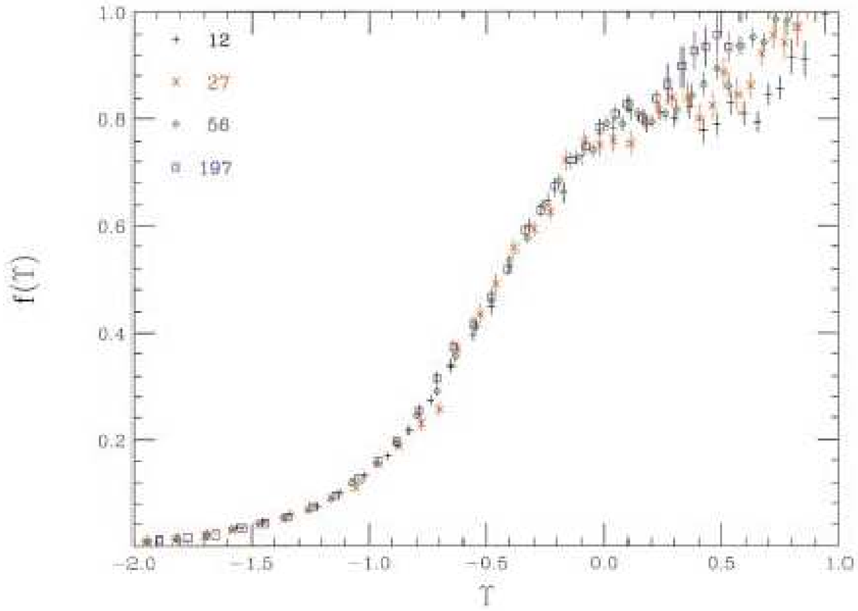

FIG. 7. (Color) Scaling function $f(\Upsilon)$ for nuclei $A = 12–197$ at 3.6 GeV energy and 16° scattering angle as a function of the scaling variable Υ.

065502-8

Scaling in the QE peak

Summary of past work by Donnelly & Sick PRC 60 (1999)

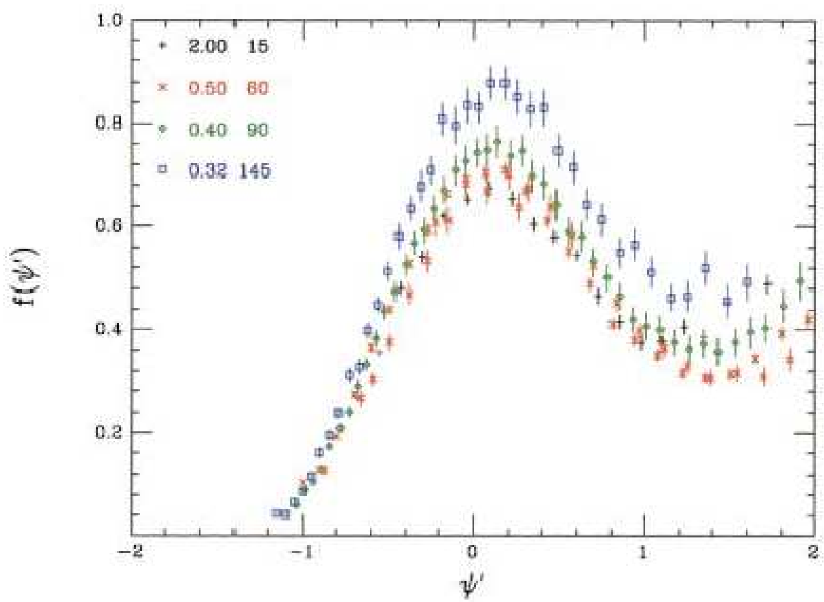

FIG. 8. (Color) Scaling function for ^{12}C at approximately constant $q \approx 500$ MeV/c, but varying angle. The energies (in GeV) and angles (in degrees) of the different data sets are identified in the plot.

Scaling in the QE peak

Summary of past work by Donnelly & Sick PRC 60 (1999)

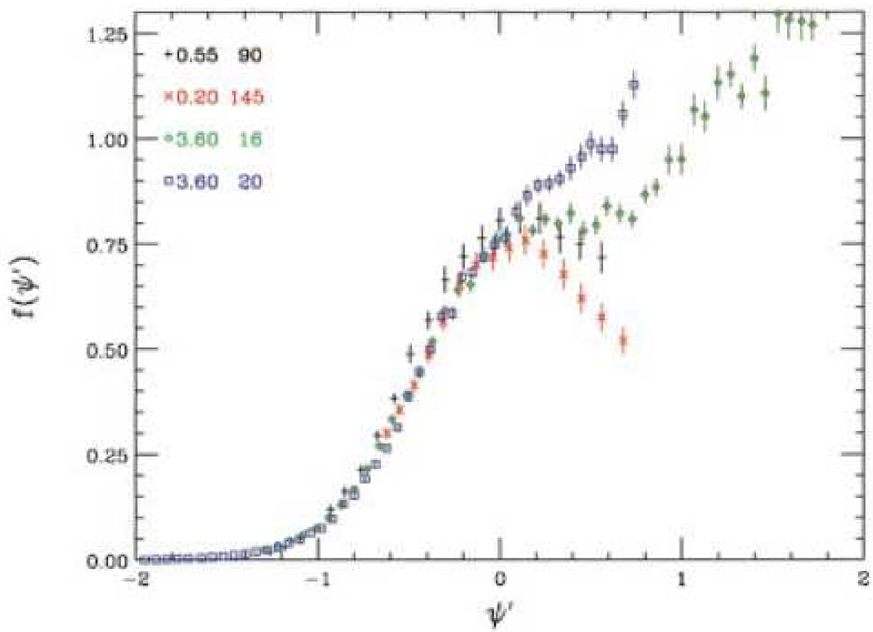

FIG. 9. (Color) Scaling function for ^{12}C and roughly constant ratio of the longitudinal and transverse *e-p* elastic cross section, as a function of the momentum transfer *q*.

Scaling in the QE peak

Summary of past work by Donnelly & Sick PRC 60 (1999)

SUPERSCALING OF INCLUSIVE ELECTRON . . . PHYSICAL REVIEW C **60** 065502

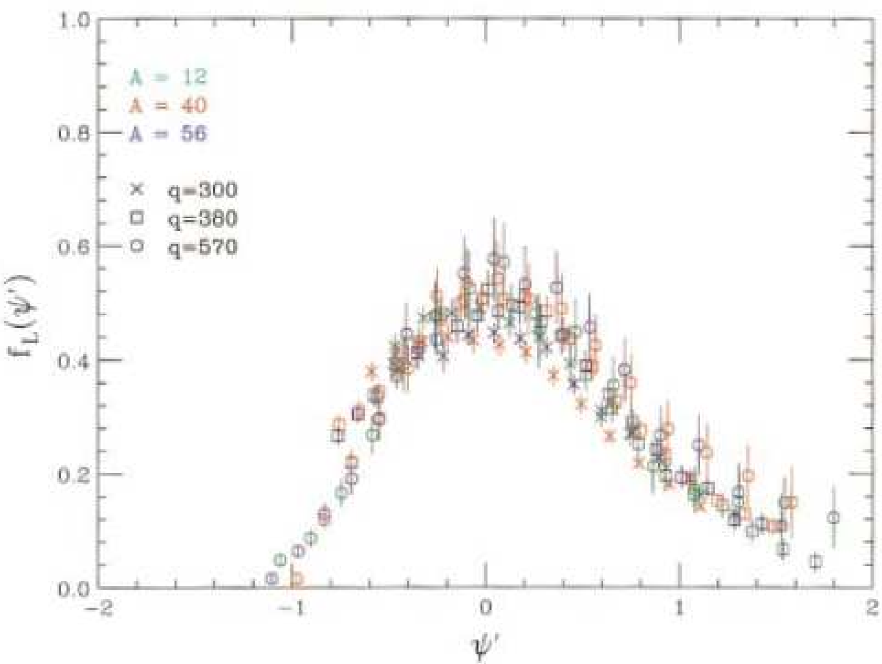

FIG. 10. (Color) Scaling function $f_L(\psi')$ from the longitudinal response.

Scaling in the QE peak

Summary of past work by Donnelly & Sick PRC 60 (1999)

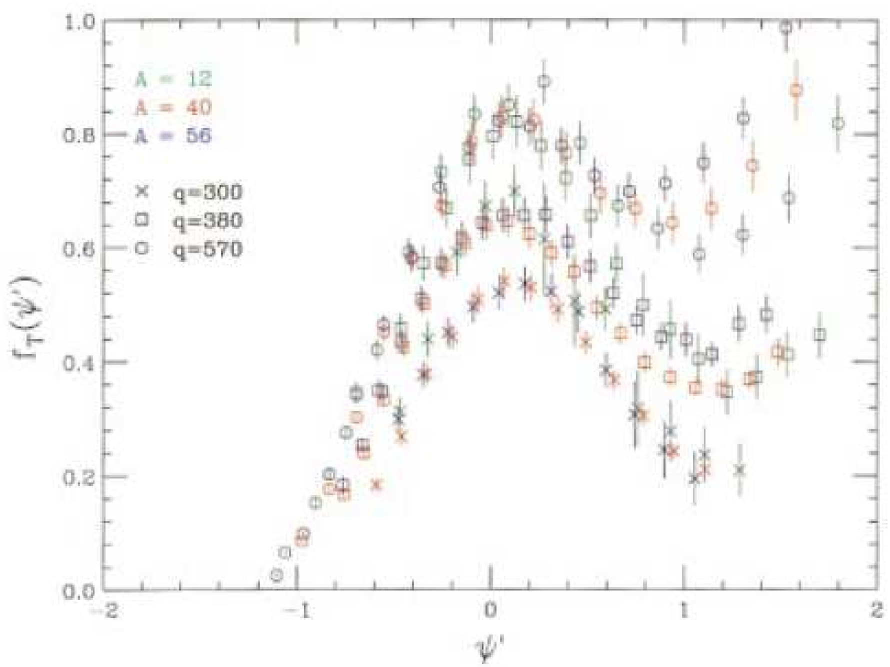

FIG. 11. (Color) Scaling function $f_T(\psi')$ from the transverse response.

Scaling properties of data

- Good 1st-kind scaling below the QE peak (scaling region)

Scaling properties of data

- Good 1st-kind scaling below the QE peak (scaling region)
- Above the peak the scaling is broken (Δ region)

Scaling properties of data

- Good 1st-kind scaling below the QE peak (scaling region)
- Above the peak the scaling is broken (Δ region)
- Scaling of the 2nd-kind works well in the scaling region

Scaling properties of data

- Good 1st-kind scaling below the QE peak (scaling region)
- Above the peak the scaling is broken (Δ region)
- Scaling of the 2nd-kind works well in the scaling region
- The longitudinal response appears to superscale

Scaling properties of data

- Good 1st-kind scaling below the QE peak (scaling region)
- Above the peak the scaling is broken (Δ region)
- Scaling of the 2nd-kind works well in the scaling region
- The longitudinal response appears to superscale
- Scaling violations reside in the transverse response,

Fit in the Quasi-elastic peak

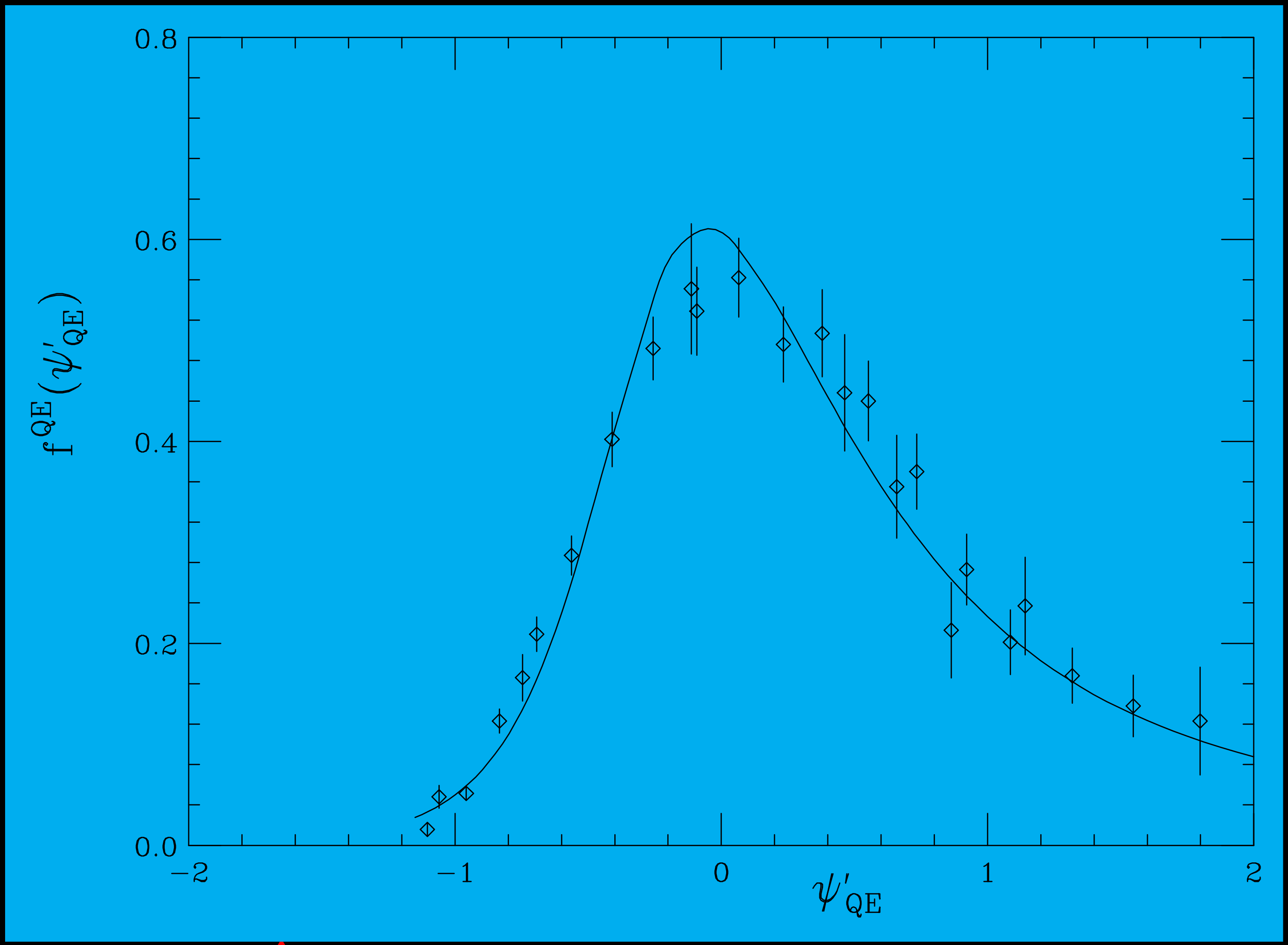

Fit in the Quasi-elastic peak

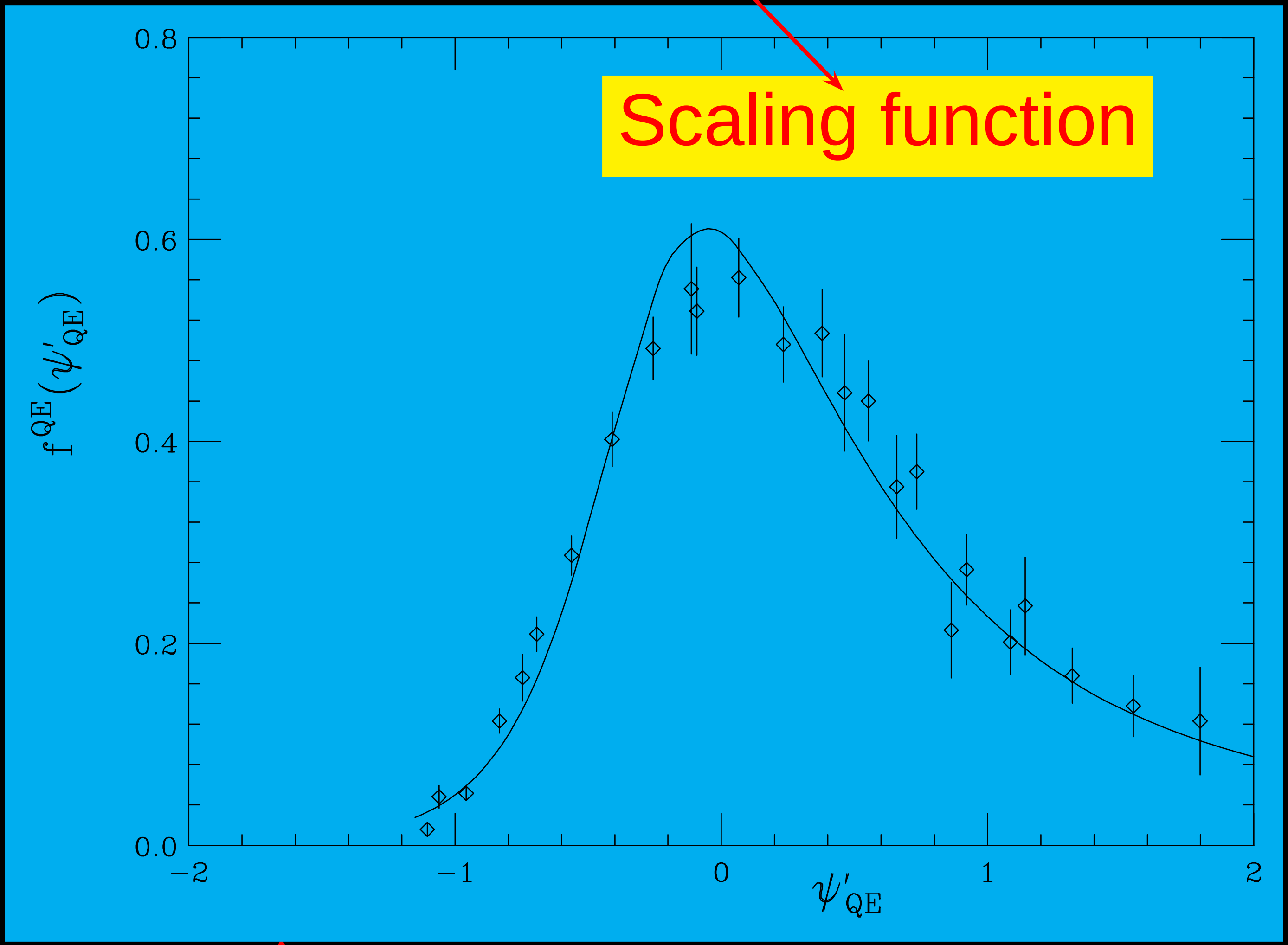

Fit in the Quasi-elastic peak

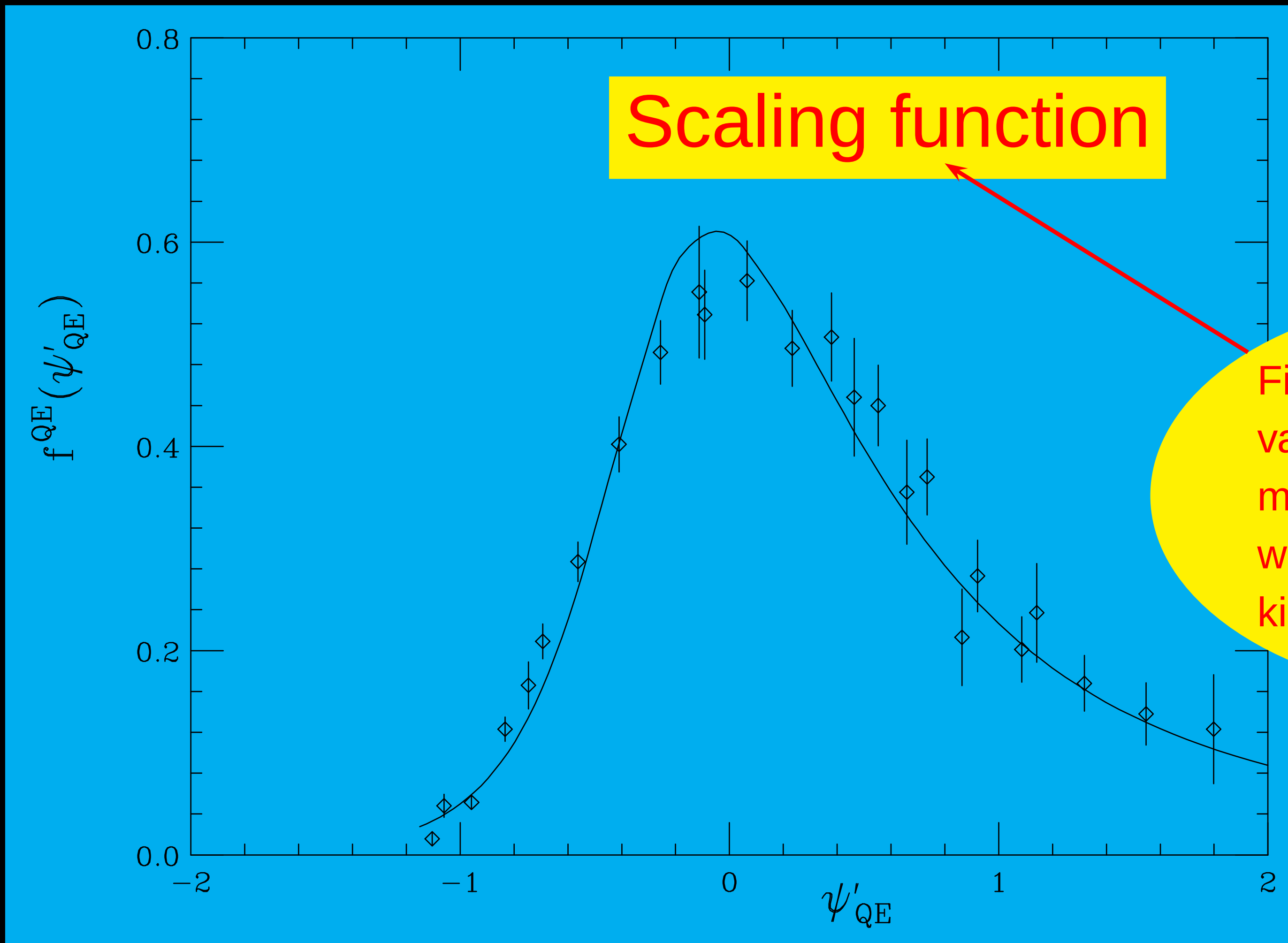

Fitted to the set of f_L values for the higher momentum transfer where scaling of the first kind is seen to occur

SuSA (Super Scaling Analysis)

- Using the experimental (e, e') scaling function to predict neutrino cross sections

NUINT 09

SuSA (Super Scaling Analysis)

- Using the experimental (e, e') scaling function to predict neutrino cross sections
- Use the RFG equations to compute the (ν_l, l^-) response functions with the substitution $f_{RFG}(\psi) \longrightarrow f_{exp}(\psi)$

SuSA (Super Scaling Analysis)

- Using the experimental (e, e') scaling function to predict neutrino cross sections
- Use the RFG equations to compute the (ν_l, l^-) response functions with the substitution $f_{RFG}(\psi) \longrightarrow f_{exp}(\psi)$
- Needed to justify theoretically the validity of SuSA

The semirelativistic shell model

- Study the scaling properties in realistic models

The semirelativistic shell model

- Study the scaling properties in realistic models
- Estimate the validity range of SuSA

The semirelativistic shell model

- Study the scaling properties in realistic models
- Estimate the validity range of SuSA
- Include relativistic effects in the model

The semirelativistic shell model

- Study the scaling properties in realistic models
- Estimate the validity range of SuSA
- Include relativistic effects in the model
- Compare with the experimental scaling function

The continuum shell-model (CSM)

- Closed-shell nuclei ^{12}C, ^{16}O and ^{40}Ca,
- Initial state $|i\rangle$: Slater determinant with all shells occupied.
- Impulse approximation: final states are particle-hole excitations coupled to total angular momentum

$$|f\rangle = |(ph^{-1})J\rangle$$

- Single hole wave function $|h\rangle = |\epsilon_h l_h j_h\rangle$
- Single particle wave function $|p\rangle = |\epsilon_p l_p j_p\rangle$
- Obtained by solving the Schrödinger equation

Woods-Saxon potential

$$V(r) = -V_0 f(r,R_0,a_0) + \frac{V_{ls}}{m_\pi^2 r}\frac{df(r,R_0,a_0)}{dr}\mathbf{l}\cdot\boldsymbol{\sigma} + V_C(r)$$

$$f(r,R,a) = \frac{1}{1+e^{(r-R)/a}}$$

$V_C(r)$: Coulomb potential.

	V_0^p	V_{LS}^p	V_0^n	V_{LS}^n	r_0	a_0
^{12}C	62.0	3.20	60.00	3.15	1.25	0.57
^{16}O	52.5	7.00	52.50	6.54	1.27	0.53
^{40}Ca	57.5	11.11	55.00	8.50	1.20	0.53

The SR approach

A **Expand the relativistic single-nucleon current**

$$j^\mu(\vec{p}',\vec{p}) = \overline{u}(\vec{p}')\Gamma^\mu(Q)u(\vec{p})$$

in powers of $\vec{\eta} = \vec{p}/m_N$. to first order $O(\eta)$

Not expand in $\vec{p}'/m_N$.

$\Longrightarrow q,\omega$ can be large

Relativistic kinematics

B

USE RELATIVISTIC KINEMATICS.

- The energy transfer is the difference between the (non-relativistic) single-particle energies of particle and hole $\omega = \epsilon_p - \epsilon_h$.
- The relativistic kinematics are taken into account by the substitution

$$\epsilon_p \longrightarrow \epsilon_p(1 + \epsilon_p/2m_N)$$

as the eigenvalue of the Schrödinger equation for the particle

The SR vector current

$$
\begin{aligned}
J_V^0 &= \xi_0 + i\xi_0'(\boldsymbol{\kappa} \times \boldsymbol{\eta}) \cdot \boldsymbol{\sigma} \\
\mathbf{J}_V^{\perp} &= \xi_1 \boldsymbol{\eta}^{\perp} + i\xi_1' \boldsymbol{\sigma} \times \boldsymbol{\kappa} \,,
\end{aligned}
$$

(q,ω)-dependent factors:

$$
\xi_0 = \frac{\kappa}{\sqrt{\tau}} 2G_E^V \quad , \quad \xi_0' = \frac{2G_M^V - G_E^V}{\sqrt{1+\tau}}
$$

$$
\xi_1' = 2G_M^V \frac{\sqrt{\tau}}{\kappa} \quad , \quad \xi_1 = 2G_E^V \frac{\sqrt{\tau}}{\kappa}
$$

provide the required relativistic behavior.

The longitudinal component is given from vector current conservation, $J_V^3 = \frac{\lambda}{\kappa} J_V^0$.

The SR axial-vector current

$$\mathbf{J}_A^\perp = \zeta_1' \boldsymbol{\sigma}^\perp, \quad \zeta_1' = \sqrt{1+\tau} G_A \ .$$

Transverse

Neglect the terms of order $O(\eta)$

$$\begin{aligned} J_A^0 &= \zeta_0' \boldsymbol{\kappa} \cdot \boldsymbol{\sigma} + \zeta_0'' \boldsymbol{\eta}^\perp \cdot \boldsymbol{\sigma} \\ J_A^z &= \zeta_3' \boldsymbol{\kappa} \cdot \boldsymbol{\sigma} + \zeta_3'' \boldsymbol{\eta}^\perp \cdot \boldsymbol{\sigma} \ , \end{aligned}$$

Time component

Longitudinal component

The SR axial-vector current

$$\mathbf{J}_A^{\perp} = \zeta_1' \boldsymbol{\sigma}^{\perp}, \quad \zeta_1' = \sqrt{1+\tau} G_A \,.$$

Transverse

Neglect the terms of order $O(\eta)$

$$\begin{aligned} J_A^0 &= \zeta_0' \boldsymbol{\kappa} \cdot \boldsymbol{\sigma} + \zeta_0'' \boldsymbol{\eta}^{\perp} \cdot \boldsymbol{\sigma} \\ J_A^z &= \zeta_3' \boldsymbol{\kappa} \cdot \boldsymbol{\sigma} + \zeta_3'' \boldsymbol{\eta}^{\perp} \cdot \boldsymbol{\sigma} \,, \end{aligned}$$

Time component

Longitudinal component

$$\zeta_0' = \frac{1}{\sqrt{\tau}} \frac{\lambda}{\kappa} G_A' \quad , \quad \zeta_0'' = \frac{\kappa}{\sqrt{\tau}} \left[G_A - \frac{\lambda^2}{\kappa^2 + \kappa\sqrt{\tau(\tau+1)}} G_A' \right]$$

$$\zeta_3' = \frac{1}{\sqrt{\tau}} G_A' \quad , \quad \zeta_3'' = \frac{\lambda}{\sqrt{\tau}} \left[G_A - \frac{\kappa}{\kappa + \sqrt{\tau(\tau+1)}} G_A' \right]$$

$G_A' = G_A - \tau G_P$ small due to cancellations

The $O(\eta)$ term, proportional to $\vec{\eta}^{\perp} \cdot \vec{\sigma}$ is dominant

Test of the SR approach: V responses

^{2}C

$k_F = 220$ MeV/c

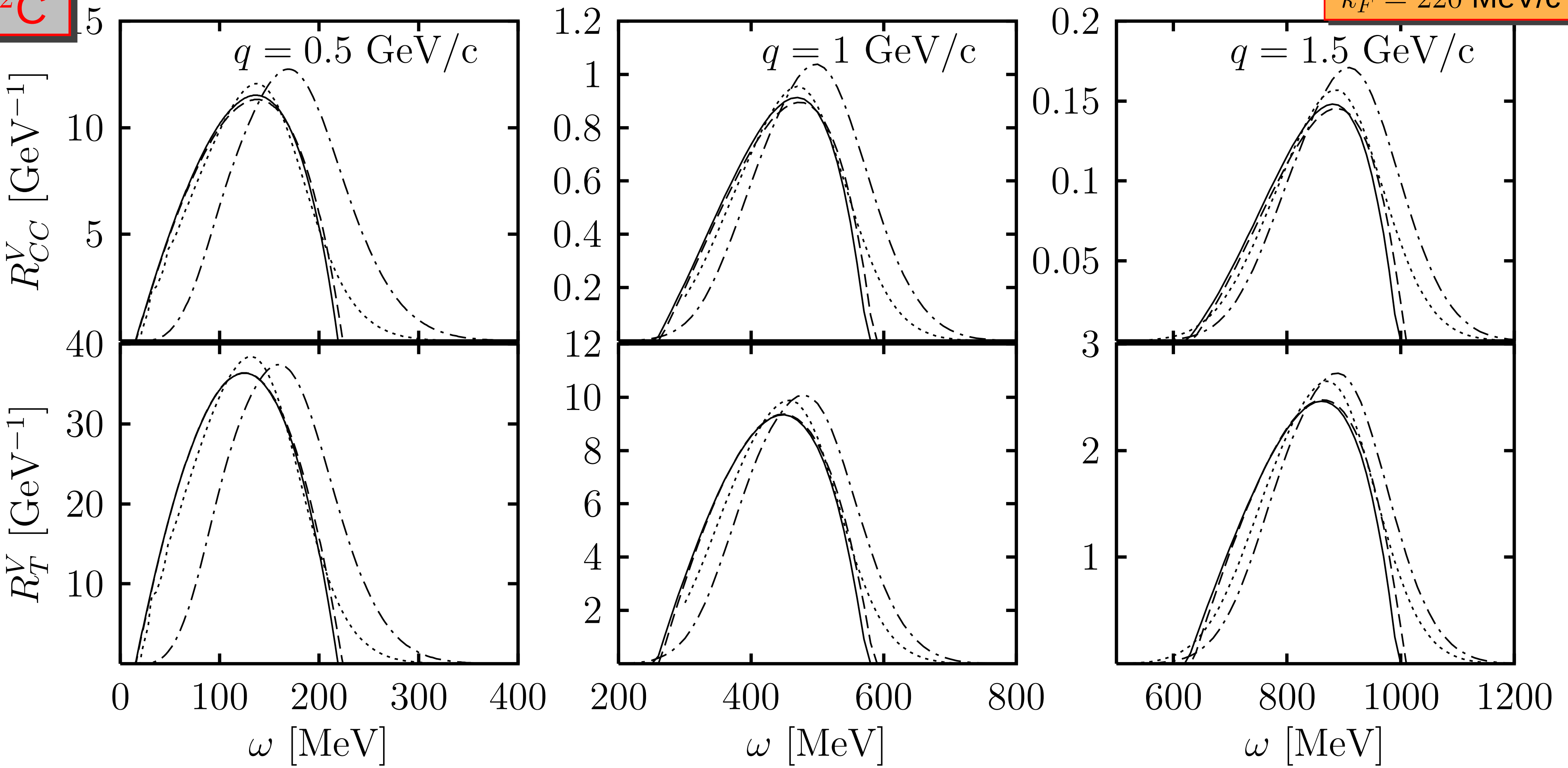

Solid lines: RFG   Dashed lines: SRFG

Dotted: CSM   Dot-dashed: PWIA.

A responses

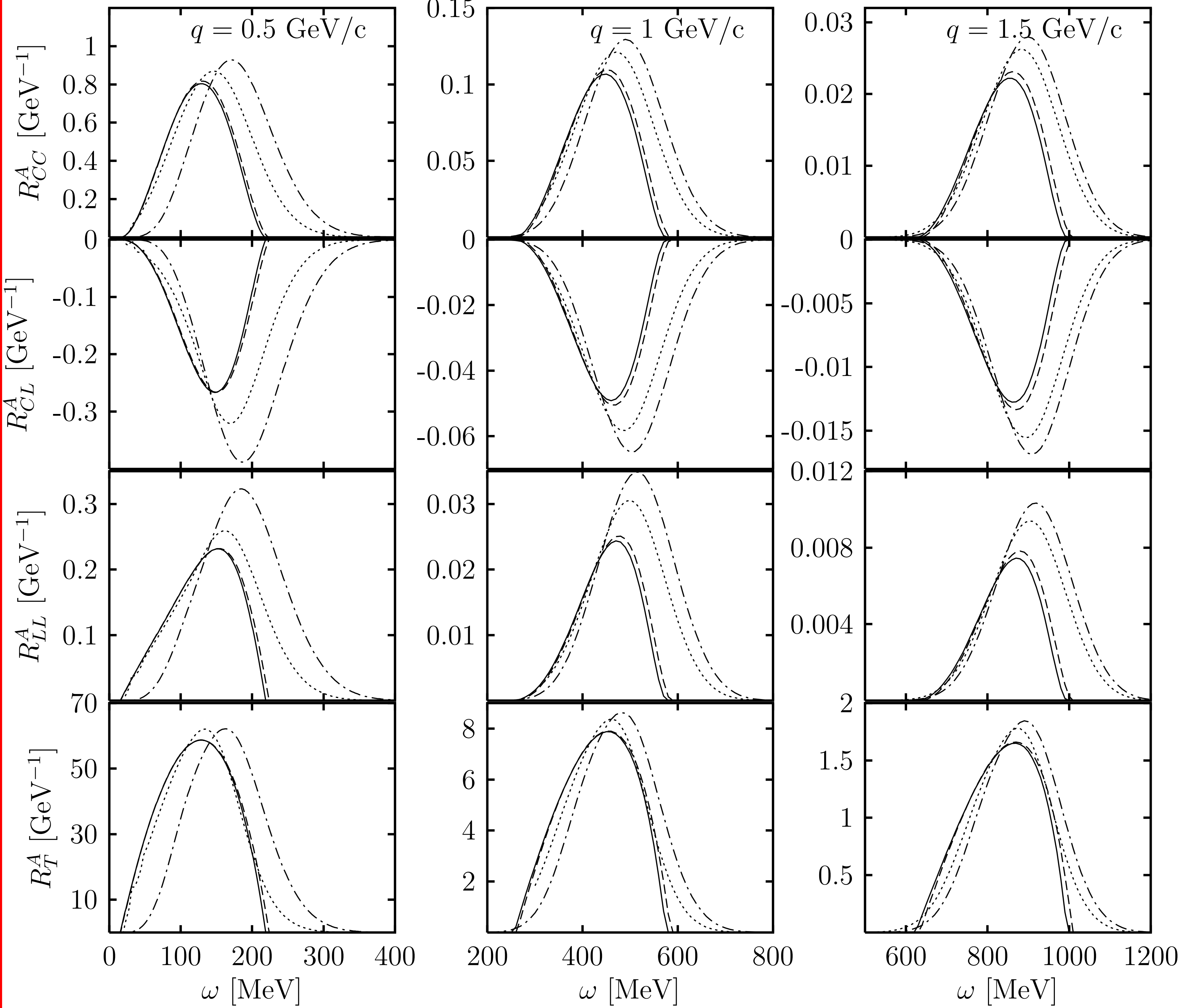

$q = 0.5$ GeV/c
$q = 1$ GeV/c
$q = 1.5$ GeV/c
R^A_{CC} [GeV^{-1}]
R^A_{CL} [GeV^{-1}]
R^A_{LL} [GeV^{-1}]
R^A_T [GeV^{-1}]
ω [MeV]
ω [MeV]
ω [MeV]

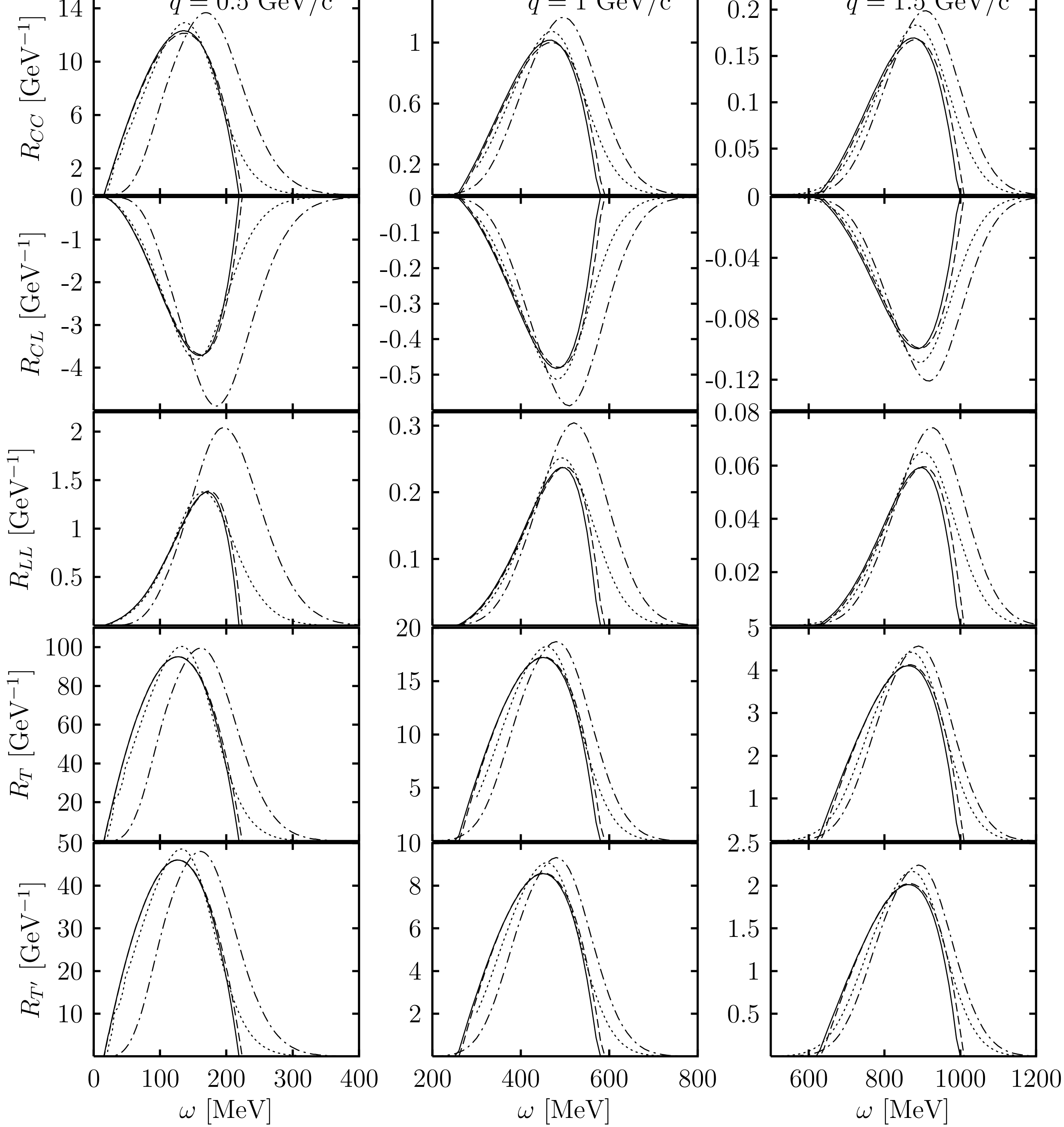

Total responses

$^{12}\mathrm{C}(\nu_\mu, \mu^-)$

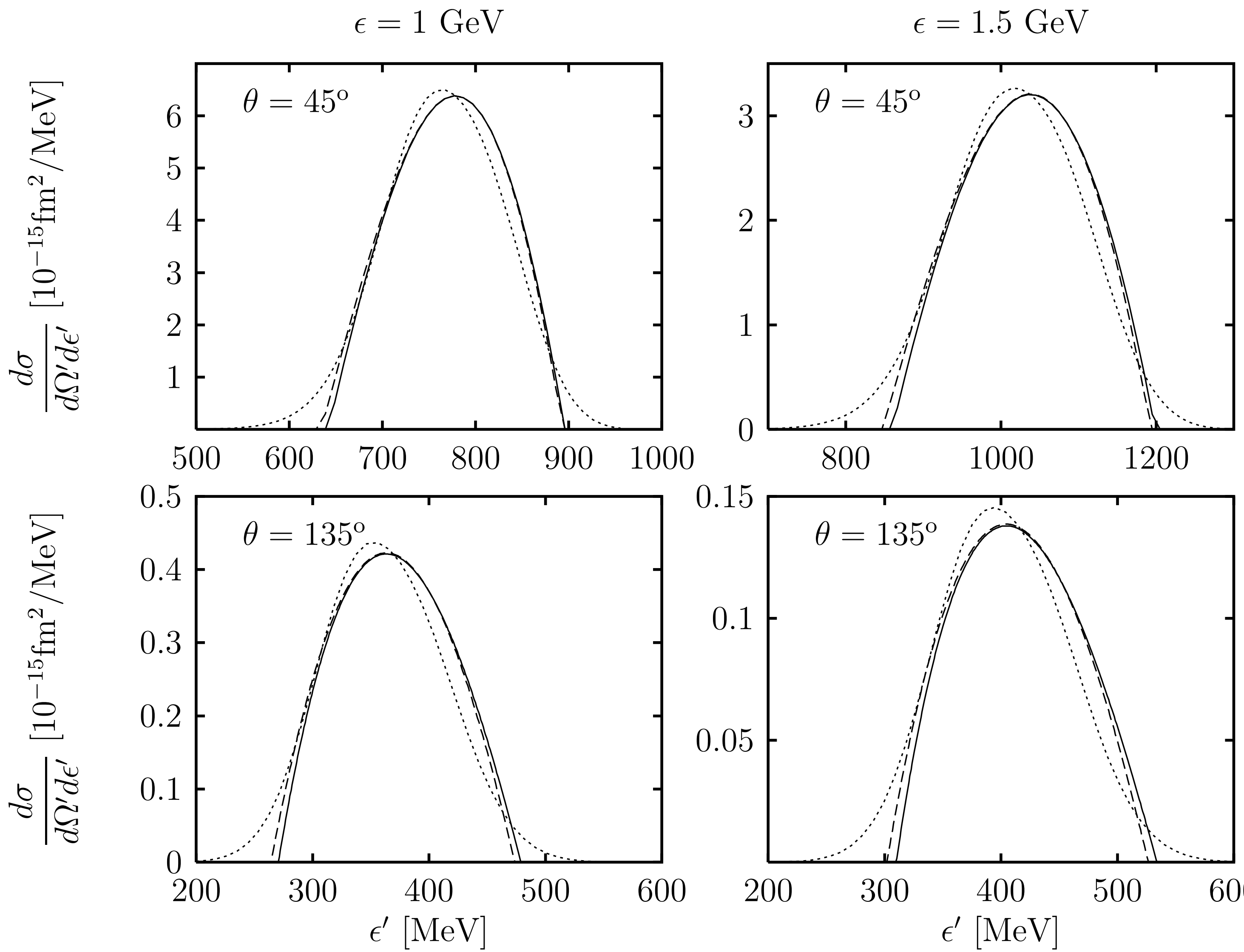

Scaling of the first kind

Scaling of the first ki

Curves for
$q = 0.5, 0.7, 1, 1.3, 1.5$ GeV
collapse into one

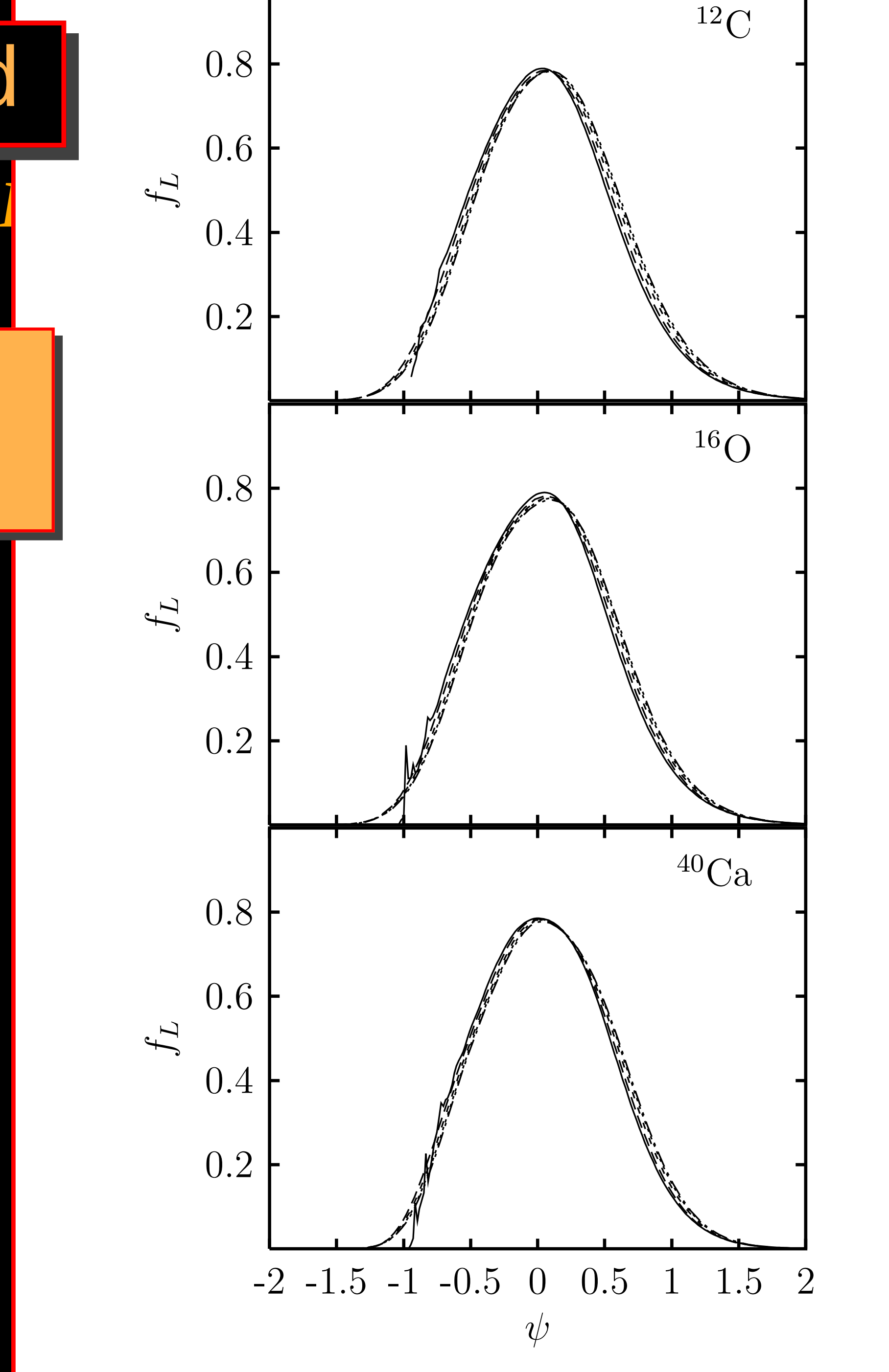

Scaling of the second kind

Curves for
^{12}C, ^{16}O and ^{40}Ca
collapse into one

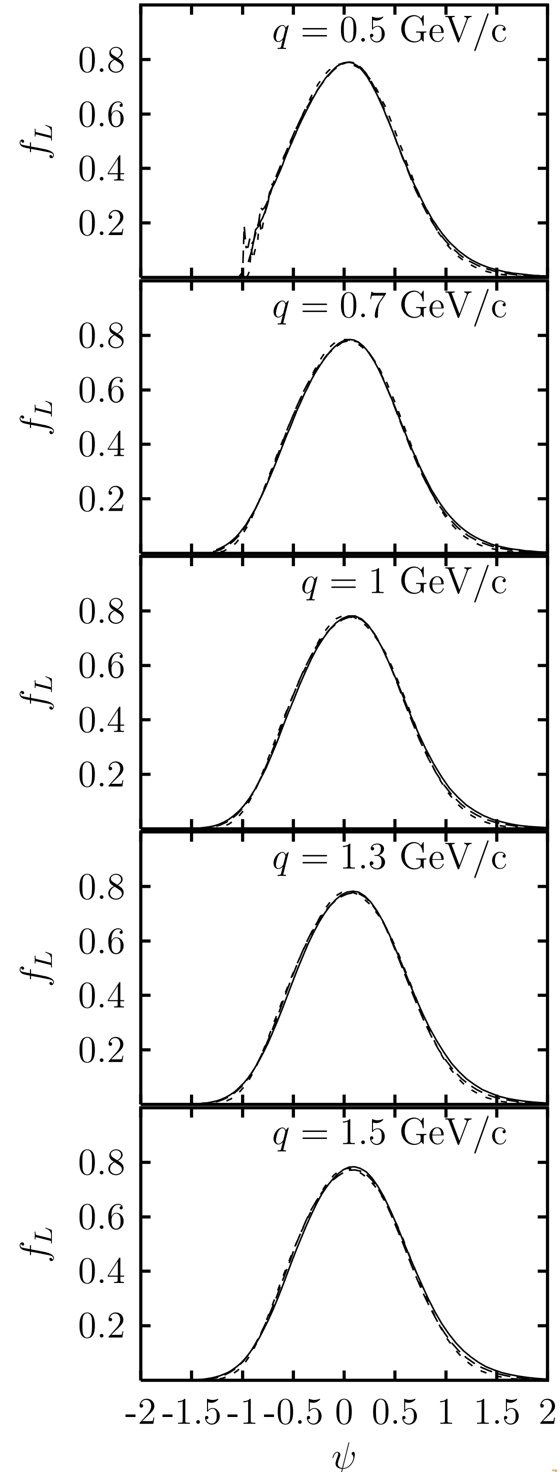

Superscaling

Scaling of the first kind

+ Scaling of the second kind

= Superscaling
in the CSM

Improvement of the FSI

C

DEB+D potential (Dirac-equation-based plus Darwin term) in the final state:

- Rewrite Dirac eqution as a second-order equation for the up component $\psi_{up}(\vec{r})$
- Darwin term: $\psi_{up}(\vec{r}) = K(r,E)\phi(\vec{r})$
- The function $\phi(\vec{r})$ verifies the Schrödinger equation

$$\left[-\frac{1}{2m_N}\nabla^2 + U_{DEB}(r,E)\right]\phi(\vec{r}) = \frac{E^2 - m_N^2}{2m_N}\phi(\vec{r})$$

- Both the DEB potential $U_{DEB}(r,E)$ and Darwin term $K(r,E)$ are energy-dependent

DEB+D FSI effect

Dotted: SR Woods-Saxon
Solid: SR DEB+D
Dashed: RMF

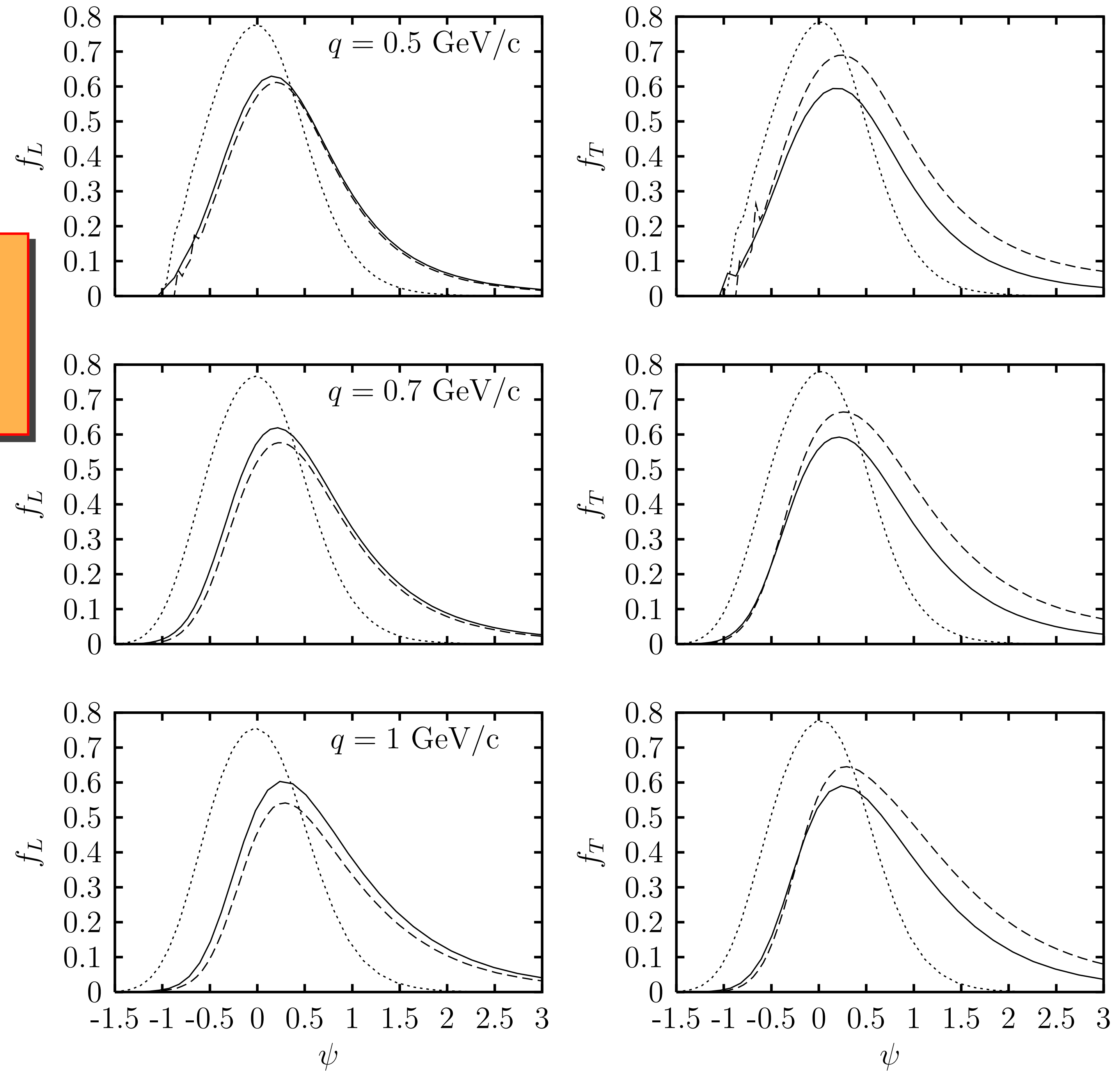

Scaling of 1st kind DEB+D

$q = 0.5$, 0.7
1.0, 1.3
and 1.5 GEV/c

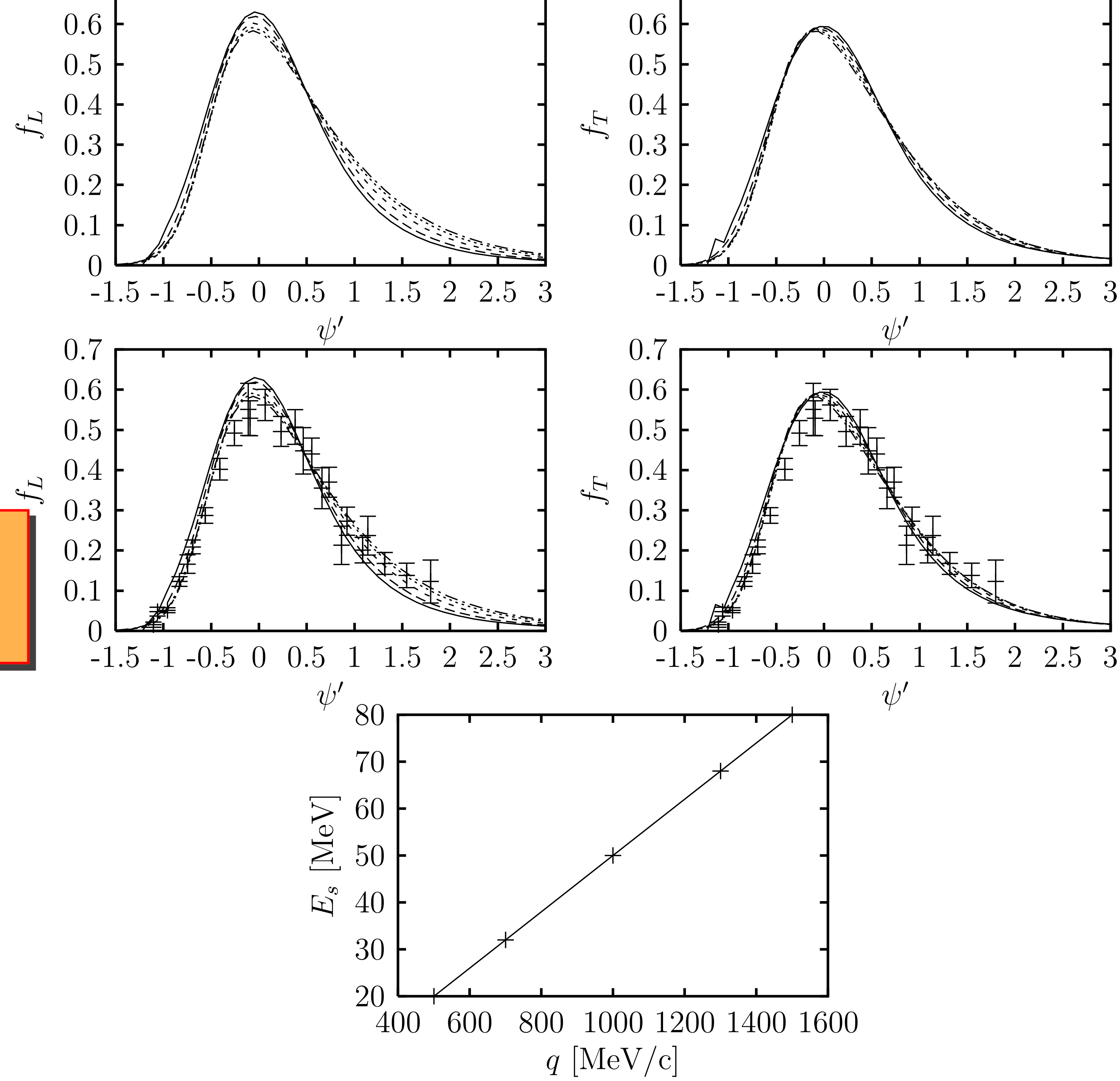

CC neutrino reactions

- SuSA reconstruction of the (ν_μ, μ^-) cross section from the (e, e') one
- Test of the SuSA in the CSM
- The CSM electromagnetic scaling function is used to compute neutrino cross sections.
- Compare with the exact CSM result

$^{12}\mathrm{C}(\nu_\mu, \mu^-)$

$\epsilon = 1$ GeV

Dotted: Woods-Saxon
Solid: DEB+D
Dashed: SuSA

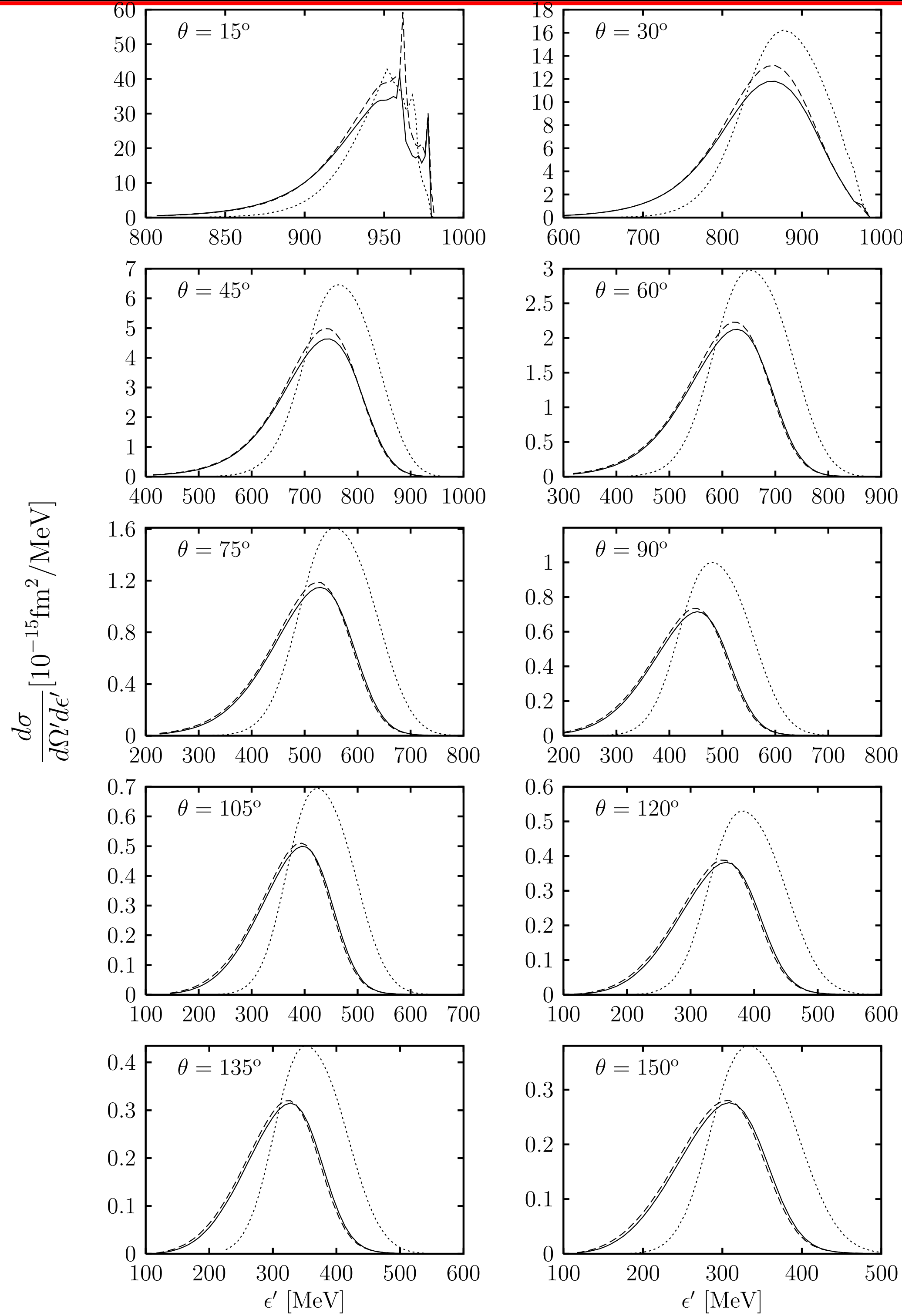

Scaling violation for low q

Scaling violation for low q

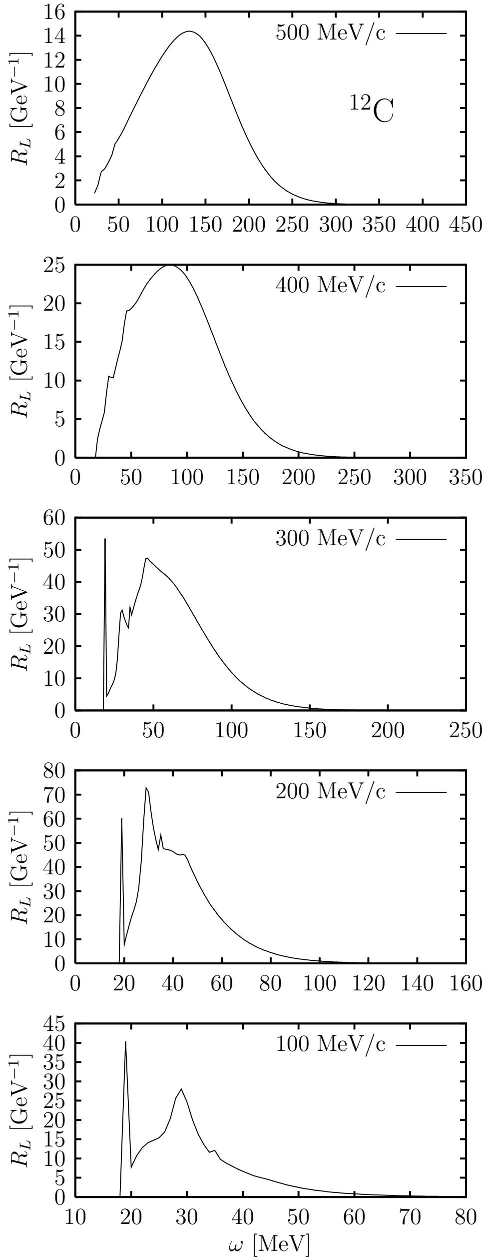

Scaling violation for low q

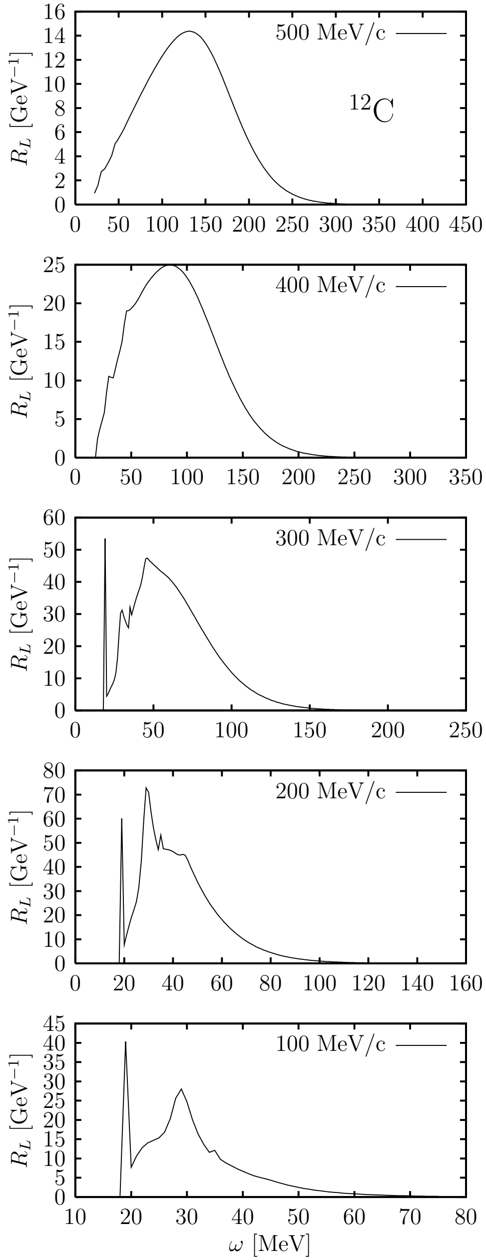

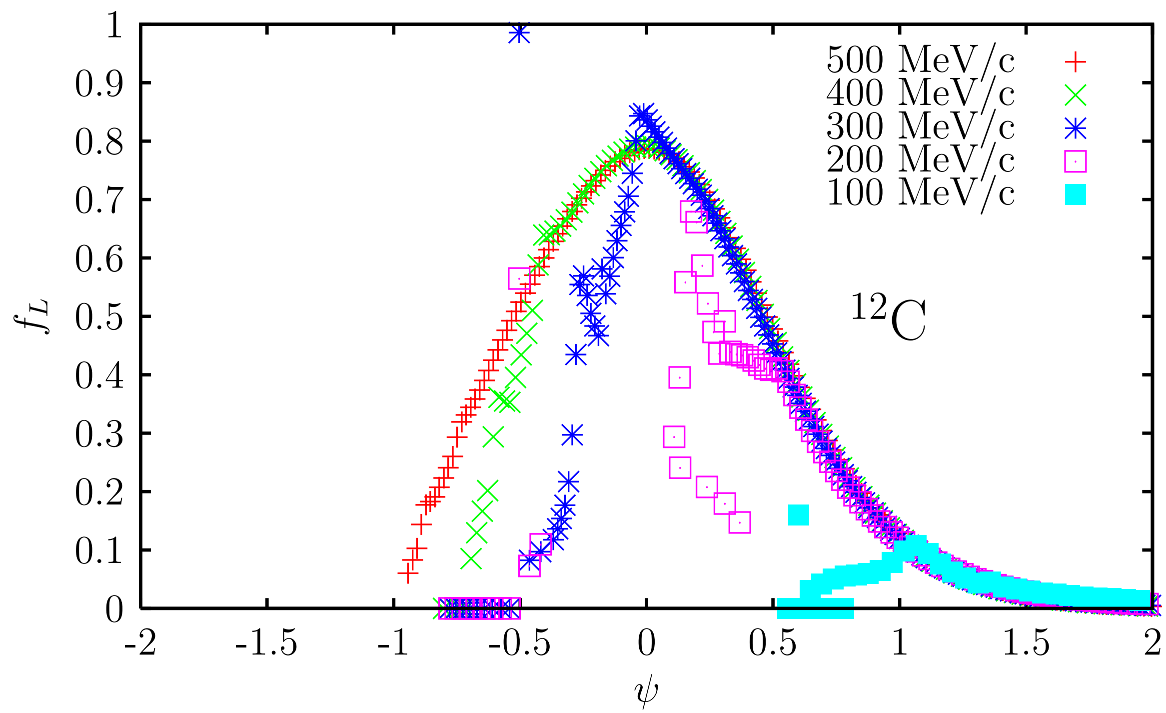

5 *The Relativistic Mean Field (RMF)*

- Solve the exact relativistic Dirac equation for the initial and final nucleons
- Use the exact relativistic V and A current operators
- Describe the bound nucleon states as self-consistent Dirac-Hartree solutions using a lagrangian containing σ, ω and ρ mesons
- Use the same relativistic Diract-Hartree potential for the final states (FSI)

(ν_μ, μ^-) results with the RMF

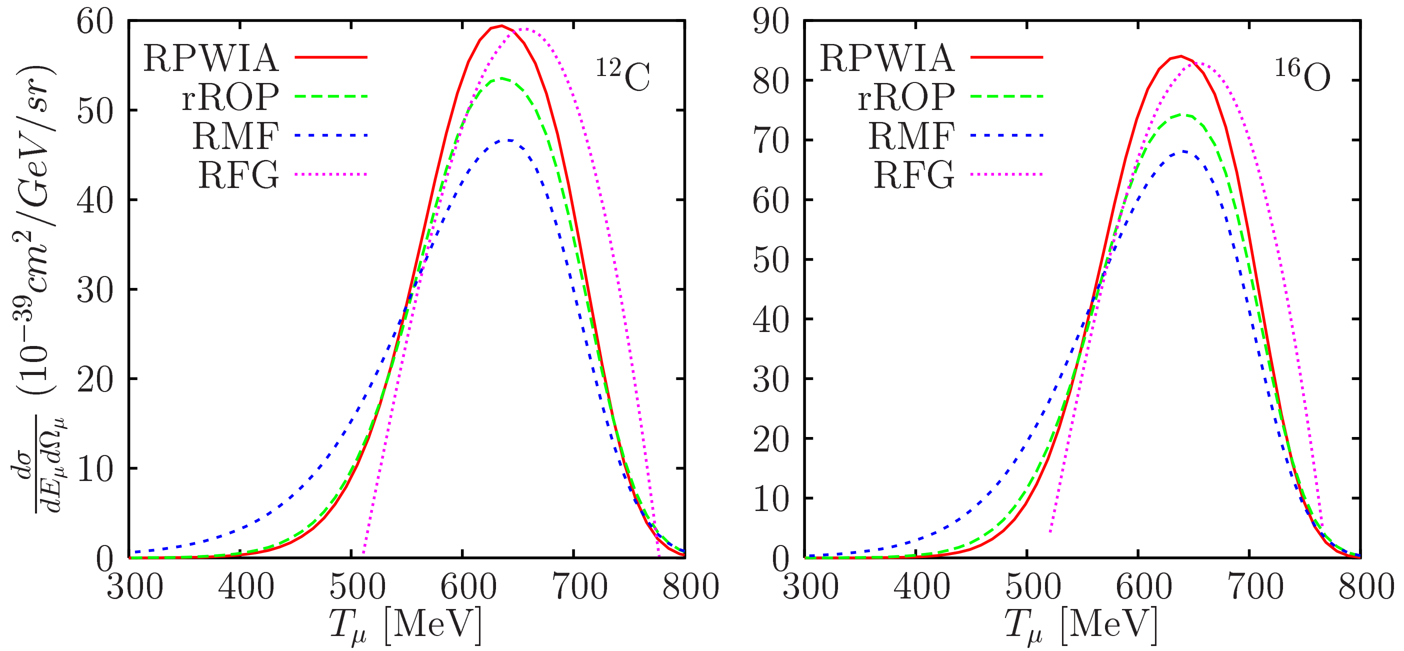

Quasi-elastic differential cross section $d\sigma/dE_\mu/d\Omega_\mu$ for (ν_μ, μ^-)

- Incident neutrino energy $\varepsilon_\nu = 1$ GeV.
- Muon scattering angle $\theta_\mu = 45^o$.
- RPWIA (solid), rROP (dashed) and RMF (dot-dashed), RFG (dotted).

From Caballero, Amaro, Barbaro, Donnelly, Maieron, and Udias, PRL 95 (2005)

(ν_μ, μ^-) results with the RMF

Neutrino scaling function Compared to the experimental scaling function

- RPWIA (solid),
- rROP (dashed)
- RMF (dot-dashed)
- Parameterization of data (dotted)

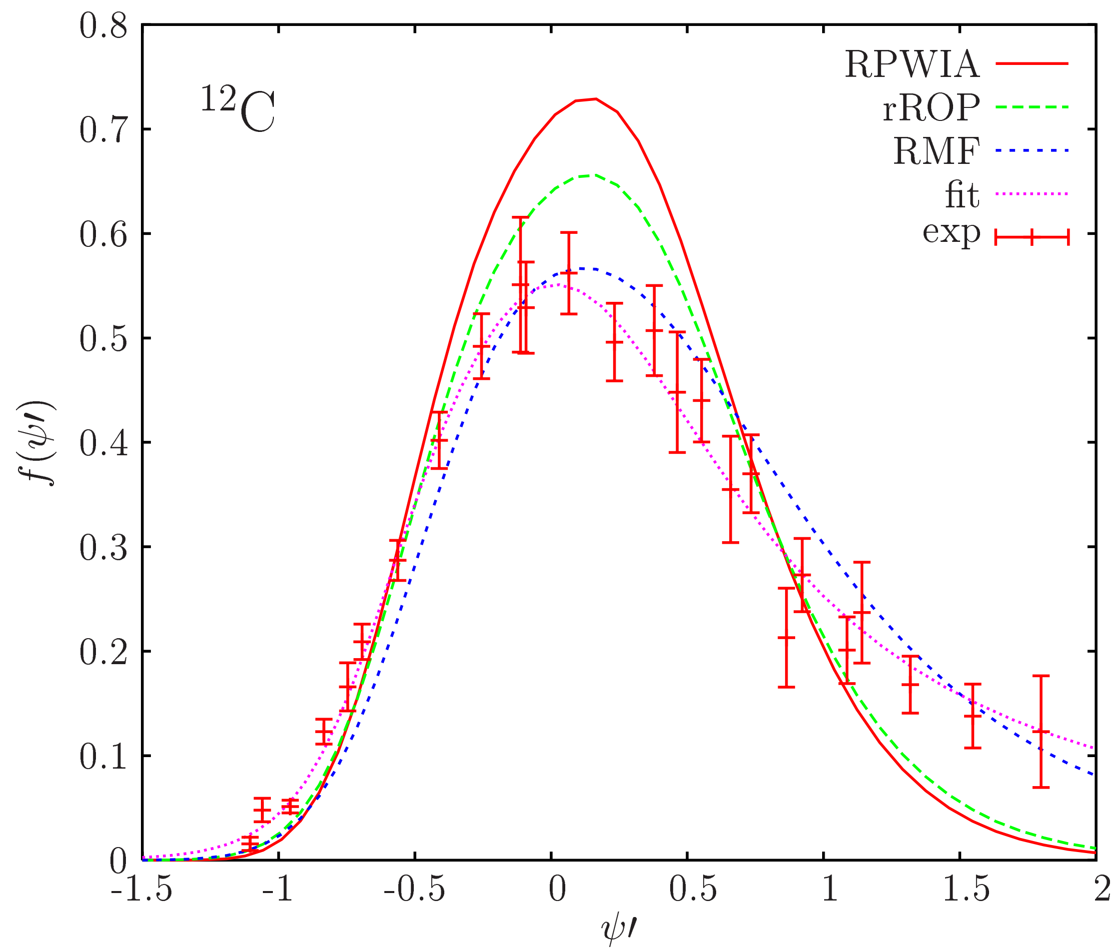

From Caballero, Amaro, Barbaro, Donnelly, Maieron, and Udias, PRL 95 (2005)

(ν_μ, μ^-) results with the RMF

Total integrated (ν_μ, μ) QE cross section for ^{12}C
as a function of the incident neutrino energy.

- RMF (squares),
- RFG (solid line)
- SuSA (dashed line),
- RPWIA (dot-dashed line)
- SRWS (circles)
- SRWS-tot (crosses).

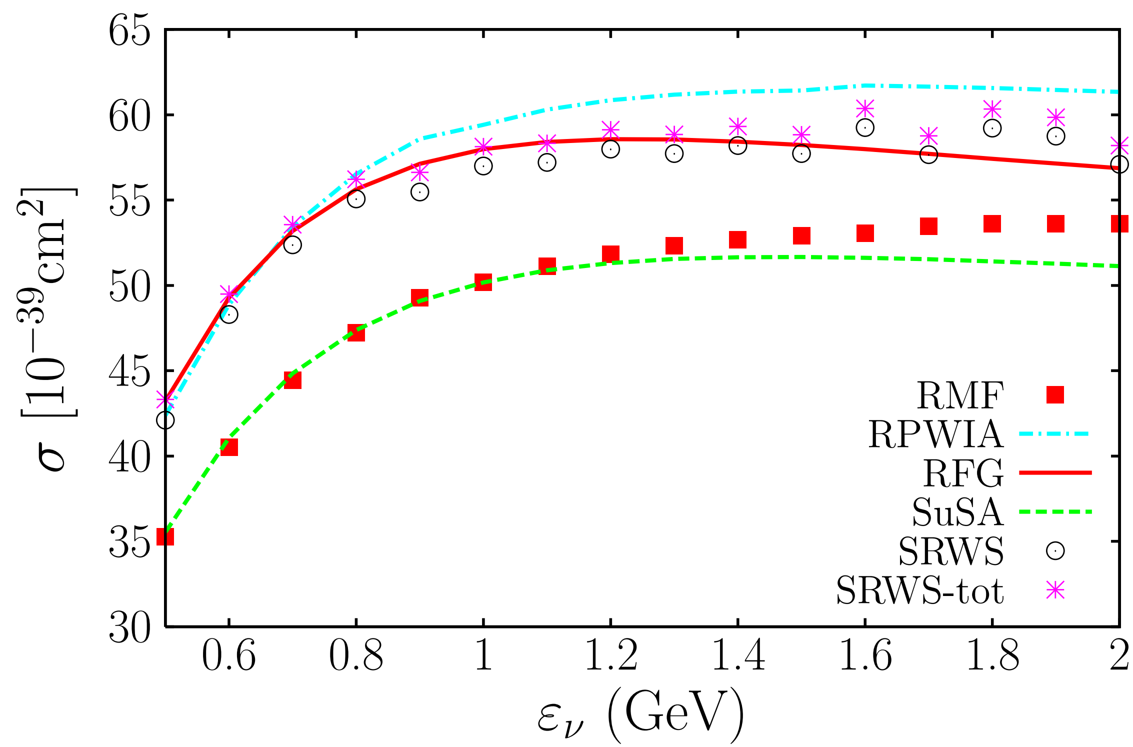

From Amaro, Barbaro, Caballero, Donnelly Phys. Rev. Lett. 98 (2007)

6 Neutrino excitation of the Δ peak

J.E. Amaro, M.B. Barbaro, J.A. Caballero, T.W. Donnelly, A. Molinari, Nucl. Phys. A **657** (1999) 161.

New scaling variable for the Δ peak :

$$\psi_\Delta \equiv \left[\frac{1}{\xi_F}\left(\kappa\sqrt{\rho_\Delta^2+1/\tau}-\lambda\rho_\Delta-1\right)\right]^{1/2} \times \begin{cases} +1 & \lambda \geq \lambda_\Delta^0 \\ -1 & \lambda \leq \lambda_\Delta^0 \end{cases}$$

$$\lambda_\Delta^0 = \frac{1}{2}\left[\sqrt{\mu_\Delta^2+4\kappa^2}-1\right], \qquad \mu_\Delta \equiv m_\Delta/m_N$$

$$\rho_\Delta \equiv 1+\beta_\Delta/\tau \qquad \beta_\Delta \equiv \frac{1}{4}\left(\mu_\Delta^2-1\right)$$

ψ_Δ Vanishes at the Δ peak $\Longrightarrow \omega = \omega_\Delta^0 = \sqrt{m_\Delta^2+q^2}-m_N$

Include a small energy shift $\omega \rightarrow \omega' \equiv \omega - E_{shift}$. yielding a shifted scaling variable ψ'_Δ.

RFG responses in the Δ peak

ignoring terms of order η_F^2:

$$
\begin{aligned}
R_L^\Delta(\kappa,\lambda)_0 &= \frac{1}{2}\Lambda_0\frac{\kappa^2}{\tau}\left[\left(1+\tau\rho_\Delta^2\right)w_2^\Delta(\tau)-w_1^\Delta(\tau)\right]\times f_{RFG}(\psi_\Delta)\\
R_T^\Delta(\kappa,\lambda)_0 &= \frac{1}{2}\Lambda_0\left[2w_1^\Delta(\tau)\right]\times f_{RFG}(\psi_\Delta),
\end{aligned}
$$

$$\Lambda_0 = \frac{\mathcal{N}}{2\kappa k_F}$$

One should add the contributions:

$\mathcal{N} = Z$ and the $p \to \Delta^+$ structure functions

$\mathcal{N} = N$ and the $n \to \Delta^0$ responses.

Experimental Δ scaling function

- Substract from the total (e,e') experimental cross section the QE cross section recalculated using $f^{QE}(\psi'_{QE})$
- Divide by $S^{\Delta} \equiv \sigma_M \left[v_L G_L^{\Delta} + v_T G_T^{\Delta} \right]$

$$
\begin{aligned}
G_L^{\Delta} &= \frac{\kappa}{2\tau k_F} \left[\mathcal{N} \left\{ \left(1+\tau\rho_{\Delta}^2\right) w_2^{\Delta}(\tau) - w_1^{\Delta}(\tau) \right\} \right] + \mathcal{O}(\eta_F^2) \\
G_T^{\Delta} &= \frac{1}{\kappa k_F} \left[\mathcal{N} \left\{ w_1^{\Delta}(\tau) \right\} \right] + \mathcal{O}(\eta_F^2).
\end{aligned}
$$

Scaling function in the Δ peak

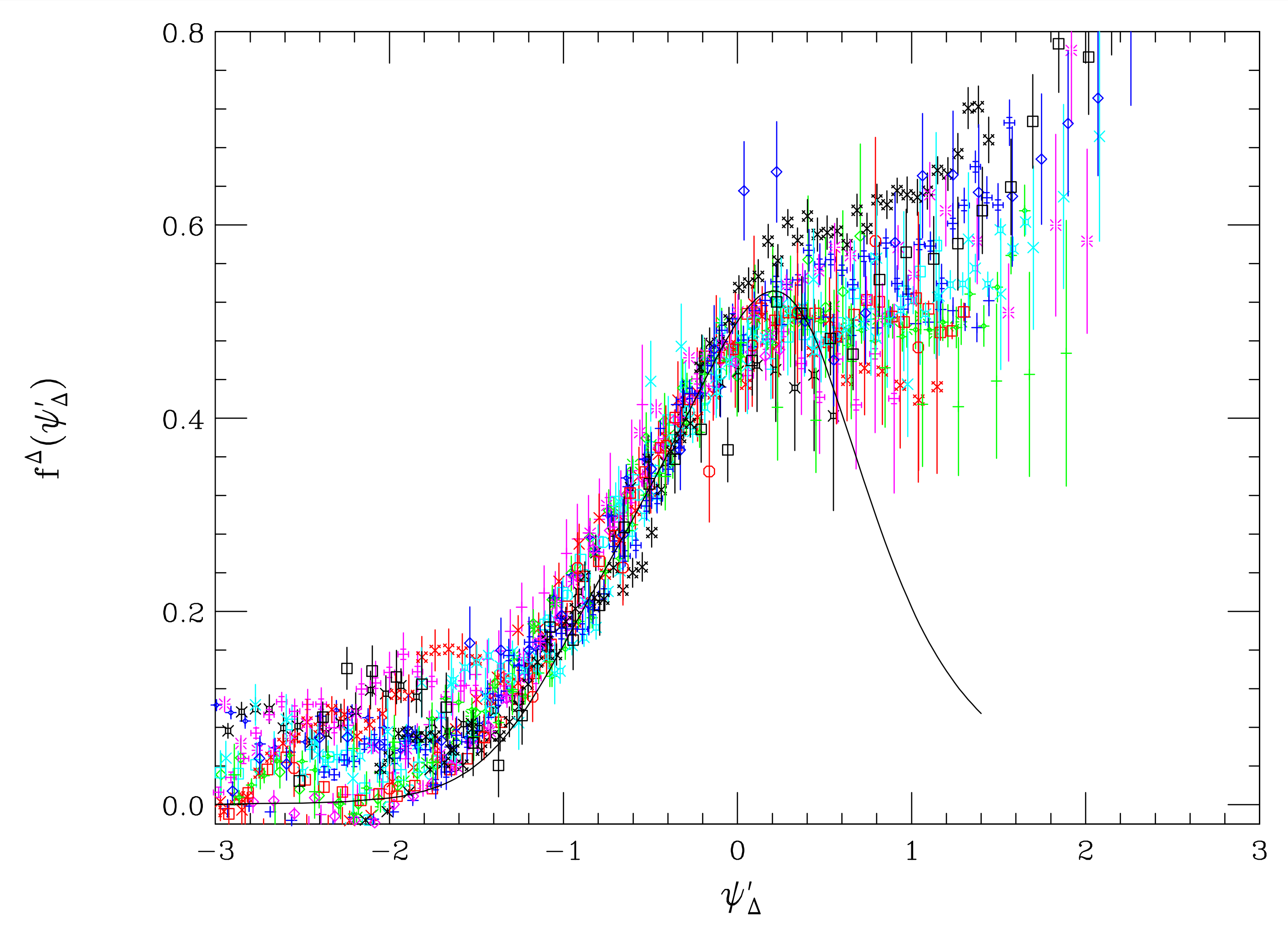

Scaling function in the Δ peak

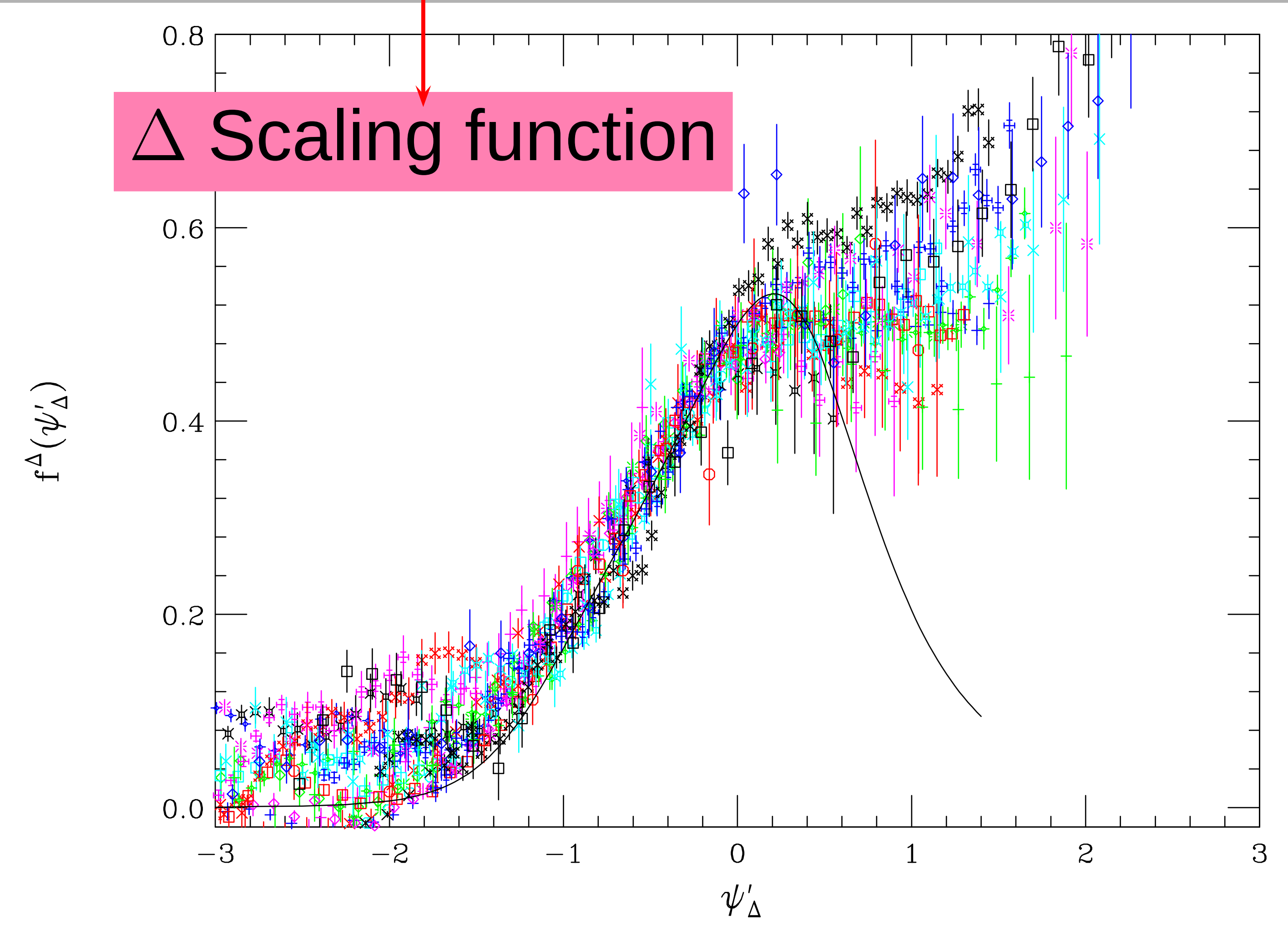

Scaling function in the Δ peak

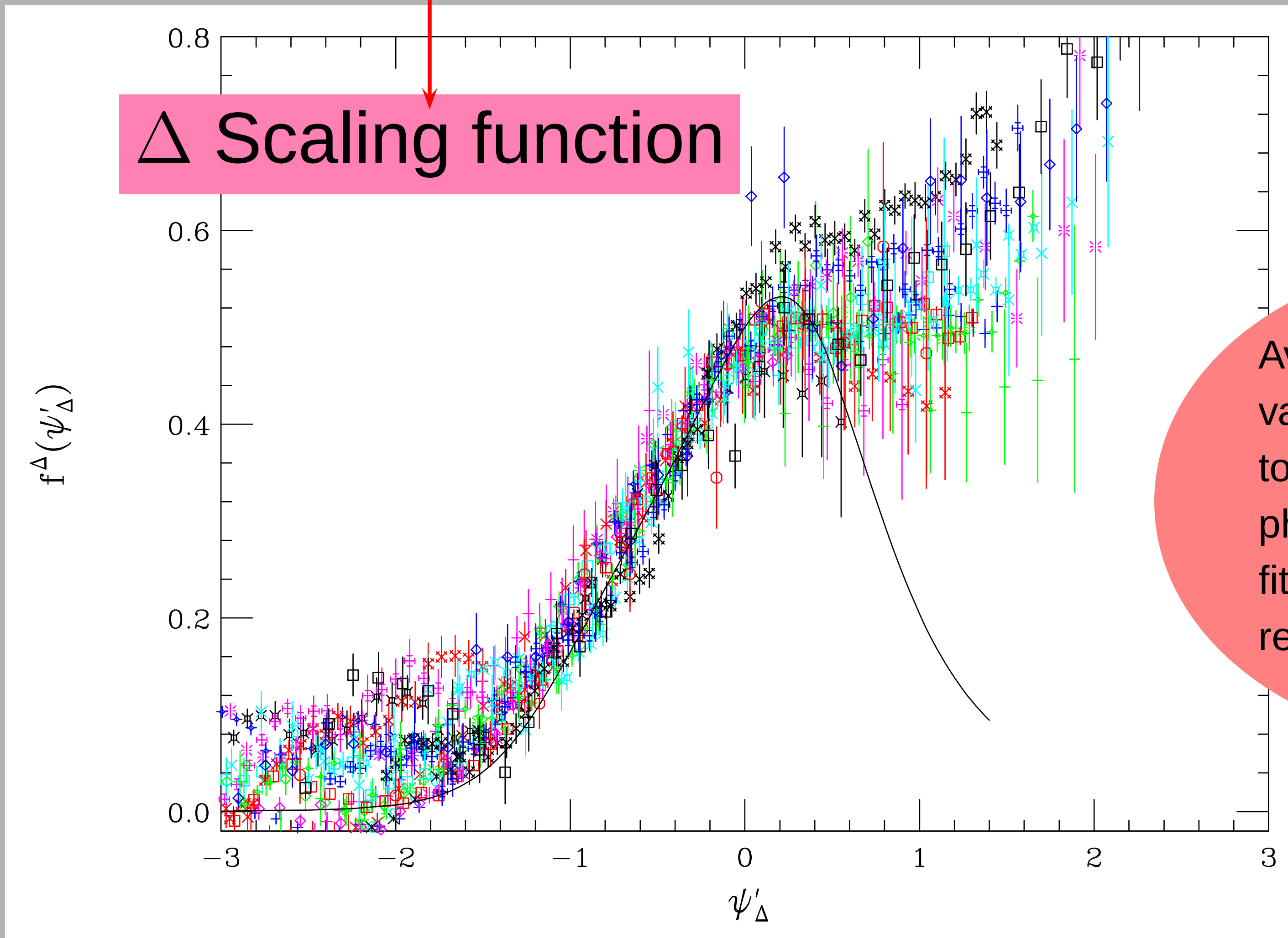

Averaged experimental values of $f^{\Delta}(\psi'_{\Delta})$ together with a phenomenological fit (whose validity is restricted to $\psi'_{\Delta} < 0$).

(e,e') *SuSA results (I)*

Cross section computed with scaling functions

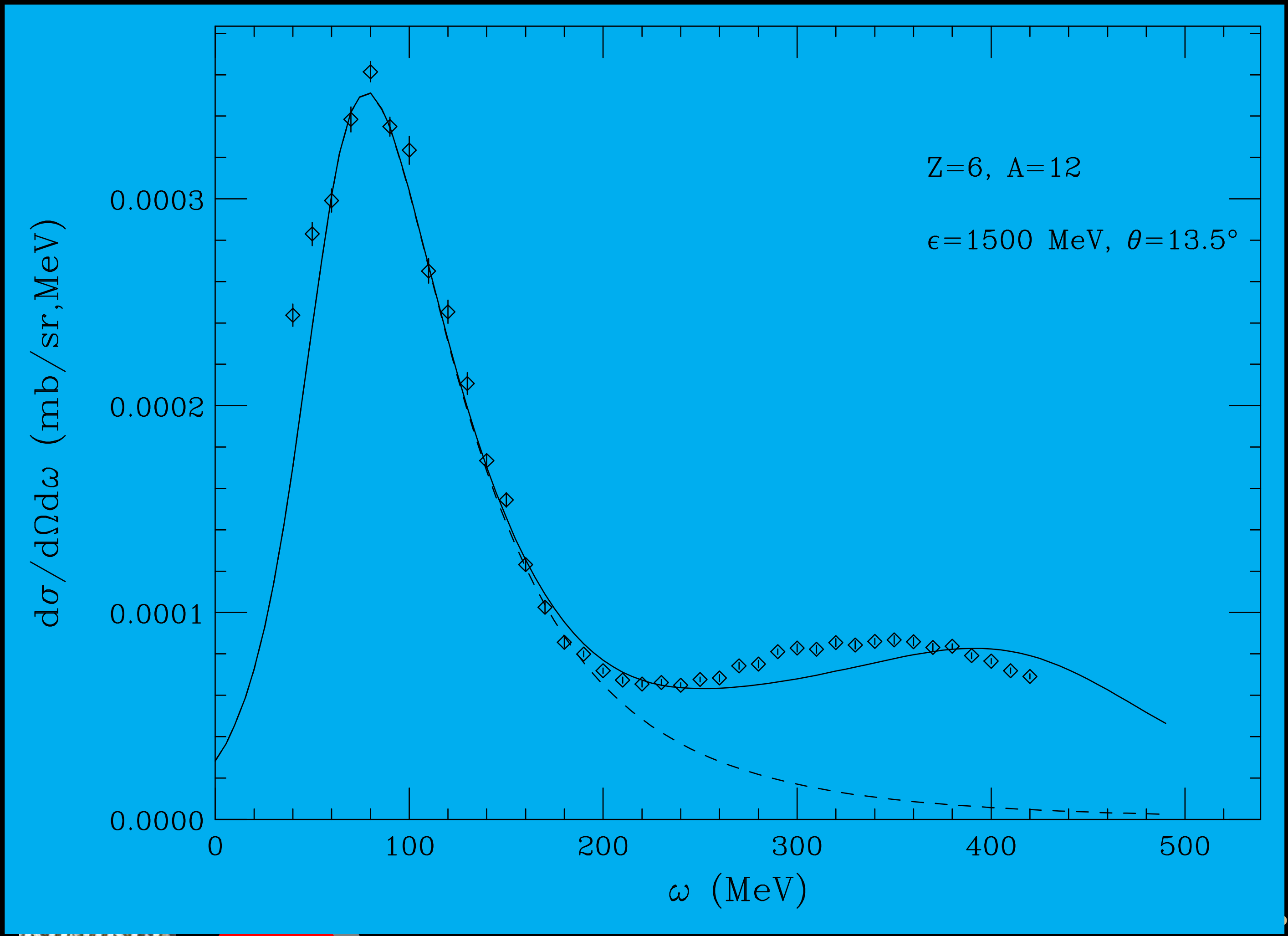

(e, e') *SuSA results (I)*

Cross section computed with scaling functions

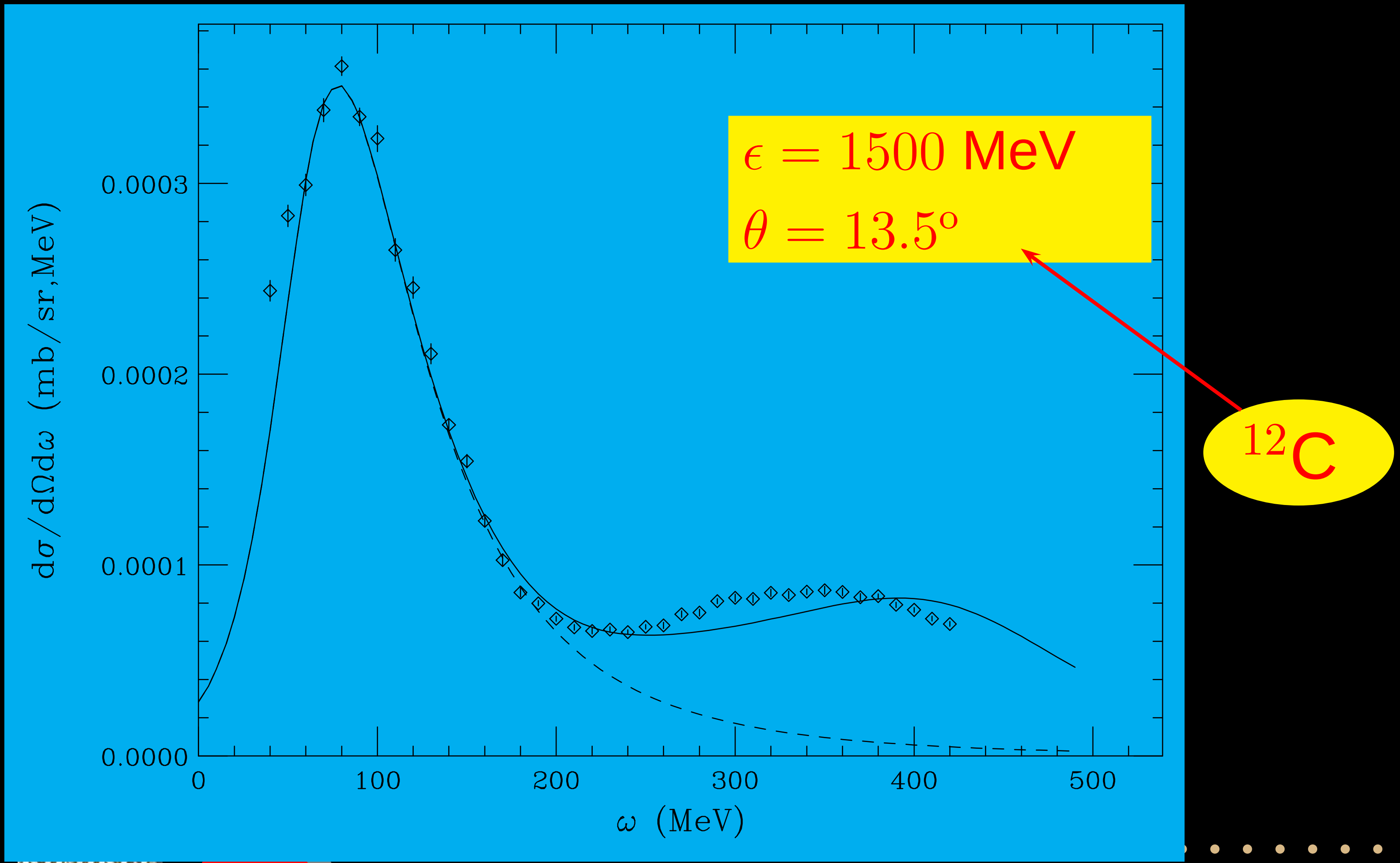

(e, e') *SuSA results (II)*

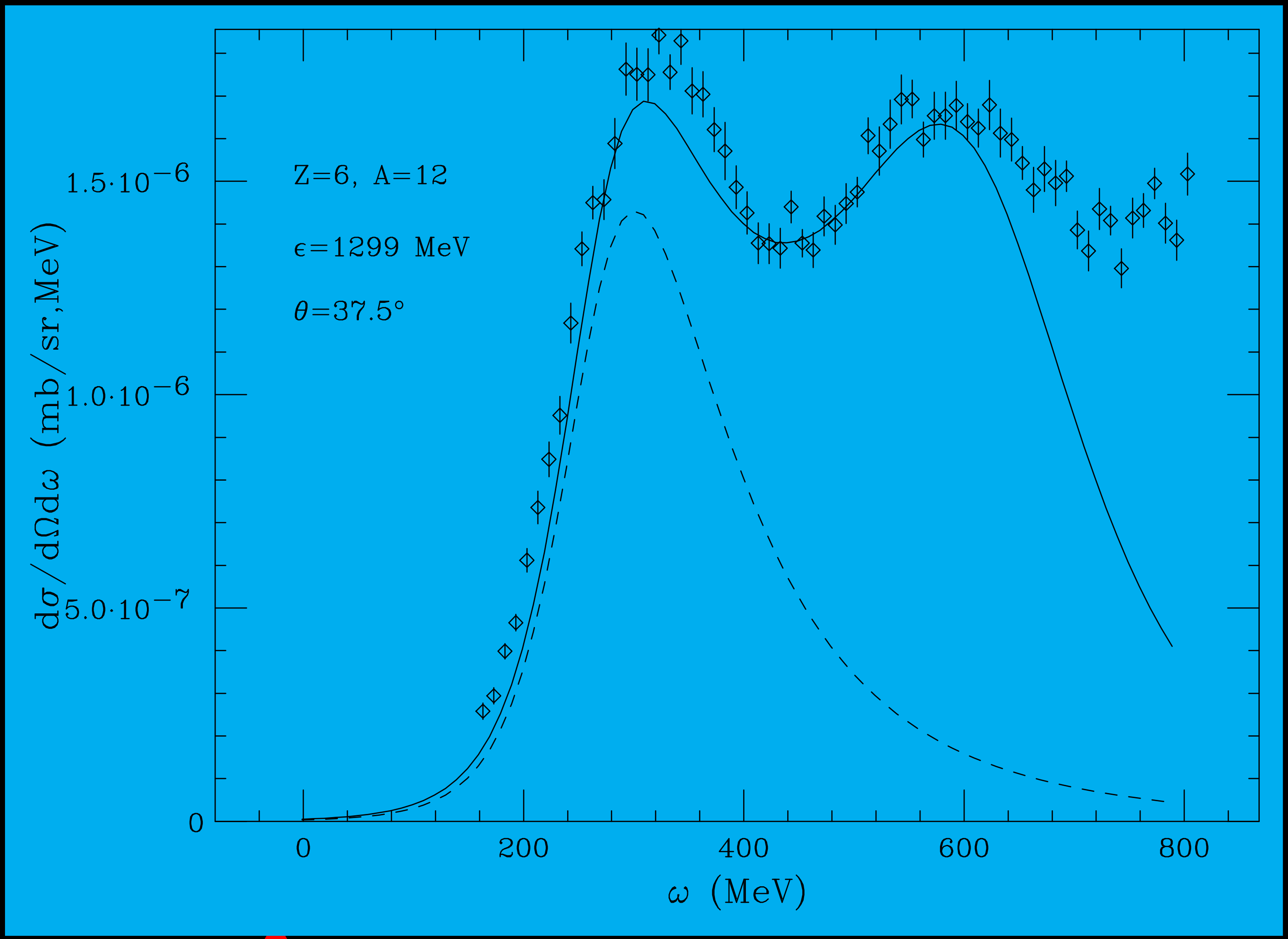

(e,e') *SuSA results (II)*

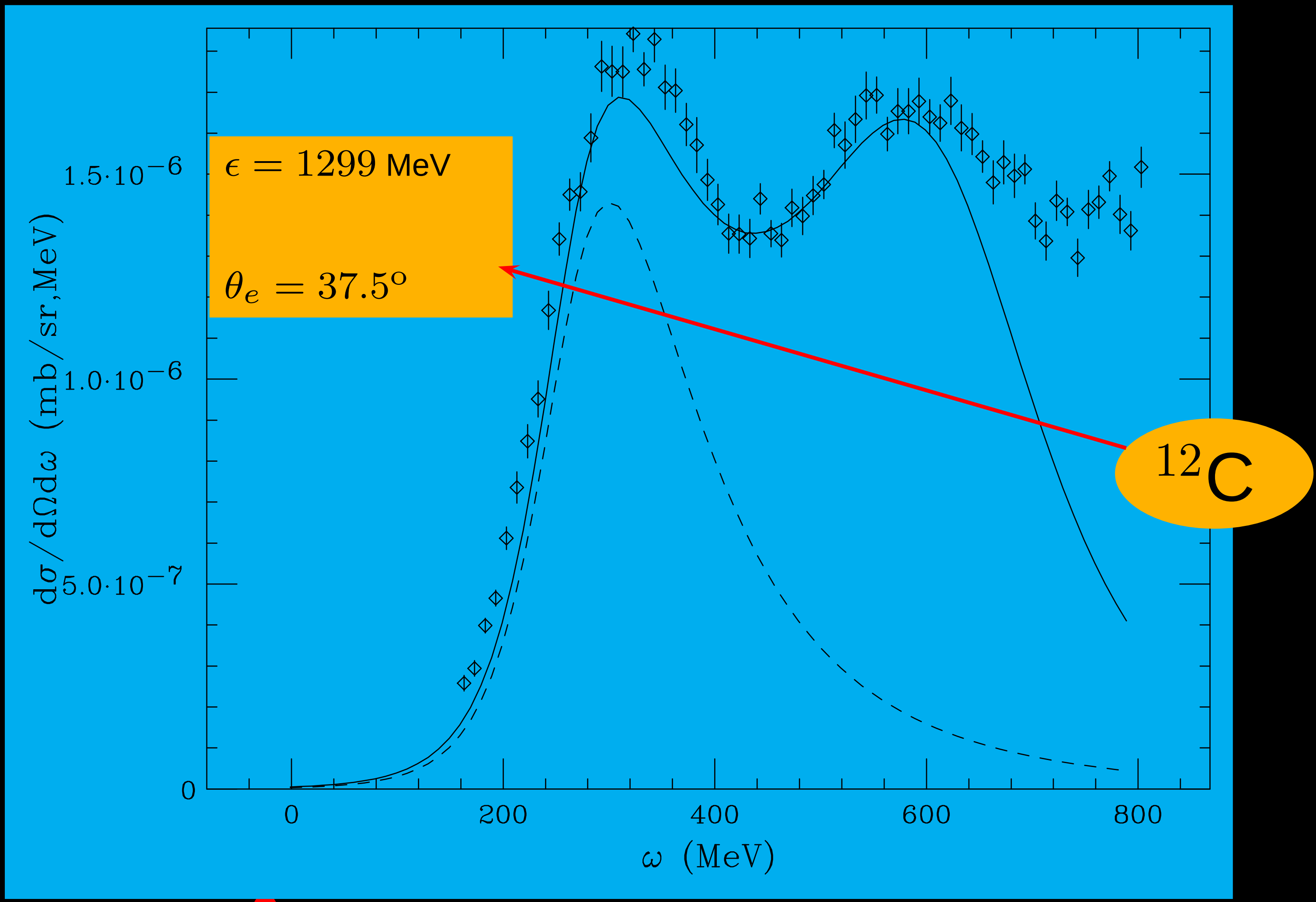

(e, e') *results (III)*

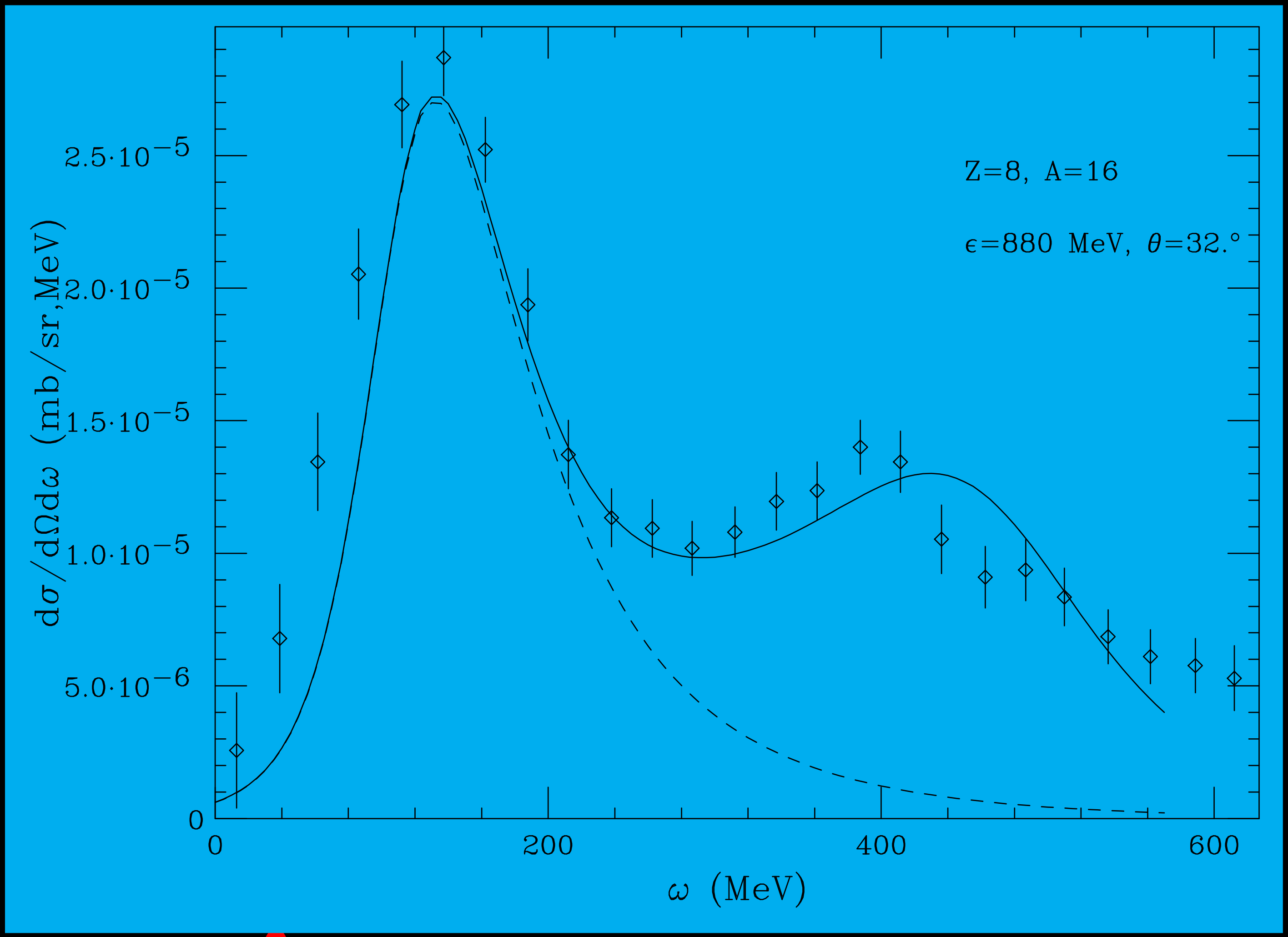

(e, e') *results (III)*

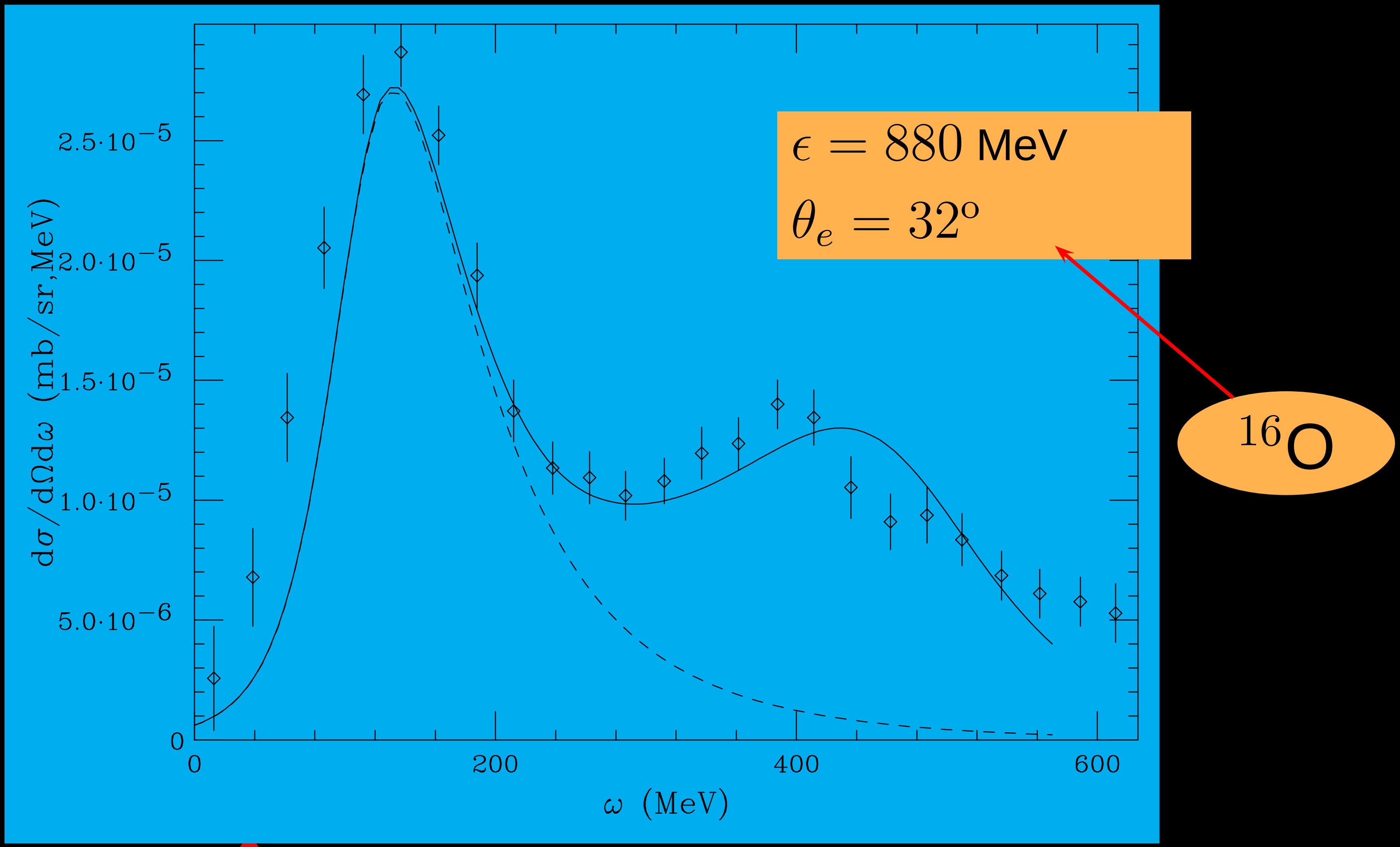

$N(\nu_\mu, \mu^-)\Delta$ *model*

Elementary reactions

$$
\begin{aligned}
\nu_\mu p &\longrightarrow \mu^- \Delta^{++} && (1)\\
\nu_\mu n &\longrightarrow \mu^- \Delta^{+} && (2)\\
\bar{\nu}_\mu p &\longrightarrow \mu^+ \Delta^{0} && (3)\\
\bar{\nu}_\mu n &\longrightarrow \mu^+ \Delta^{-}\ . && (4)
\end{aligned}
$$

Associated currents [Alvarez-Ruso et al. (1998)]:

$$J^\mu(q) = \mathcal{T}\bar{u}^{(\Delta)}_\alpha(p', s')\Gamma^{\alpha\mu}u(p, s), \qquad (5)$$

isospin factor: $\mathcal{T} = \sqrt{3}$ for Δ^{++} and Δ^- production and $= 1$ for Δ^+ and Δ^0 production,

$u^{(\Delta)}_\alpha(p', s')$: Rarita-Schwinger spinor

$N(\nu_\mu, \mu^-)\Delta$ *model*

Vertex tensor [Alvarez-Ruso (1998)]

$$
\begin{aligned}
\Gamma^{\alpha\mu} &= \\
&= \left[\frac{C_3^V}{m_N} (g^{\alpha\mu} \not{q} - q^\alpha \gamma^\mu) + \frac{C_4^V}{m_N^2} \left(g^{\alpha\mu} q \cdot p' - q^\alpha p'^\mu \right) + \frac{C_5^V}{m_N^2} (g^{\alpha\mu} q \cdot p - q^\alpha p^\mu) \right] \gamma_5 \\
&+ \left[\frac{C_3^A}{m_N} (g^{\alpha\mu} \not{q} - q^\alpha \gamma^\mu) + \frac{C_4^A}{m_N^2} \left(g^{\alpha\mu} q \cdot p' - q^\alpha p'^\mu \right) + C_5^A g^{\alpha\mu} + \frac{C_6^A}{m_N^2} q^\alpha q^\mu \right]
\end{aligned}
$$

CVC implies $C_6^V = 0$ and PCAC yields
$C_6^A = C_5^A (\mu_\pi^2 + 4\tau)^{-1}$, with $\mu_\pi = m_\pi / m_N$

SuSA (ν_μ, μ) *predictions* Δ *peak*

Neutrino energy: $\epsilon = 1$ GeV

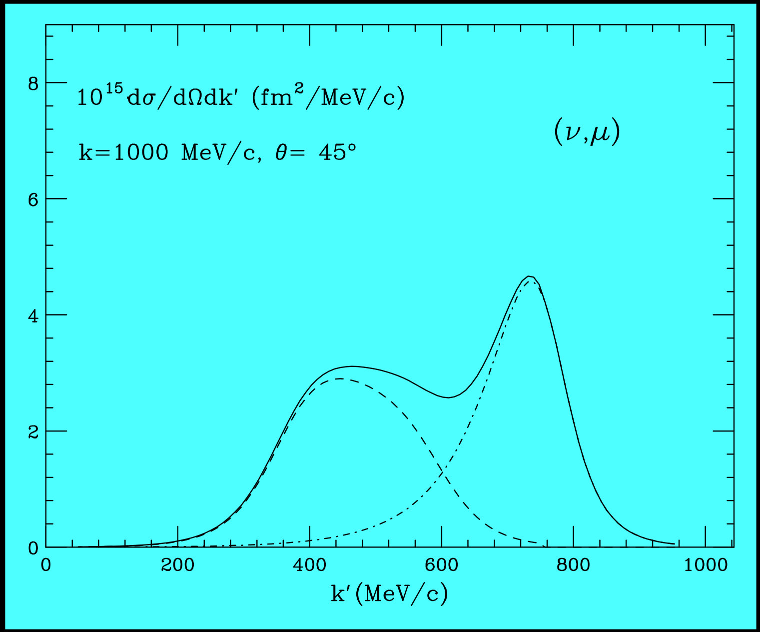

$\theta = 45^o$

SuSA (ν_μ, μ) *predictions* Δ *peak*

Neutrino energy: $\epsilon = 1$ GeV

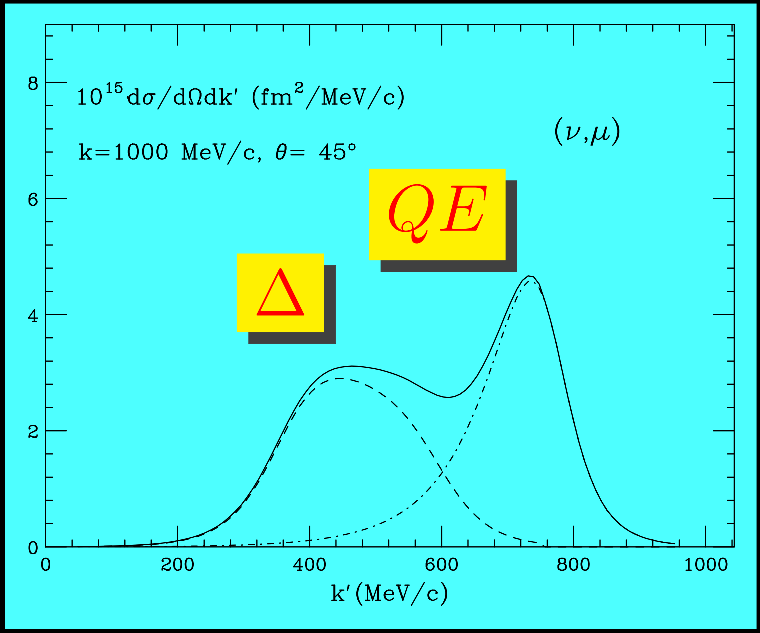

$\theta = 45^o$

SuSA (ν_μ, μ) *predictions* Δ *peak*

Neutrino energy: $\epsilon = 1$ GeV

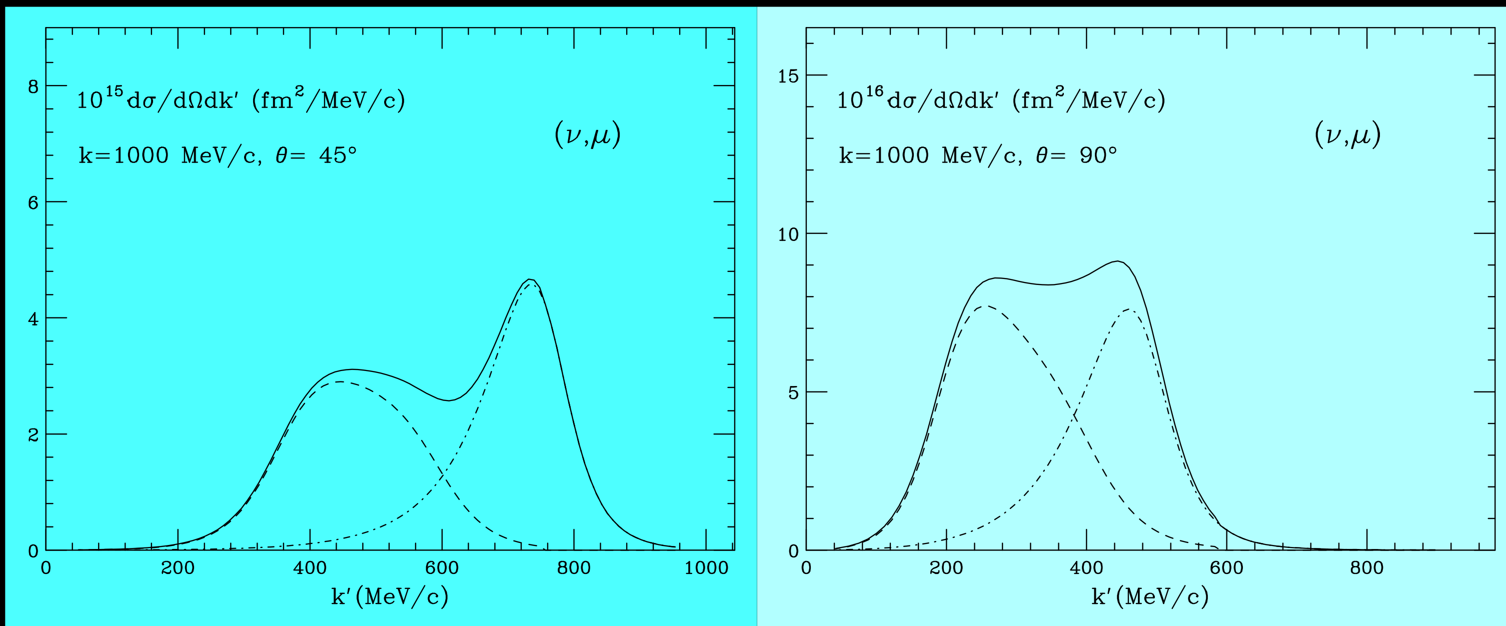

$\theta = 45^o$

$\theta = 90^o$

SuSA (ν_μ, μ) predictions Δ peak

Neutrino energy: $\epsilon = 1$ GeV

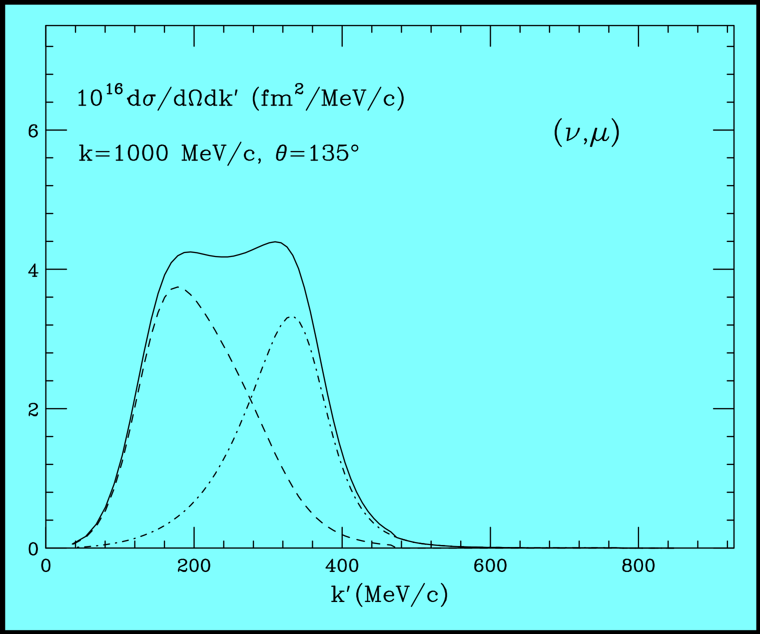

$\theta = 135^\circ$

SuSA (ν_μ, μ) *predictions* Δ *peak*

Neutrino energy: $\epsilon = 1$ GeV

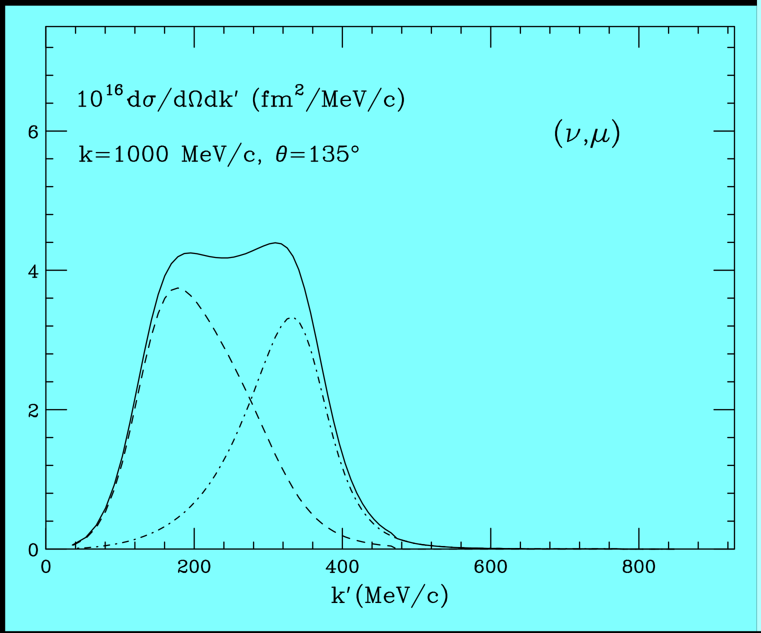

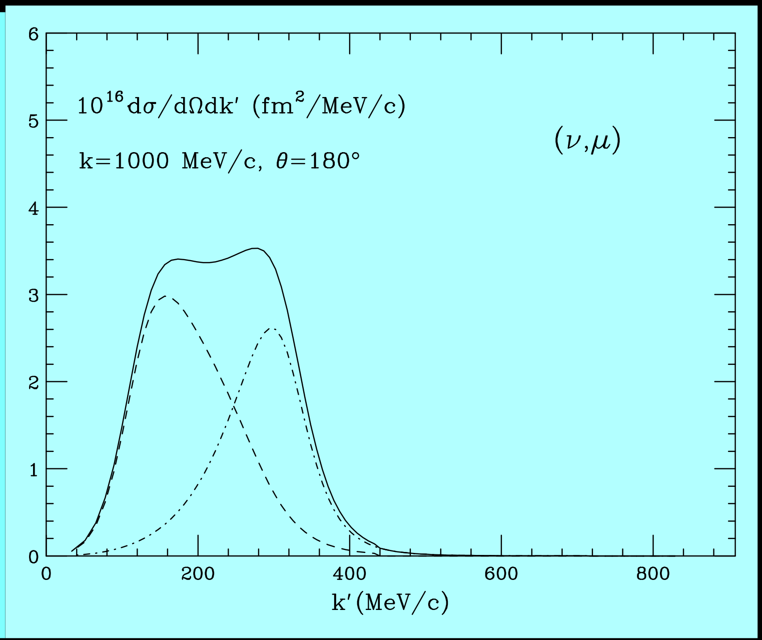

$\theta = 135^\circ$

$\theta = 180^\circ$

SuSA $(\overline{\nu}_\mu, \mu^+)$ *predictions* Δ *peak*

Neutrino energy: $\epsilon = 1$ GeV

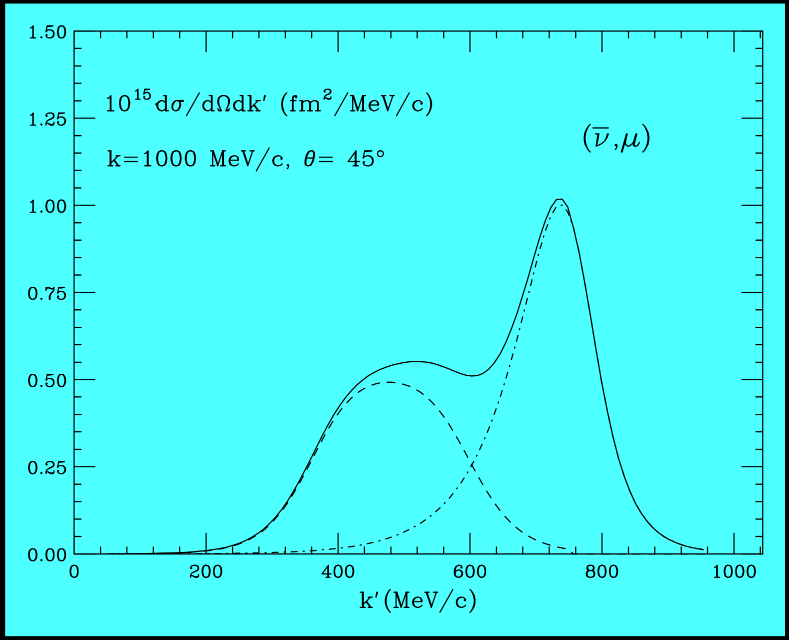

$$\theta = 45^o$$

SuSA $(\overline{\nu}_\mu, \mu^+)$ predictions Δ peak

Neutrino energy: $\epsilon = 1$ GeV

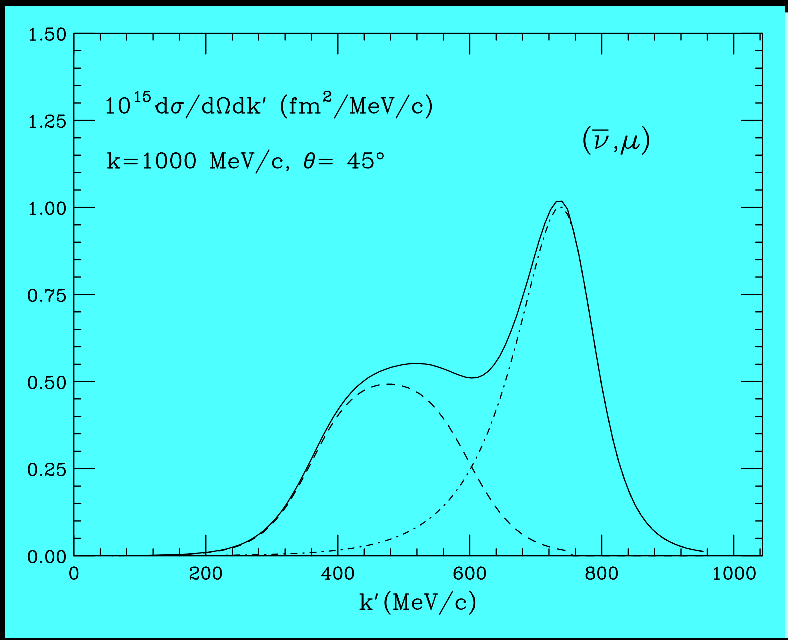

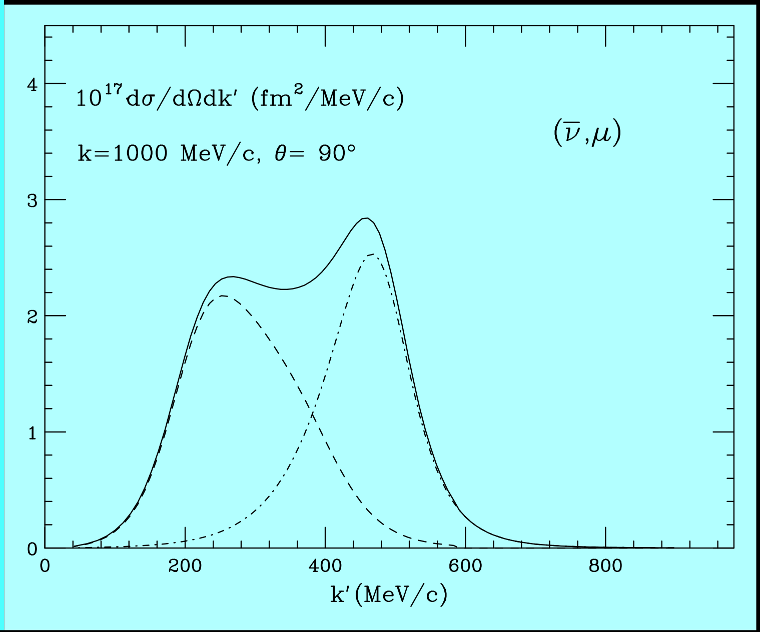

$\theta = 45^{\circ}$

$\theta = 90^{\circ}$

$(\overline{\nu}_\mu, \mu^+)$ *predictions (II)*

Neutrino energy: $\epsilon = 1$ GeV

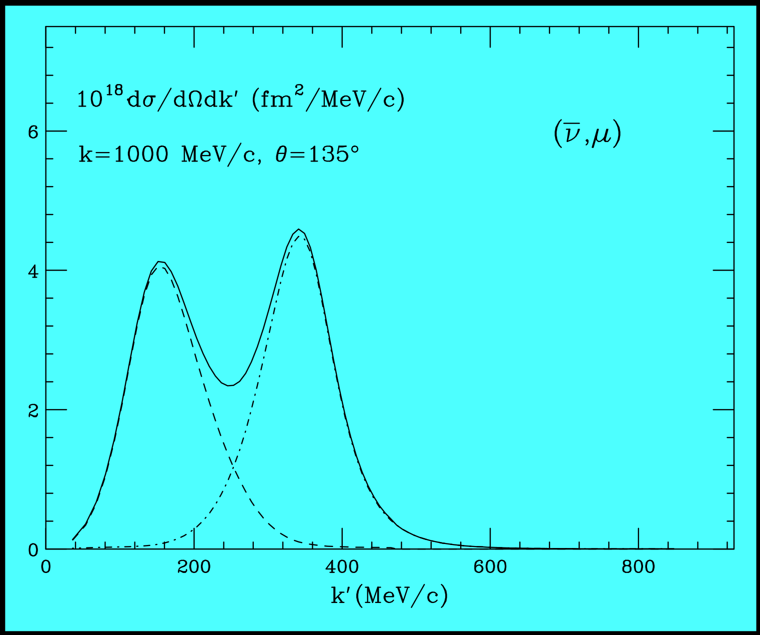

$\boxed{\theta = 135^{\rm o}}$

$(\overline{\nu}_\mu, \mu^+)$ *predictions (II)*

Neutrino energy: $\epsilon = 1$ GeV

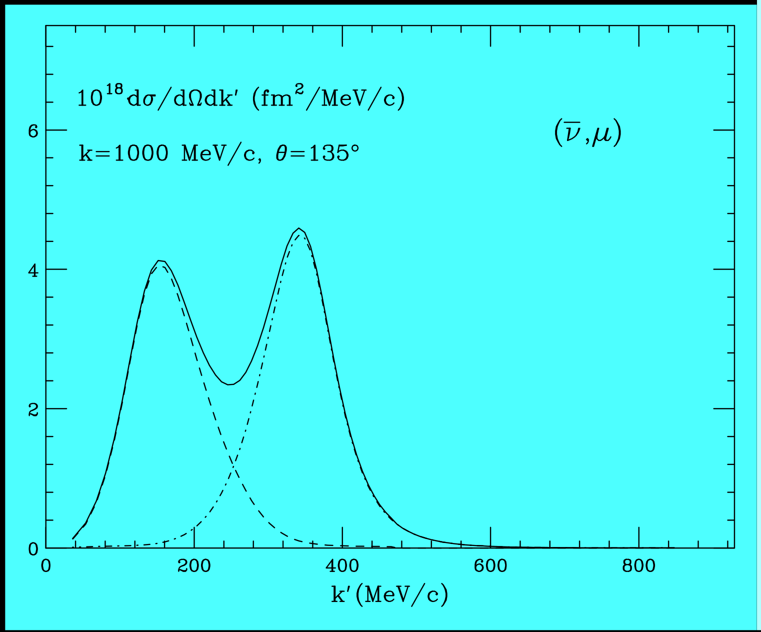

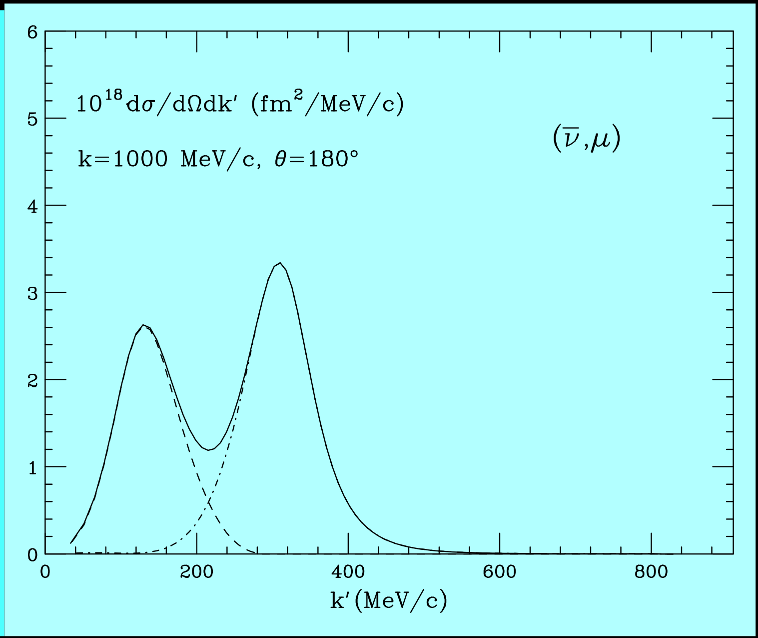

$\theta = 135^o$

$\theta = 180^o$

Angular distribution

At the tops of the QE and Δ peaks - $\epsilon = 1$ GeV

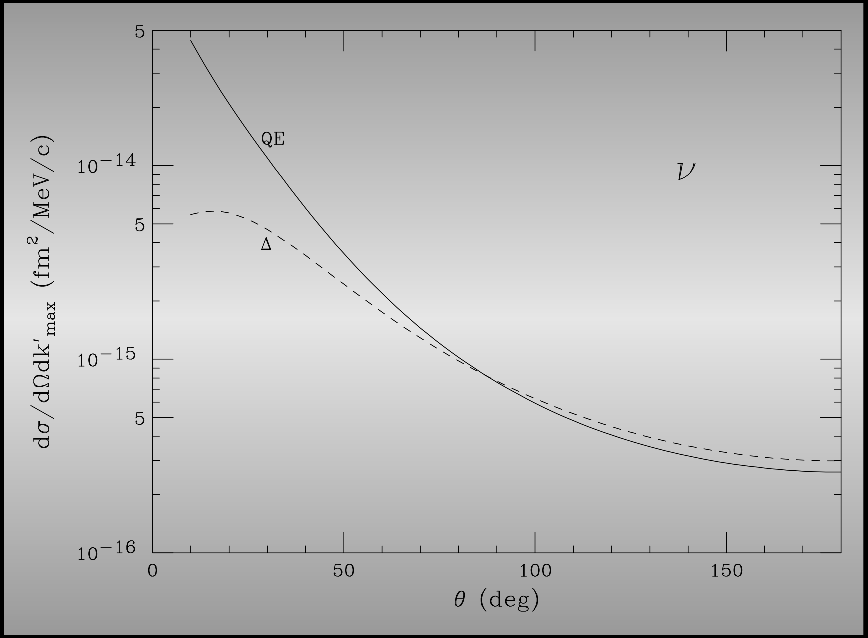

(ν_μ, μ)

Angular distribution

At the tops of the QE and Δ peaks - $\epsilon = 1$ GeV

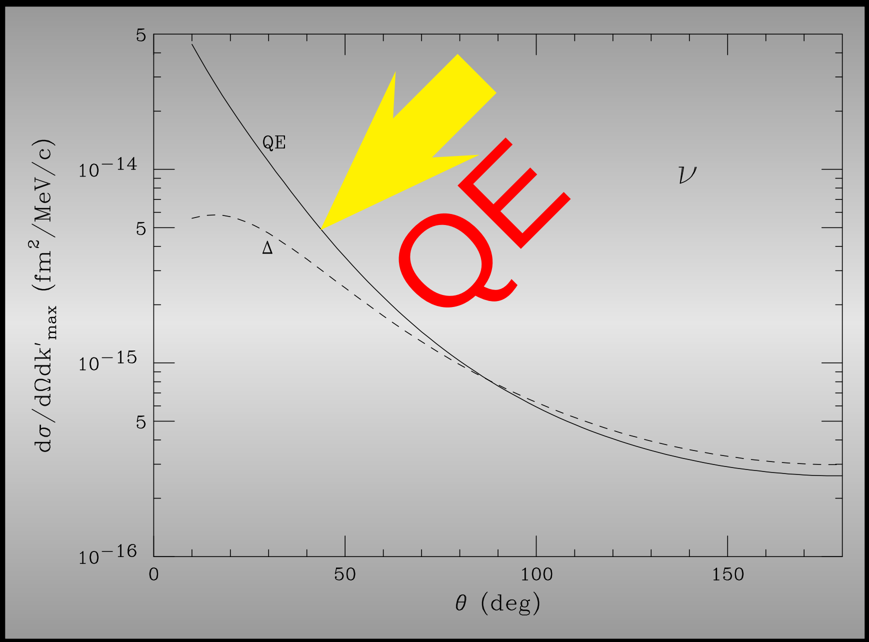

(ν_μ, μ)

Angular distribution

At the tops of the QE and Δ peaks - $\epsilon = 1$ GeV

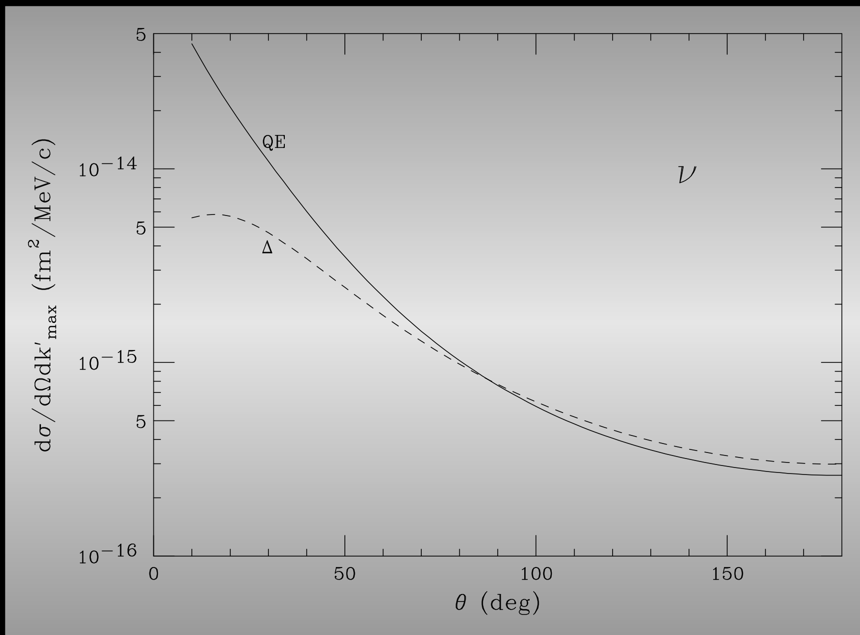

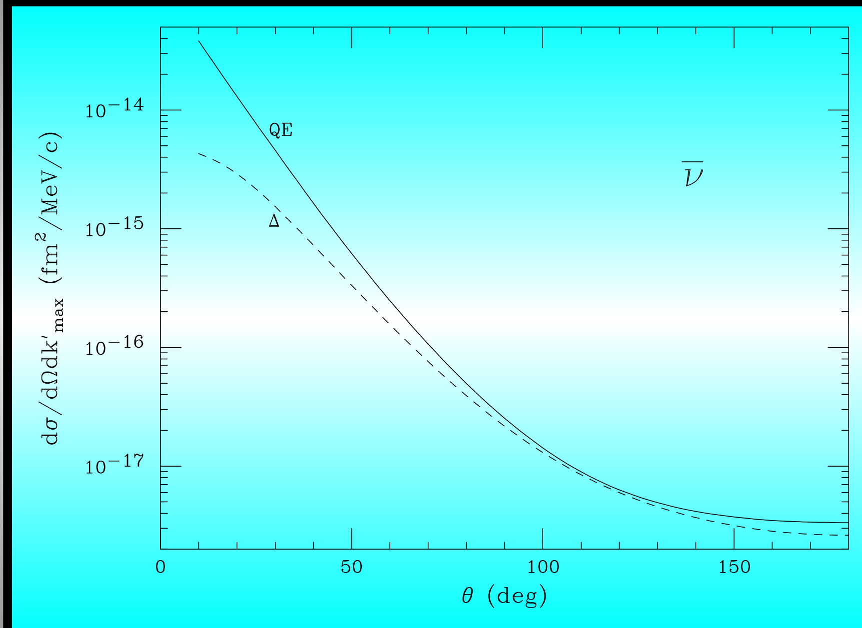

(ν_μ, μ) $(\overline{\nu}_\mu, \mu^+)$

Comparison with the RFG

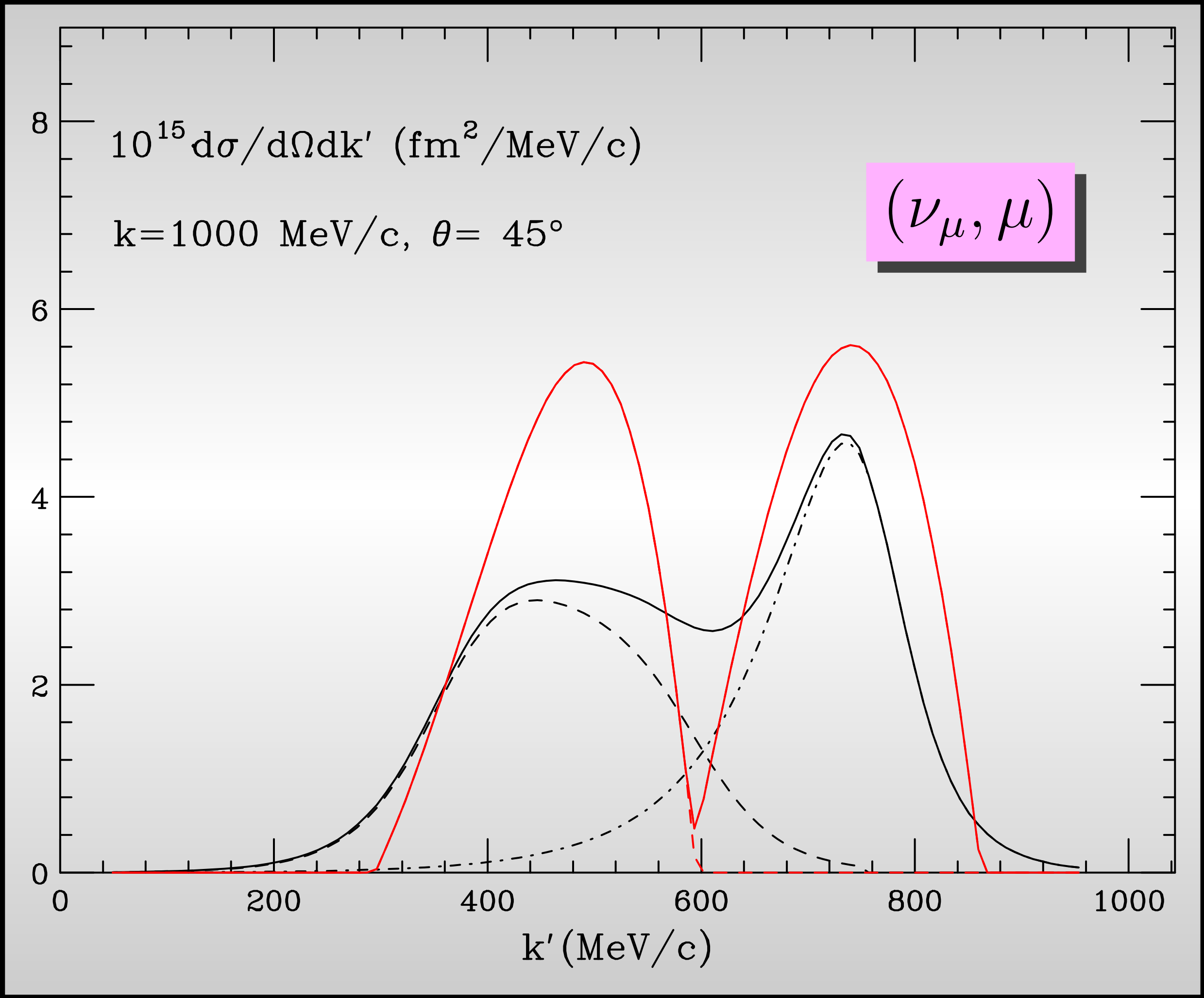

Comparison with the RFG

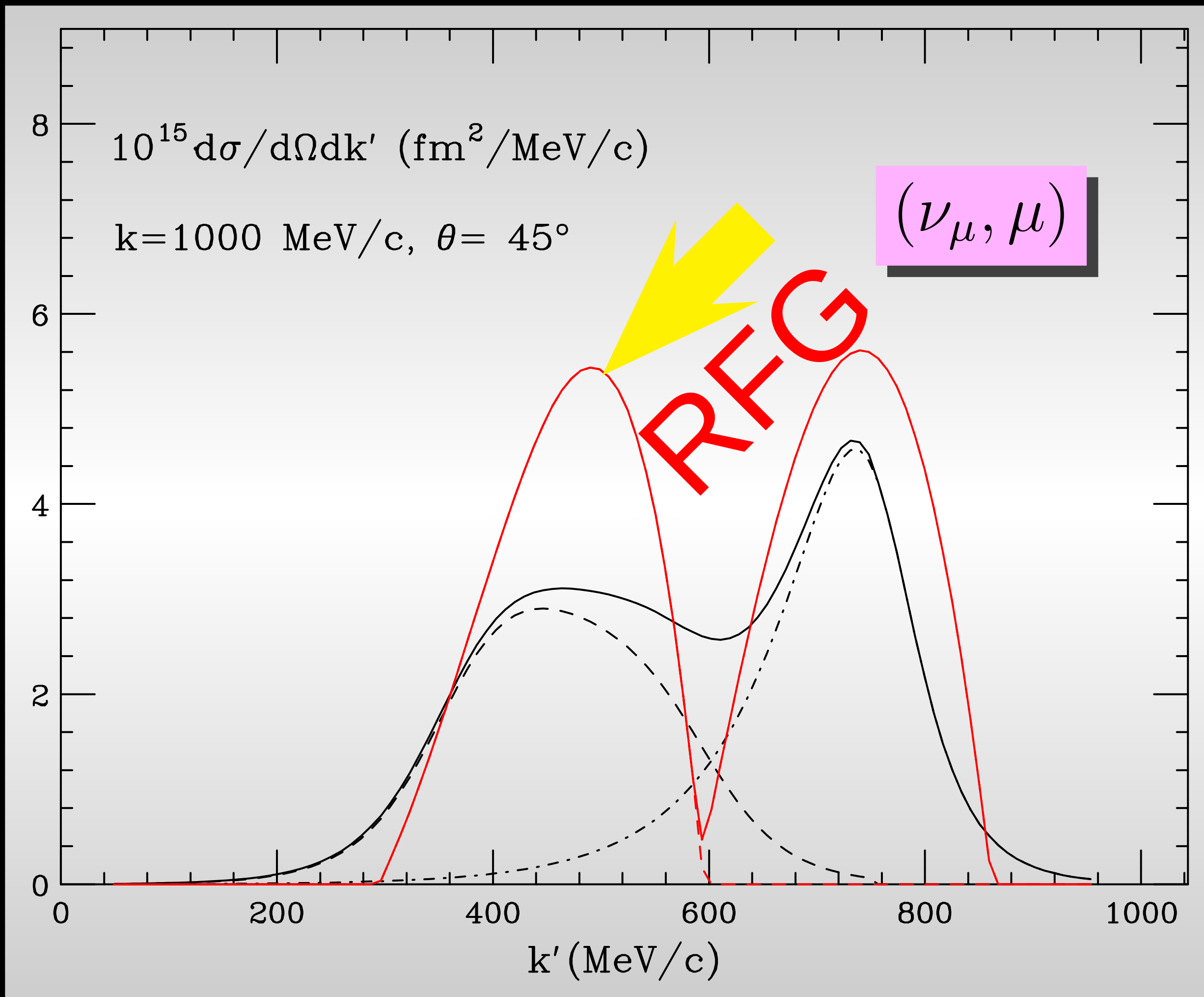

7 Neutral current neutrino reactions

t - Channel inclusive scattering

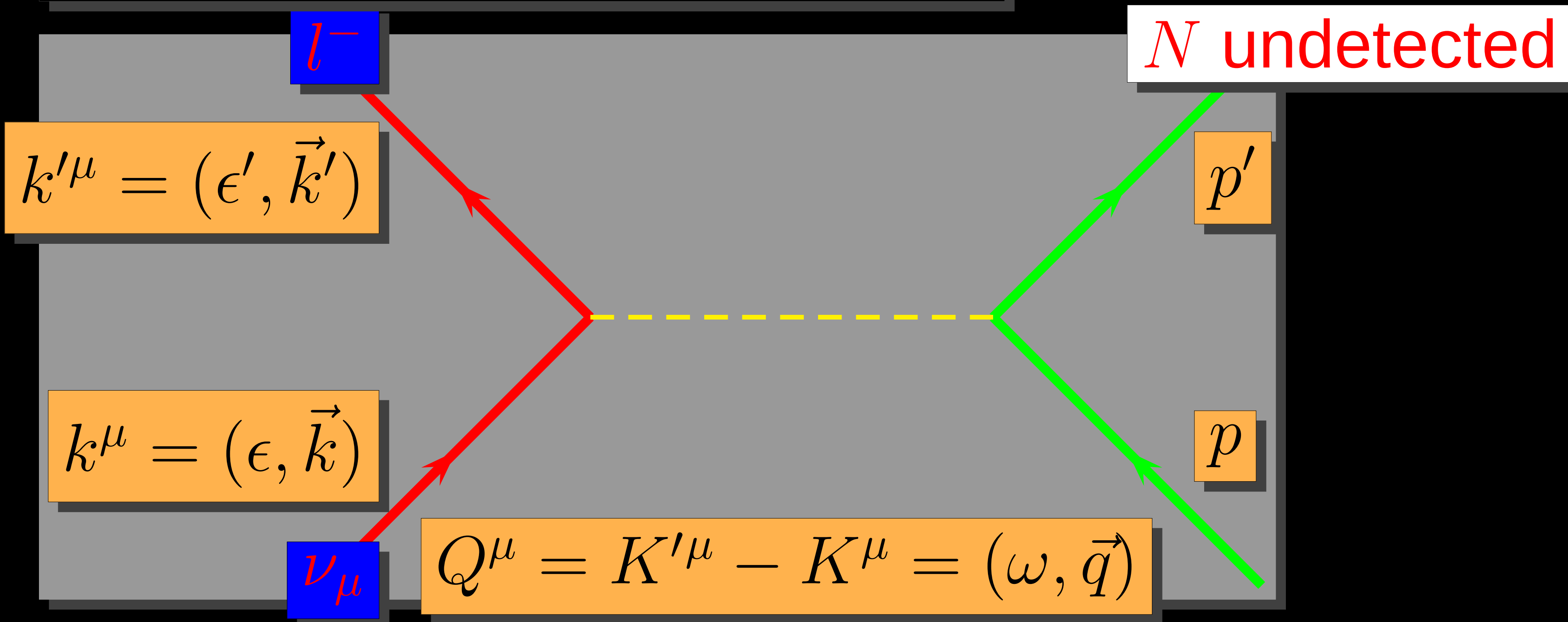

$$\lambda = \frac{\omega}{2m_N} \qquad \kappa = \frac{q}{2m_N} \qquad \tau = \kappa^2 - \lambda^2$$

7 Neutral current neutrino reactions

u - Channel inclusive scattering

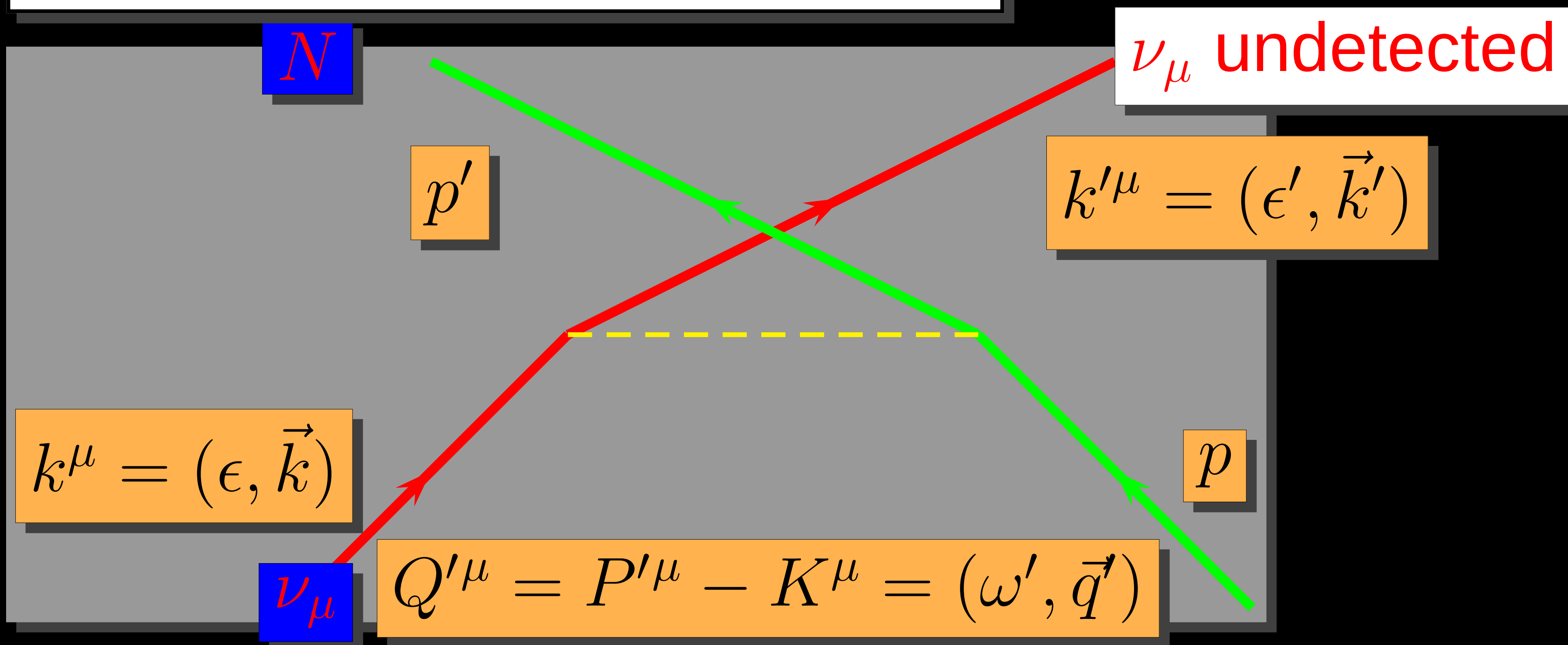

$$\lambda' = \frac{\omega'}{2m_N} \qquad \kappa' = \frac{q'}{2m_N} \qquad \tau' = \kappa'^2 - \lambda'^2$$

SuSA approach to NC neutrino scattering

t-channel (ν_l, l^-)

$$\frac{d\sigma}{d\Omega_{k'}dk'} = \int d\Omega_N dp_N \frac{d\sigma}{d\Omega_{k'}dk'd\Omega_N dp_N} \simeq \overline{\sigma}_{sn}^{(t)} F^{(t)}(\psi^{(t)})$$

Valid exactly for the RFG

u-channel (ν_l, N)

$$\frac{d\sigma}{d\Omega_N dp_N} = \int d\Omega_{k'}dk' \frac{d\sigma}{d\Omega_{k'}dk'd\Omega_N dp_N} \simeq \overline{\sigma}_{sn}^{(u)} F^{(u)}(\psi^{(u)})$$

Good approximation in the RFG

- Extend the SuSA model to the neutral current u-channel
- Assume that $F^{(u)}(\psi) = F^{(t)}(\psi)$
- Use the phenomenological scaling function extracted from (e, e') data to predict NC ν-nucleus cross sections.

Proton knock-out from ^{12}C

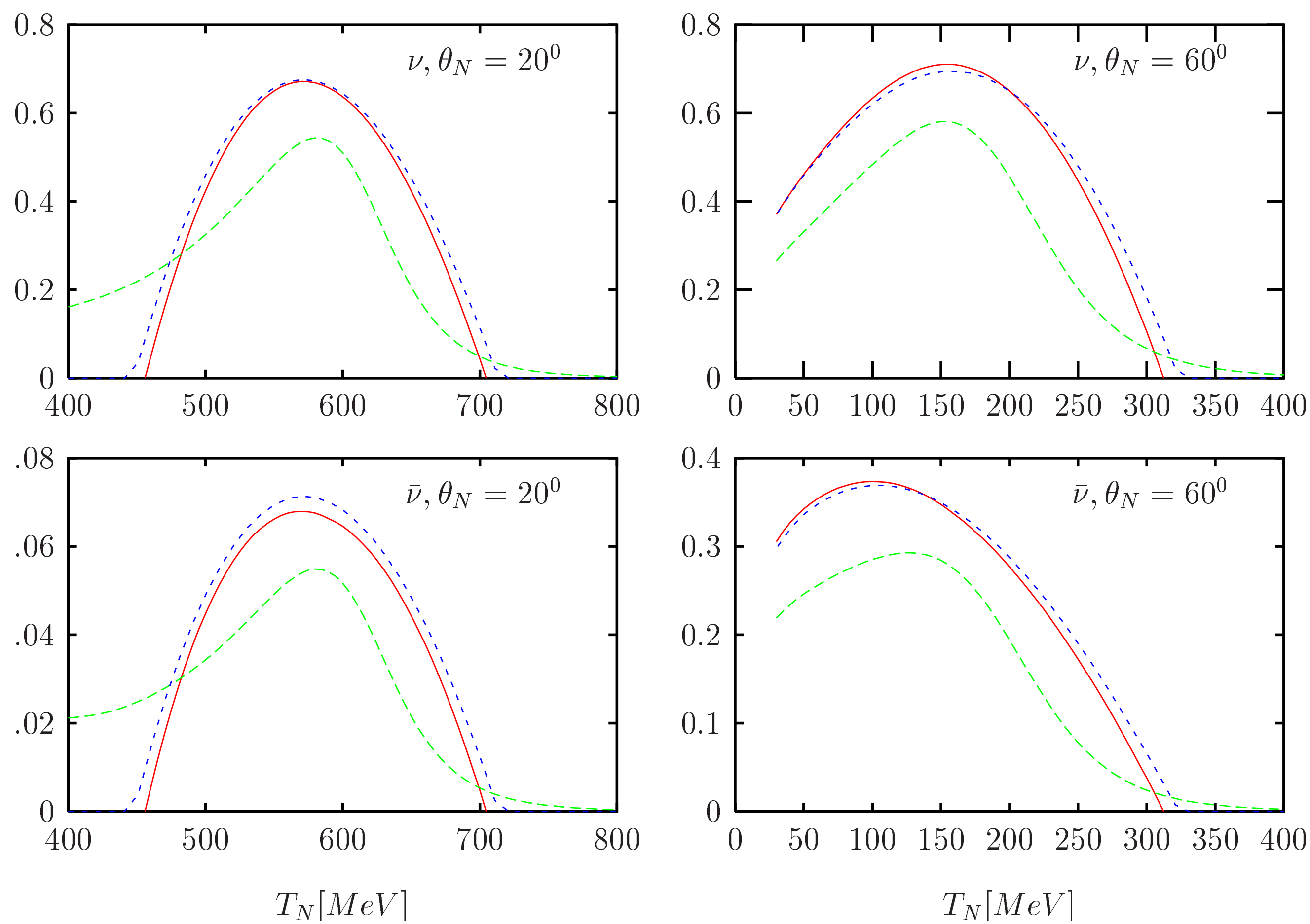

- Blue: RFG
- Red: factorized RFG
- Green: Phenomenological SuSA model

Nucleon strangeness effects

$^{12}\mathrm{C}(\nu_\mu, p)$

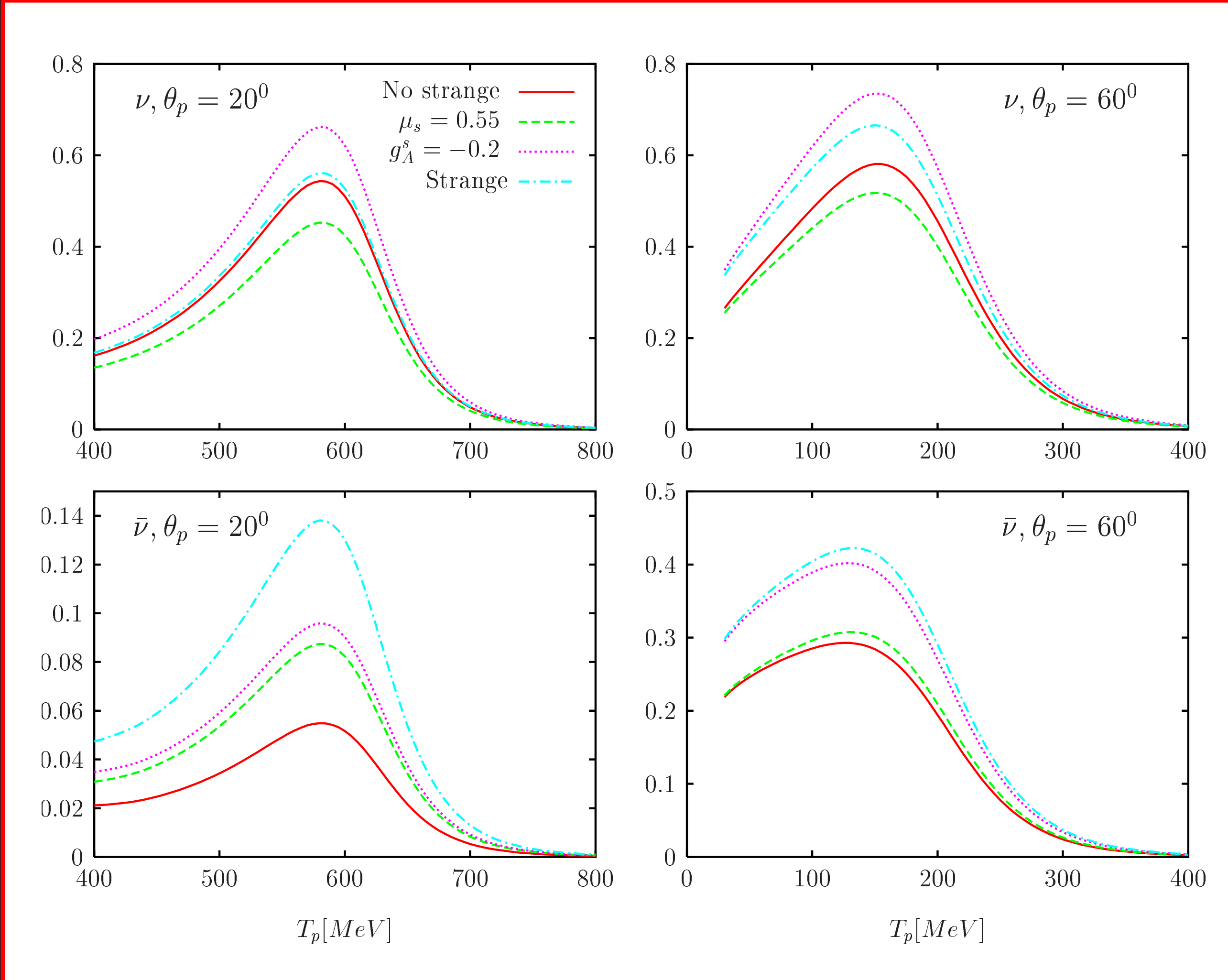

- Blue: strangeness
- Red: no strangeness

Nucleon strangeness effects

$^{12}\mathrm{C}(\nu_\mu, n)$

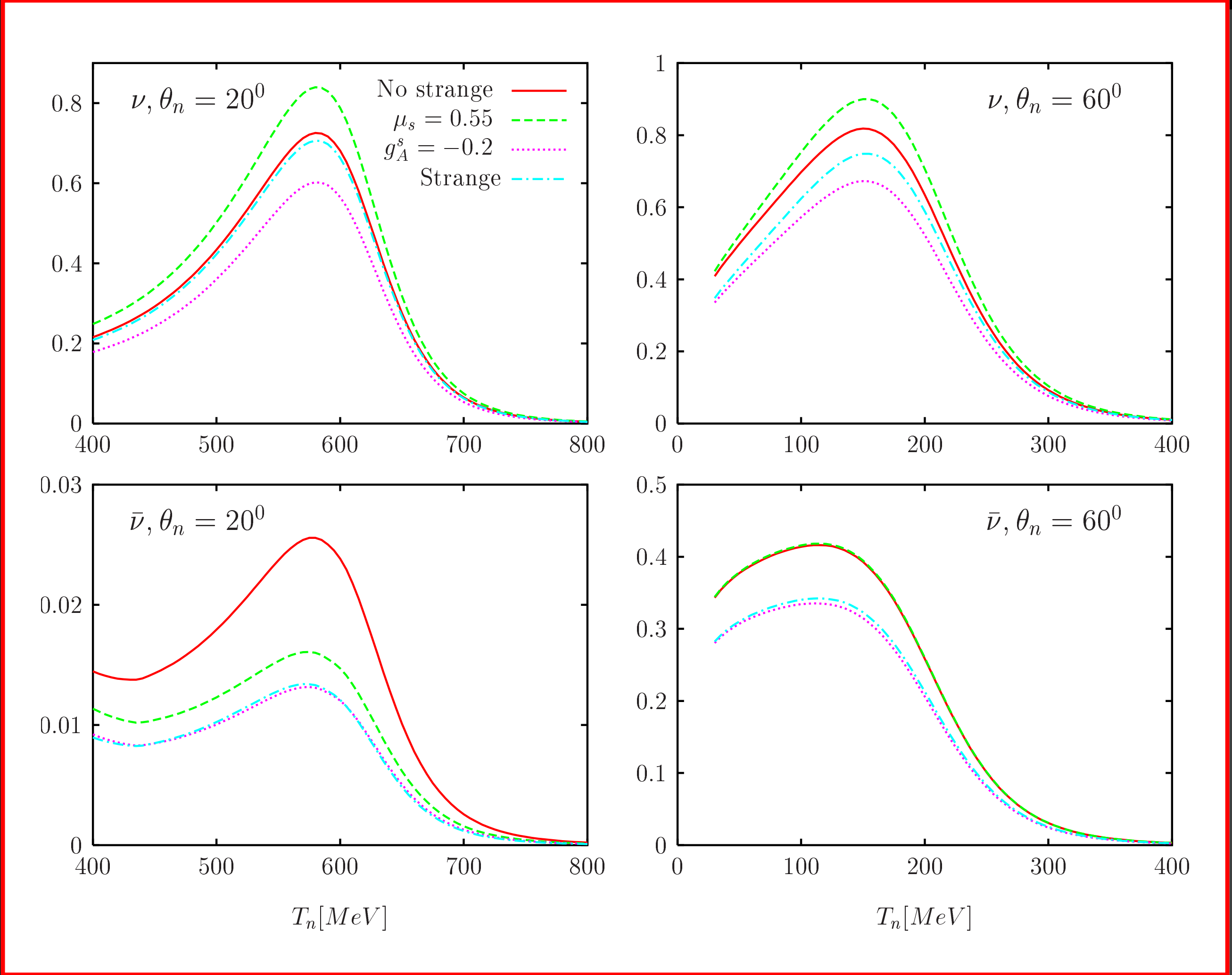

- Blue: strangeness
- Red: no strangeness

8 Coherent pion production

$$\begin{aligned}
\nu_l(k) + X &\longrightarrow l^-(k') + X + \pi^+(k_\pi) \\
\nu_l(k) + X &\longrightarrow \nu_l^-(k') + X + \pi^0(k_\pi)
\end{aligned}$$

- Coherent pion production is sensitive to the nuclear form factor $F(\vec{q} - \vec{k}_\pi)$
- Maximum when $\vec{q}$ and $\vec{k}_\pi$ are parallel
- The vector contribution is purely transverse and vanishes $\Longrightarrow$ small for electromagnetic pion production
- The axial contribution does not vanishes for neutrino-induced reactions

NUINT 09

8 *Coherent pion production*

$$\nu_l(k) + X \longrightarrow l^-(k') + X + \pi^+(k_\pi)$$
$$\nu_l(k) + X \longrightarrow \nu_l^-(k') + X + \pi^0(k_\pi)$$

- Microscopic model for coherent CC and NC pion production Amaro, E. Hernandez, J. Nieves and M. Valverde, PRD 79 (2009)
- The model includes Δ production plus background terms
- Good description of neutrino-induced pion production off the nucleon Hernandez, Nieves and Valverde, PRD 76 (2007)]

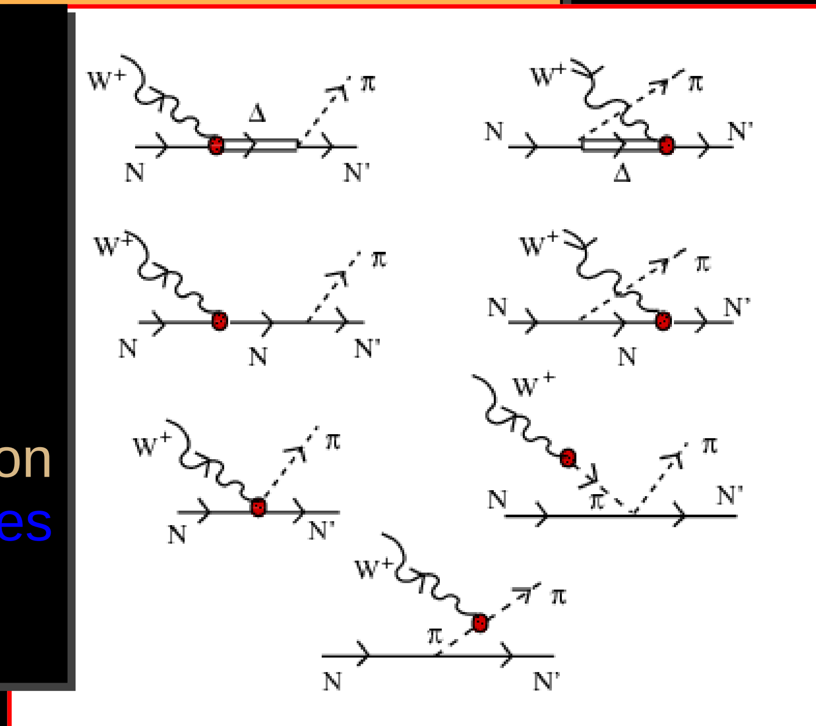

8 Coherent pion production

The model provides accurate coherent pion production cross sections

- Takes into account the relevant nuclear effects
- Δ self-energy in the medium and Pauli-blocking effects in the width.
- Local density aproximation assuming initial and final nucleon momenta $\vec{p} = (\vec{k_\pi} - \vec{q})/2 \; \vec{p'} = -(\vec{k_\pi} - \vec{q})/2$
- Pion distortion effects solving the Klein-Gordon equation for the pion with optical potential

$$[-\nabla^2 + m_\pi^2 + 2E_\pi V_{\rm opt}(\vec{r})]\varphi^*(\vec{r}) = E_\pi^2 \varphi^*(\vec{r})$$

- M
p
N
- T
b
- G
p
a

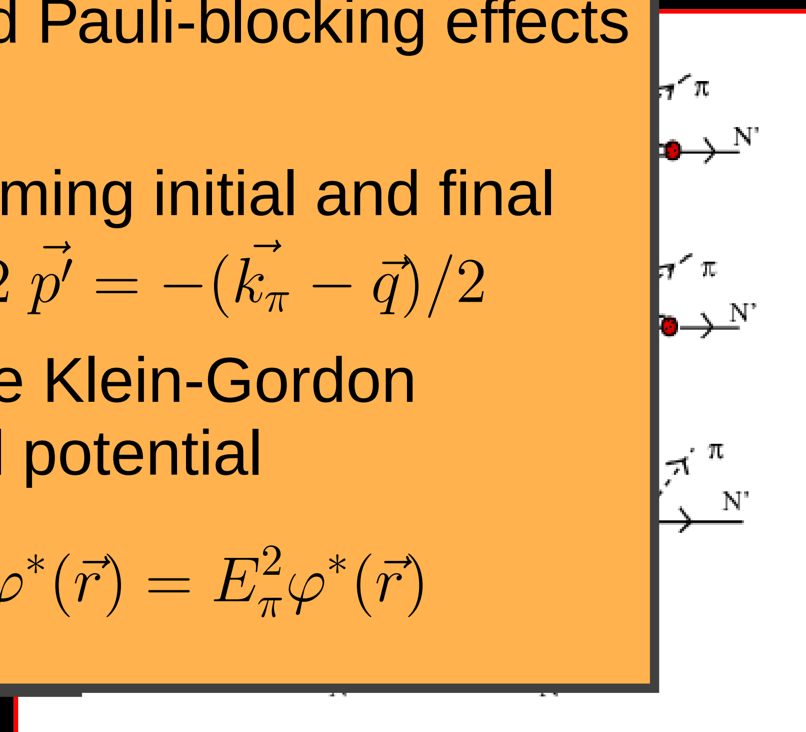

π momentum distribution

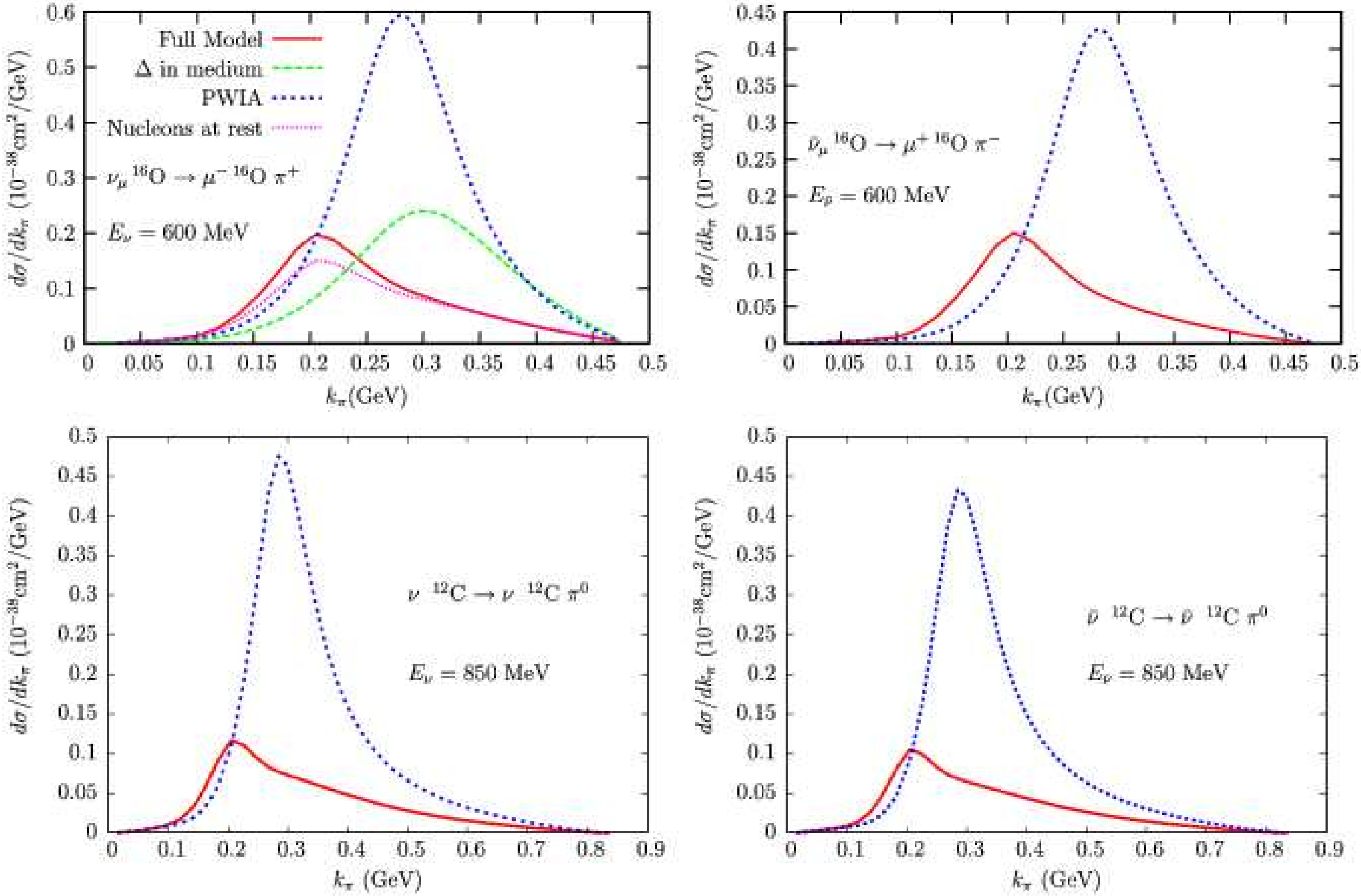

FIG. 2 (color online). Pion momentum differential cross section in the LAB frame for different coherent pion production reactions. Short-dashed line (in blue) has been calculated using planes waves for the outgoing pion and without including any in-medium correction for the Δ. Results with Δ nuclear medium effects are shown in the upper-left panel by the long-dashed line (in green). Our full model calculation, including medium effects on the Δ and the distortion of the outgoing pion wave function, is shown by the solid line (in red). Finally, the effect of putting the nucleons at rest is shown in the upper-left panel by the dotted line (in magenta).

Coherent π predictions

 PHYSICAL REVIEW D **79,** 013002 (2009)

TABLE II. NC/CC muon neutrino and antineutrino coherent pion production total cross sections for K2K, MiniBooNE and T2K experiments. In the case of CC K2K, the experimental threshold for the muon momentum $|\vec{k}'| > 450$ MeV is taken into account. To convert the cross section ratio given in [11] into a coherent cross section (K2K), we use the value of 1.07×10^{-38} cm^2/nucleon for the total CC cross section, as quoted in [11]. For the MiniBooNE NC* entry, we present our results when an optical pion-nucleus potential with an imaginary part due to absorption and inelastic channels alone is used to compute the distortion of the outgoing pion (see text for more details). The absolute NC π^0 coherent cross section quoted in the PhD thesis of Ref. [77] should be taken with extreme caution, since in the published paper (Ref. [18]) it is not given. There, it is quoted the ratio of the sum of the NC coherent and diffractive modes over all exclusive NC π^0 production at MiniBooNE. Some details on the flux convolution are compiled in the last three columns.

Reaction	Experiment	$\bar{\sigma}$ [10^{-40} cm^2]	$\sigma_{\rm exp}$ [10^{-40} cm^2]	$E^i_{\rm max}$ [GeV]	$\int_{E^i_{\rm low}}^{E^i_{\rm max}} dE\phi^i(E)\sigma(E)$ [10^{-40} cm^2]	$\int_{E^i_{\rm low}}^{E^i_{\rm max}} dE\phi^i(E)$
CC $\nu_\mu + {}^{12}$C	K2K	4.68	<7.7 [11]	1.80	3.84	0.82
CC $\nu_\mu + {}^{12}$C	MiniBooNE	2.99		1.45	2.78	0.93
CC $\nu_\mu + {}^{12}$C	T2K	2.57		1.45	2.34	0.91
CC $\nu_\mu + {}^{16}$O	T2K	3.03		1.45	2.76	0.91
NC $\nu_\mu + {}^{12}$C	MiniBooNE	1.97	$7.7 \pm 1.6 \pm 3.6$ [77]	1.34	1.75	0.89
NC* $\nu_\mu + {}^{12}$C	MiniBooNE	2.38*	$7.7 \pm 1.6 \pm 3.6$ [77]	1.34	2.12*	0.89
NC $\nu_\mu + {}^{12}$C	T2K	1.82		1.34	1.64	0.90
NC $\nu_\mu + {}^{16}$O	T2K	2.27		1.35	2.04	0.90
CC $\nu_\mu + {}^{12}$C	T2K	2.12		1.45	1.42	0.67
NC $\nu_\mu + {}^{12}$C	T2K	1.50		1.34	0.96	0.64

The analysis of MiniBooNE overstimates our results

Coherent π predictions

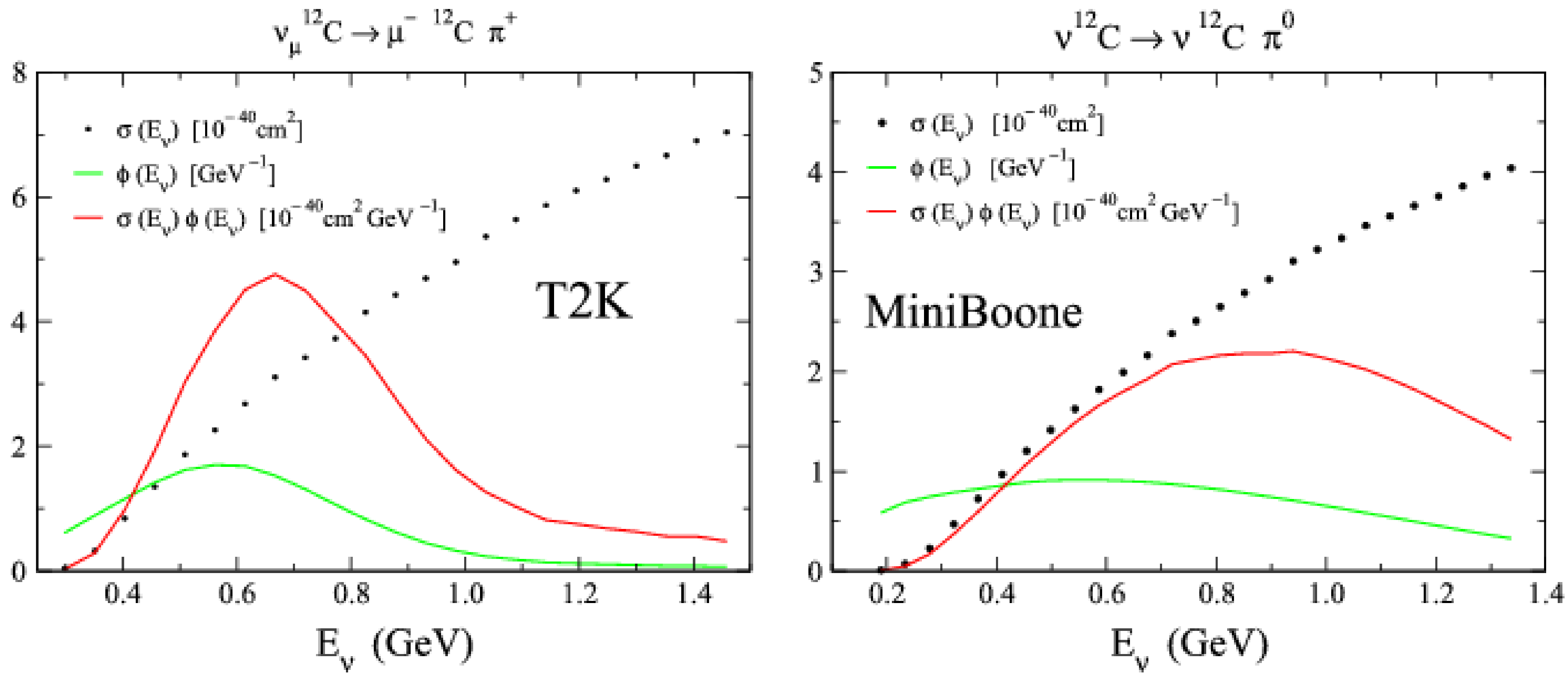

FIG. 9 (color online). CC (left) and NC (right) coherent pion production cross sections in carbon. We also show predictions multiplied by the T2K (left) and MiniBooNE (right) ν_μ neutrino energy spectra. In the region of neutrino energies around 0.6 GeV, the lower curves stand for the T2K and MiniBooNE ν_μ fluxes normalized to one.

Conclusions

Neutrino interactions importance for nuclear physics:

- We have illustrated with examples a selection of neutrino reactions on nuclei and their interplay with nuclear reaction models and structure
- Neutrino cross sections incorporate a richer information on nuclear structure and interactions than electrons.
- The availability of neutrino cross sections of different kinds will be valuable for the developement of more precise nuclear models and nuclear interaction theories